GCA TECHNICAL REPORT NO. 63-12-N

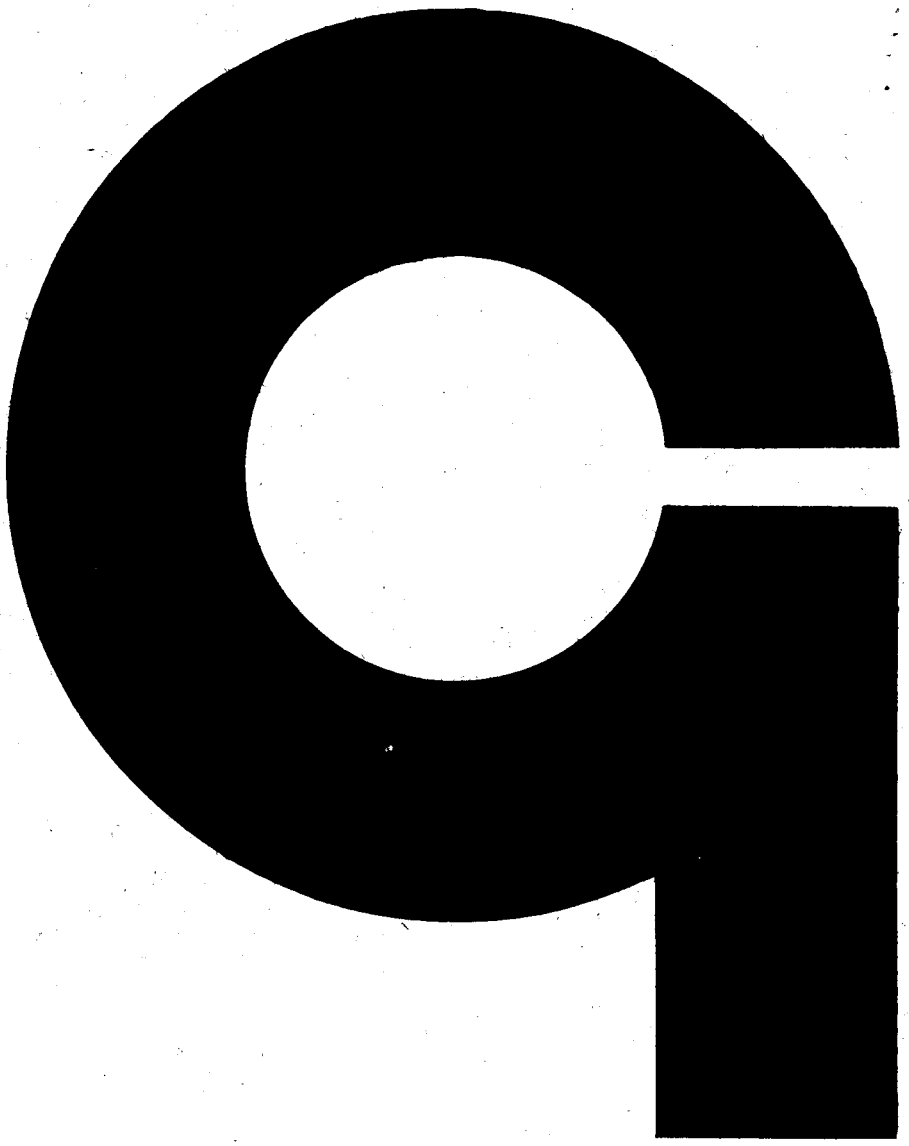

LABORATORY AND THEORETICAL STUDIES IN THE VACUUM ULTRAVIOLET

FINAL REPORT

CONTRACT NO. NASw-395

PREPARED FOR

NATIONAL AERONAUTICS AND SPACE ADMINISTRATION

HEADQUARTERS

400 MARYLAND AVENUE, S. W.

WASHINGTON 25, D. C.

GEOPHYSICS CORPORATION OF AMERICA

BEDFORD, MASSACHUSETTS

APRIL 1963

To: NASA Headquarters
400 Maryland Avenue, S.W.
Washington 25, D. C.

GCA Technical Report
No. 63-12-N

"Laboratory and Theoretical Studies in the Vacuum Ultraviolet"

prepared under

Contract No. NASw-395

FINAL REPORT

Covering the Period 2 February 1962 through 2 March 1963

by

GEOPHYSICS CORPORATION OF AMERICA
Bedford, Massachusetts

This report has been prepared by Dr. F.F. Marmo, Project Director
and Principal Investigator.

TABLE OF CONTENTS

INTRODUCTION

This is a Final Report of the work accomplished under NASA Contract No. NASw-395 covering the period from 2 February 1962 through 2 March 1963. Detailed accounts of the work accomplished during this period can be found in the ten GCA technical reports listed in the Table of Contents.

For the purposes of the present publication, the essential data have been extracted from the above-mentioned reports and presented in summary form with brief analyses when required for completeness. In most cases, details are omitted since they are included in the original reports for the interested reader. In this format, the highlights of the work accomplished under Contract No. NASw-395 can be presented in a clear and concise manner.

The material will be divided into two categories: Section I presents summaries of theoretical work, whereas Section II presents summaries of experimental work accomplished under the present contract.

SECTION I — THEORETICAL

SUMMARIES OF WORK ACCOMPLISHED UNDER CONTRACT NO. NASw-395 AND PREVIOUSLY PUBLISHED AS GCA TECHNICAL REPORT NUMBERS 62-5-N, 62-2-N, 62-11-N, 62-14-N, 62-15-N AND 63-2-N

In this section, rather comprehensive summaries of previously published GCA Technical Reports are given. Included in these summaries are the pertinent tables, figures, and data. Brief analyses are also given so that the report is able to stand on its own. To indicate the detail and scope of work covered in the original reports, in each case the summaries are preceded by (1) the original Title Page, (2) the original Table of Contents, and (3) miscellaneous items such as abstracts, lists of figures, etc.

GCA Technical Report No. 62-5-N

PLANETARY AERONOMY II: NO_2 IN THE MARTIAN ATMOSPHERE

P. Warneck and F.F. Marmo

May 1962

GEOPHYSICS CORPORATION OF AMERICA
Bedford, Massachusetts

Contract No. NASw-395

Prepared for

NATIONAL AERONAUTICS AND SPACE ADMINISTRATION
HEADQUARTERS
WASHINGTON 25, D. C.

Accepted for publication in the May 1963 issue, Journal of Atmos. Sciences.

ABSTRACT

The transmission curve of the Martian atmosphere derived by Öpik is compared with transmission curves of an atmosphere containing various amounts of nitrogen dioxide. It is found that the amount of 6×10^{18} cm^2-column NO_2 (or even less) given by Sinton as an upper limit for the Martian NO_2 content could adequately explain the phenomenon of the blue haze. This finding made it worthwhile to investigate the effect of the temperature and pressure sensitive equilibrium $2\ NO_2 \rightleftharpoons N_2O_4$ upon the total NO_2 content and the altitude-number density distributions of NO_2 and N_2O_4. Computations were carried out for surface temperatures of 273^oK, 243^oK, 213^oK and 183^oK and for three different temperature distributions. The discussion of the results leads to the suggestion of several important new experiments.

TABLE OF CONTENTS

NO_2 IN THE MARTIAN ATMOSPHERE

P. Warneck and F.F. Marmo

SUMMARY

I. INTRODUCTION

The Martian atmosphere becomes increasingly optically dense in going from the red to the blue portion of the visible spectrum.[1] This gives rise to the so-called Martian blue haze. In addition, this haze occasionally disappears to reveal the surface markings of Mars; this is called a "blue clearing". The blue haze and blue clearing have not as yet been satisfactorily explained. Recently, some attention has been given to the role of NO_2 in the Martian atmosphere and its relationship to these phenomena.[2,3]

Recent IR measurements indicate an upper limit NO_2 content of 6×10^{18} cm^2-column. In the present work, a new NO_2-content upper limit is established by employing absorption cross sections in the visible region below 5000 A. In addition, with this limit the physical-chemical behavior of the NO_2 - N_2O_4 system is given detailed attention in order to derive the variation of NO_2 content with respect to reasonable Martian temperatures and pressures. On the basis of this study, some definitive experiments are suggested.

II. COMPUTATIONS OF NO_2, N_2O_4 NUMBER DENSITIES WITH ALTITUDE

The amount of NO_2 on Mars and the distribution of NO_2 - N_2O_4 with altitude depends strongly on the assumed thermal structure of the Martian atmosphere. Thus, computations were carried out considering three cases:

(a) An isothermal atmosphere;

(b) A linear temperature decrease according to an adiabatic lapse rate of 3.7°K per km up to a tropopause at 12 km with an isothermal atmosphere above that level; and

(c) Similar to (b) with the tropopause at 24 km.

The system studied can be written as

$$2NO_2 \rightleftharpoons N_2O_4 \quad . \tag{1}$$

The equilibrium constant

$$K = \frac{kTn_1^2}{n_2} = 1.58\text{x}10^{9}\text{x}10^{-13693/4.576\text{x}T} \quad . \tag{2}$$

The integrated amount of NO_2 remains constant so that

$$\int_o^\infty n_1 dz + 2\int_o^\infty n_2 dz = C = 6\text{x}10^{18}\ \text{cm}^2\text{-column} \tag{3}$$

[after Sinton[3]]

For the models assumed, the following expressions were derived to show the variation of the number density of NO_2 with altitude:

$$n_1 = \frac{K}{4kT}\left[\left(\sqrt{1 + \frac{8kTn_o}{K}\left(\frac{H}{H_o}\right)^{\frac{1-B}{B}}}\right) - 1\right] \tag{4}$$

for that portion of the atmosphere with a linear temperature decrease whereas for the isothermal part, one can write

$$n_1 = \frac{K}{4kT}\left[\left(\sqrt{1 + \frac{8kTn^*}{K}\exp\left(-z/H^*\right)}\right) - 1\right] \qquad (5)$$

where

k = Boltzmann's constant

n_o = combined number density (NO_2 and N_2O_4 at the surface)

n_1 = number density of NO_2

H_o = scale height at the surface

H = scale height

$B = \frac{H\beta}{T}$ where $\beta = 3.7^{o}K$ per km

n^* = number density at the tropopause

H^* = scale height at tropopause

and

z = altitude .

Equations (4) and (5) were evaluated for several cases; the results are summarized in Figures 1, 2, 3, 4, and 5.

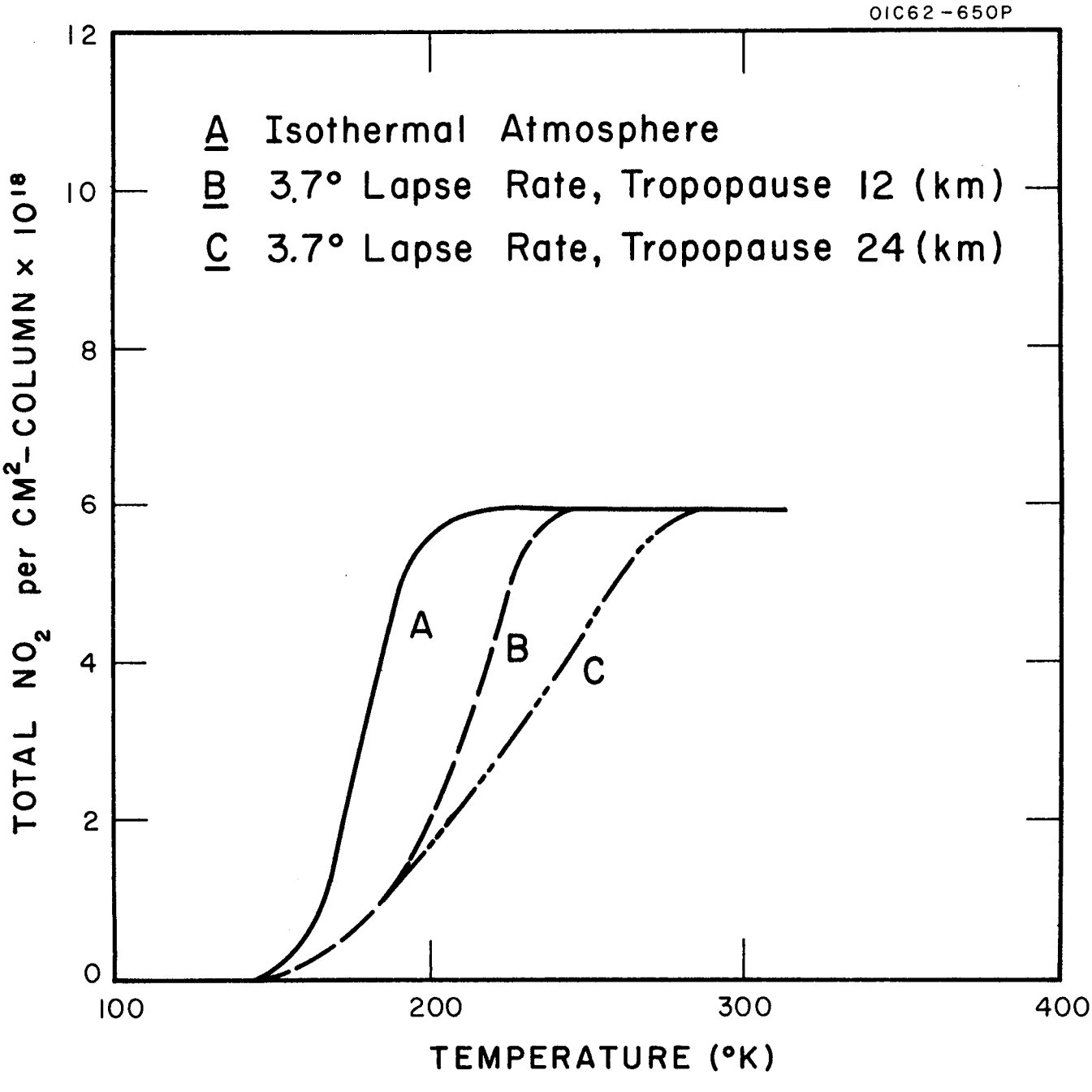

Figure 1. Variation of Total NO_2 Content of Mars with Surface Temperature.

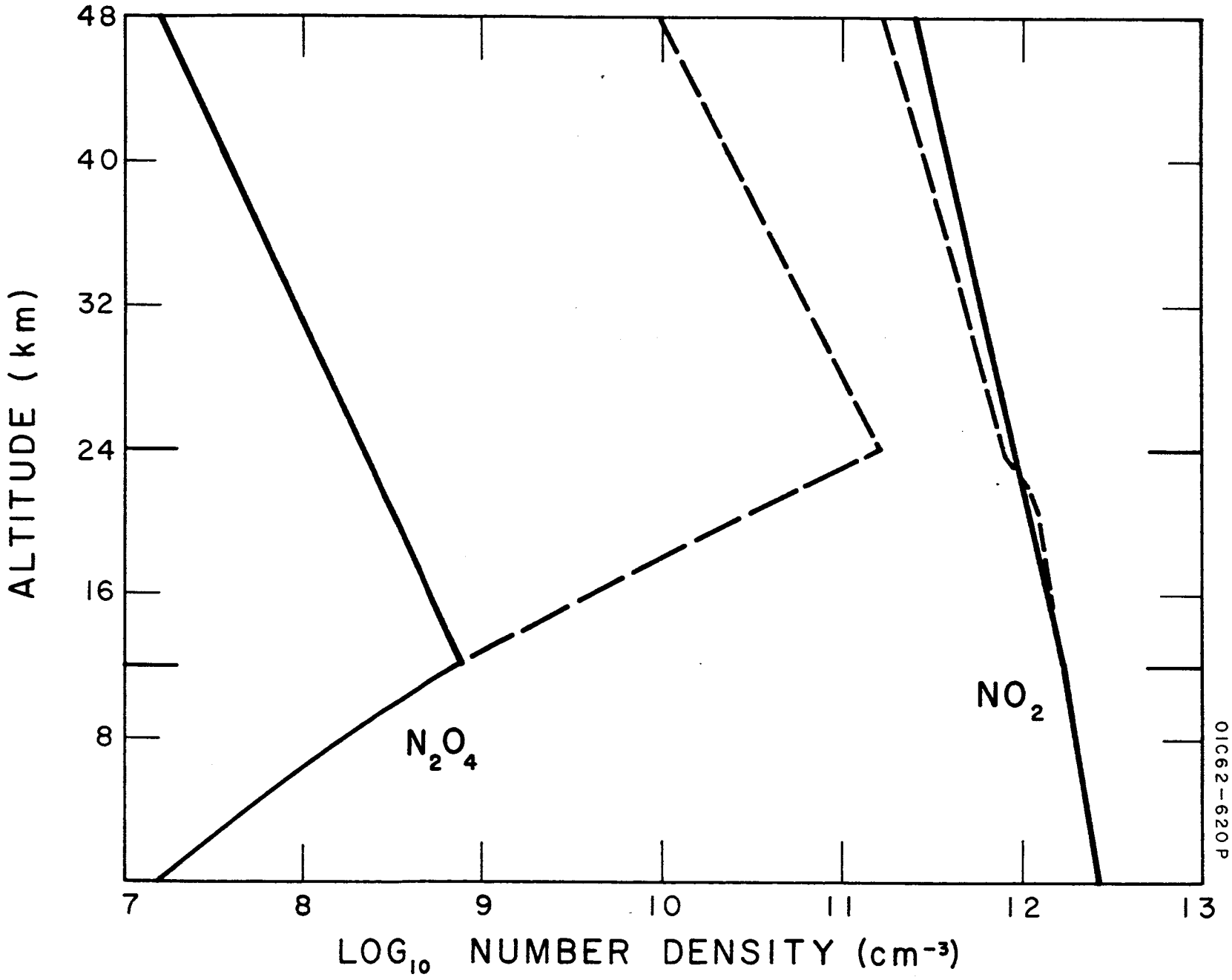

Figure 2. Distribution of NO_2 - N_2O_4 with Altitude for $T_o = 273^{\circ}K$.
Solid Curves: Tropopause at 12 km. Broken Curves: Tropopause at 24 km.

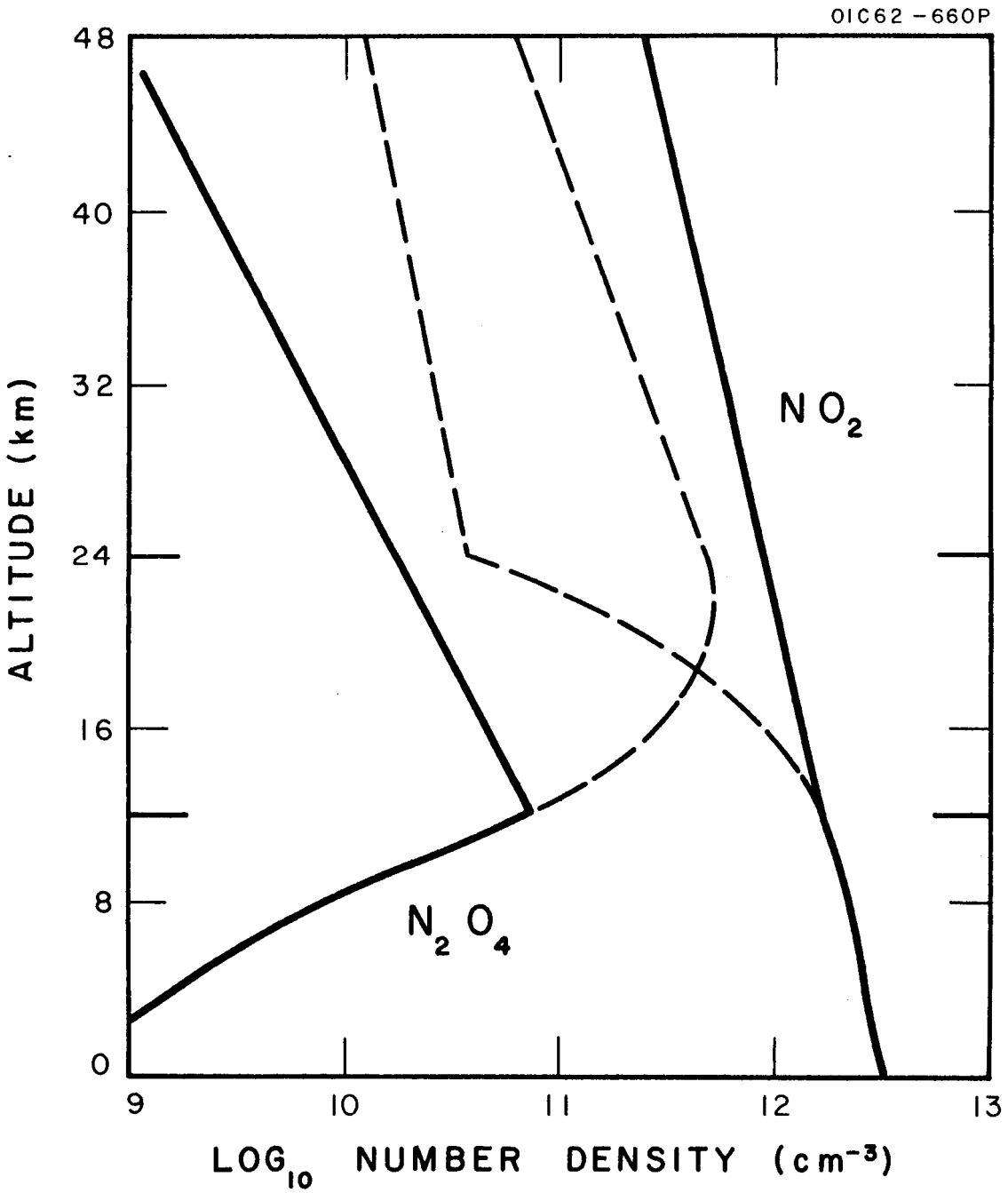

Figure 3. Distribution of NO_2 - N_2O_4 with Altitude for $T_o = 243^oK$. Solid Curves: Tropopause at 12 km. Broken Curves: Tropopause at 24 km.

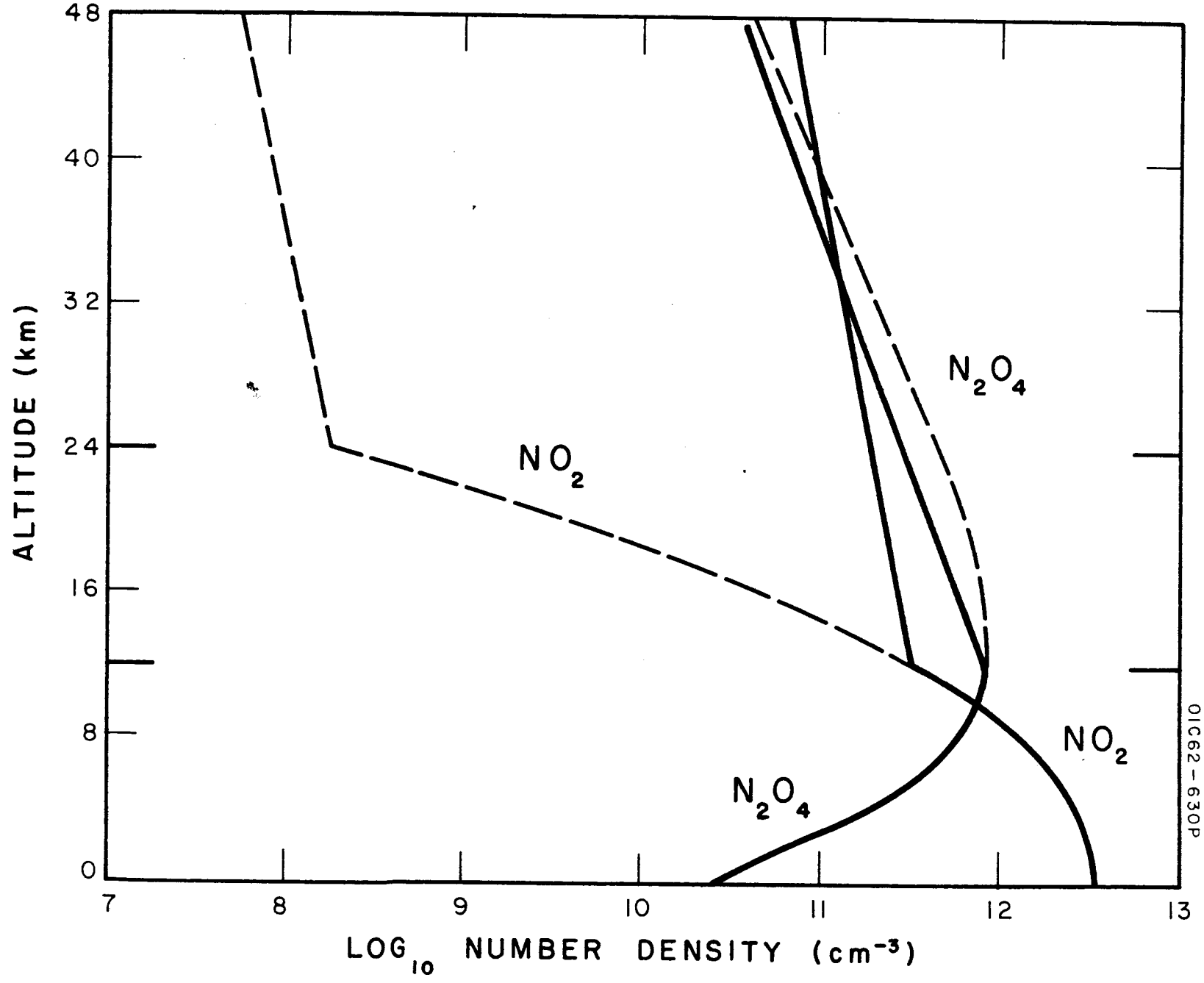

Figure 4. Distribution of NO_2 - N_2O_4 with Altitude for $T_o = 213^oK$.
Solid Curve: Tropopause at 12 km. Broken Curves: Tropopause at 24 km.

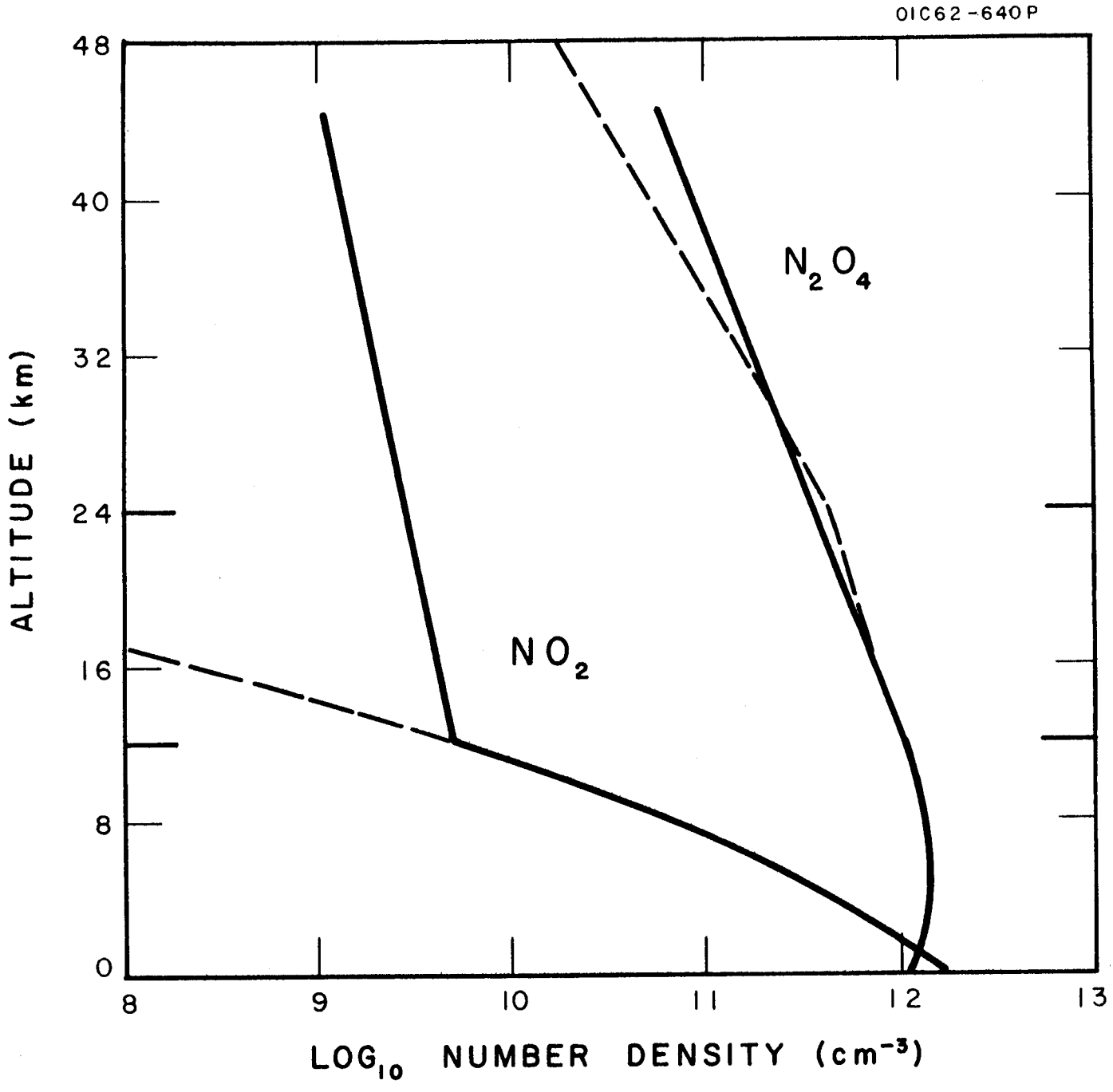

Figure 5. Distribution of NO_2 - N_2O_4 with Altitude for T_o = 183°K.
Solid Curves: Tropopause at 12 km.
Broken Curves: Tropopause at 24 km.

III. DISCUSSION OF RESULTS

On the basis of the results shown in the figures it was concluded:

(1) The hypothesis of Kiess et al.[1] could be rejected.

(2) An NO_2 content as high as 6×10^{18} cm^2-column is compatible with the results of Sinton.[3]

(3) On the basis of the calculated variation of the NO_2 content, the following experiment was suggested:

   (a) The absorption strength of the 3.43 micron band should be monitored before, during, and after a blue clearing to determine whether or not this event can be associated with Martian NO_2 depletion.

   (b) If no variation is observed, then it appears that the NO_2 hypothesis must be rejected.

   (c) On the other hand, an observed variation would then make it worthwhile to search for additional absorption bands due to N_2O_4.

   (d) If such bands are discovered, it would be worthwhile to compare the absorption intensity ratios.

   (e) To make simultaneous, independent measurements of the Martian atmosphere to check and find out if the observed NO_2 depletion can be due to temperature variations.

   (f) If the measurements in (d) and (e) are found to be not self-consistent, it is evident that the NO_2 depletion cannot be ascribed solely to temperature variations but rather are caused by other depletion mechanisms; i.e., solar photodecomposition.

REFERENCES

1. E. J. Öpik, J. Geophys. Res. 65, 3057 (1960).

2. C. C. Kiess, S. Karrer and H. K. Kiess, Pub. A.S.P. 72, 256 (1960).

3. W. M. Sinton, Pub. A.S.P. 73, 125 (1961).

GCA Technical Report No. 62-2-N

PLANETARY AERONOMY III:

DETERMINATION OF ATMOSPHERIC PARAMETERS BY THE USE OF ROCKET-BORNE MASS SPECTROMETERS

R.F.K. Herzog, F.F. Marmo, R.A. Minzner
and G.O. Sauermann

July 1962

Contract No. NASw-395

Prepared for

National Aeronautics and Space Administration
Headquarters
Washington 25, D. C.

GEOPHYSICS CORPORATION OF AMERICA
Bedford, Massachusetts

TABLE OF CONTENTS

DETERMINATION OF ATMOSPHERIC PARAMETERS BY THE USE OF ROCKET-BORNE MASS SPECTROMETERS

R. F. K. Herzog, F. F. Marmo, R. A. Minzner
and G. O. Sauermann

SUMMARY

I. INTRODUCTION

The knowledge of specific thermodynamic and hydrodynamic parameters is required in the study of almost any phase of chemical aeronomy in the upper atmosphere. Accordingly, this higher region has been the target of several detailed recent studies.[1] It is not the purpose of the present paper to review or evaluate these studies. However, it should be noted that the present state of knowledge supports several different controversial points of view. This report describes an experiment designed specifically to determine some of the more important atmospheric parameters. In the proposed experiment, a mass spectrometer will obtain number density-altitude profiles for helium and argon.

Argon measurements have been successfully performed from sounding rockets in the past[2] and no principal difficulty is expected here. On the other hand, helium measurements, although tried, have not been performed successfully as yet due to the low relative concentration of helium in the homosphere. For example, single-stage mass spectrometers are not capable of an accurate helium determination even in air at ground level since the background around the helium peak is excessively

high. This background is caused by heavy particles (N_2^+, O^+_2) which are scattered on the neutral gas molecules in the analyzer.

Recently, an experimental study was conducted as part of Contract NASw-25 to determine the feasibility of obtaining accurate helium measurements. For this purpose a special mass spectrometer was designed and built which consisted of two analyzer stages and was equipped with an electron multiplier as an ion detector. The background was suppressed and the electrical noise was made sufficiently low that it was possible to detect helium at partial pressures as low as 3×10^{-13} torr. Based on these promising results, a prototype flight model was constructed and adapted, geometrically, to the nose cone of an Aerobee-Hi rocket. The performance of this instrument is described in detail elsewhere[3] and is shown in Figure 1. It is capable of measuring the helium number density accurately as well as the total atmospheric density for conditions which correspond to altitudes greater than the peak height of the Aerobee-Hi rocket.

A very important consideration for the design of the experiment is the correlation of ambient density and the partial pressure in the mass spectrometer ion source; this aspect is discussed in the original report and not repeated here. Assuming the availability of a suitable calibrated instrument an additional study was performed to ascertain the value of utilizing this type of probe for the determination of several atmospheric dynamic and thermodynamic properties. The results

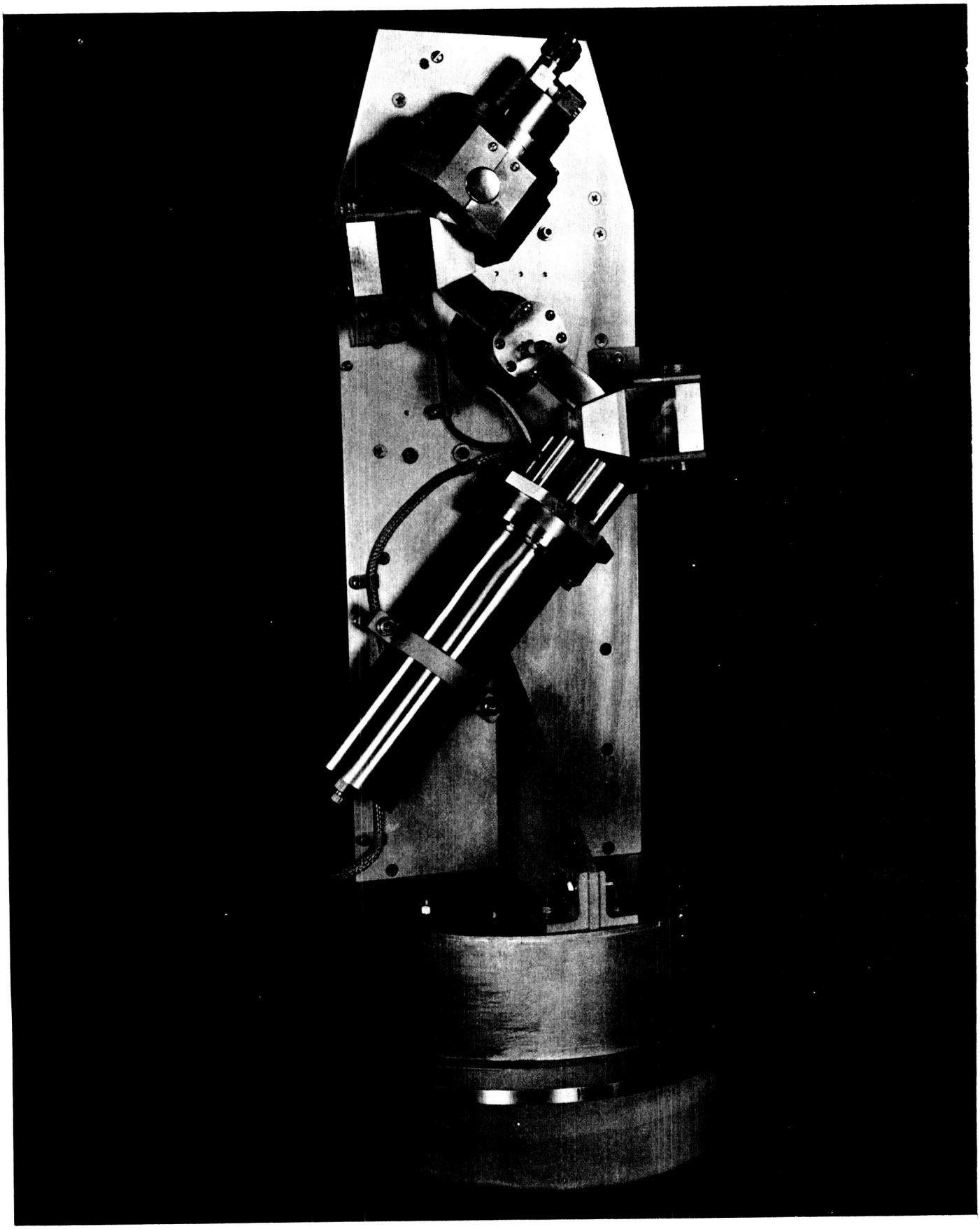

Figure 1. Photograph of the He Mass Spectrometer.

were promising in that it was found that information can be obtained for the following phenomena: (1) the beginning of the mictopause region; (2) the definition and altitude range of the transition region (between complete mixing and diffusive equilibrium; (3) separation effects in the region of complete diffusive equilibrium; (4) an approximate determination of the absolute temperature for the region of the atmosphere which is mixed; (5) an improved determination of the absolute temperature for the region of the atmosphere in diffusive equilibrium; and finally (6) the several thermodynamic properties associated with atmospheric temperature, composition, and number densities. It may be noted that Items 1, 2 and 3 can be associated with the dynamic properties of the upper atmosphere (winds) whereas Items 4, 5 and 6 can be classified as thermodynamic properties. In the original report each of these areas is discussed individually.

II. DYNAMIC AND THERMODYNAMIC PROPERTIES OF THE EARTH'S ATMOSPHERE

A. DYNAMIC PROPERTIES OF THE ATMOSPHERE

The Earth's atmosphere is well mixed below the so-called mictopause level which is assumed to be located at an altitude between 100 and 160 km. For instance, Meadows and Smith[2] collecting composition information, deduce a mictopause level between 110 and 120 km. From the surface up to these altitudes, the relative helium concentration is essentially constant (5.24×10^{-6}) so that the helium partial pressure profile is directly proportional to the total pressure. Above this level, gravitational separation causes the partial pressure of helium to decrease much slower than the total pressure. This separation effect and its relation to aeronomy has been discussed by Nicolet[4] who has shown that to obtain the theoretical density profile for helium, assumptions have to be made about the height of the mictopause (the separation level). Actually, the transition from mixing to diffusion is gradual and without sharp boundaries. Accordingly, measurement of the helium density profiles for altitudes up to 250 km (e.g. from an Aerobee-Hi rocket) can yield information on the location and nature of the mictopause region and the corresponding helium densities at much greater altitudes.

In addition to the above, it has been shown that the time constant to establish diffusive equilibrium in the atmosphere is small.

For example, P. Mange[5]--based on studies of Maris,[6] Epstein,[7] and Sutton[8]--has calculated the rapidity of diffusion in the atmosphere. From the results it can be deduced that the changes of the helium density profile at high altitudes can be correlated with the time variation of mictopause level. Previous works have shown[9] that the region above 800 km (but below about 2000 km) probably consists mainly of atomic oxygen and helium with their respective densities subject to great changes due to variations of the temperature, mictopause level, turbulence, etc. For example, the atomic-oxygen-altitude profile is very temperature sensitive (and not mictopause level sensitive), whereas the helium profile is mictopause level sensitive (but not very temperature sensitive). Accordingly, as a result, at very high altitudes (about 1600 km where helium outnumbers the oxygen), the density of the atmosphere is practically determined by phenomena which take place in the region between 100 and 150 km. In this regard, sodium measurements by E. Manring[10] show that in the region between 80 and 120 km, strong and irregular winds with shifting velocities occur which suggests that the mictopause level is subject to considerable fluctuation. On the other hand, in the region between 400 and 1000 km, where the atmosphere consists mainly of oxygen atoms, large density changes occur due to heating effects.

The previous discussion has made clear the importance of locating the mictopause level. In practice, there probably exists a transition region rather than a sharp level. Diffusive separation should become

apparent as the probe operates somewhat above 100 km. In this region, the separation ratio, r, can be determined by dividing the ratio argon-to-helium number density, as measured during the flight at a particular altitude, by the calibration ratio of argon-to-helium number density for normal, mixed, ground-level air. In other words, for r = 1, no diffusive separation is present; for r = 0, separation is complete. Several investigators[2] have probed the argon-nitrogen ratio as a function of altitude. The current experiment is analogous to these except that in this case, the argon-to-helium number density ratio is employed.

The simple theory shows that the separation ratio behaves according to

$$r = \exp\ (-h/H_1) \qquad (1)$$

where

$$H_1 = \frac{RT}{g(M^*-M)} \ ,$$

and

r = separation ratio

h = altitude interval above mictopause level

R = universal gas constant

T = average absolute temperature in interval h

g = average local value of gravity in interval h

M*= mass number of heavy gas (i.e., argon)

M = mass number of light gas (i.e., helium).

The use of helium in place of nitrogen in the proposed experiments results in a ratio of molecular weights (therefore, scale heights) of 10 compared with less than 1.5 for the case of nitrogen. This factor will aid in a more accurate and sensitive determination of the height of the beginning of diffusive separation. It may be pointed out that although previous investigations have indicated the beginning of the diffusion level, none have successfully defined the region in which complete diffusive equilibrium prevails. Much of the difficulty was due to the fact that nitrogen was one of the gases probed. Accordingly, it becomes difficult--if not impossible--to correlate the peak heights against the ambient nitrogen content due to chemical reactivity, photo-ionization, instrumental dissociation, etc. These difficulties are minimized in the present probe.

B. THERMODYNAMIC PROPERTIES OF THE ATMOSPHERE

The knowledge of the temperature profile (i.e., the temperature distribution with height) is of great importance for the proper interpretation of many physical effects in any planetary atmosphere and for the understanding of the mechanism involved. In particular, even small changes in the temperature profile can have considerable accumulative effects on the pressure and density distribution which, in turn, can affect the entire aeronomy of the upper atmosphere. Accordingly, the temperature, and the manner in which temperature varies with height, is one of the most important basic

parameters associated with many other physical properties of an atmosphere. Thus, temperature measurements have been attempted by several investigators who have employed "pressure" measuring devices and have obtained T/M ratio values. In the present experiment, T is measured explicity by employing the mass spectrometric techniques described.

In the following there will first be developed (1) a series of equations relating upper atmospheric number densities with temperatures. The application of these equations results in a temperature determination at one altitude only if the temperature is known or estimated at some reference altitude. Further development yields (2) a dual gas equation in which the requirement for a known reference temperature is eliminated but the experimental requirement is correspondingly increased.

1. Single Gas Relation Between Number Density and Temperature

To derive the general equation for a number density-temperature relation, the differential equation relating the density, ρ, to the hydrostatic pressure, p, is a good starting point:

$$dp = -g \rho \, dz \qquad (2)$$

where g denotes the acceleration of gravity and z is the geometrical altitude. For convenience, the entire calculations will be made in

terms of geopotential altitude, h, which eliminates the necessity to account for changes in the acceleration of gravity with altitude. The transformation from a geometrical altitude element, dz, into a geopotential altitude element, dh, can be made so that Equation (2) may be written as

$$dp = -G \rho \, dh \tag{3}$$

Use of the well-known relation P = nkT, derived from the universal gas law, results in

$$d(nT) = -\frac{1}{k} G \rho \, dh \tag{4}$$

$$\left[nT \right]_b^a = -\frac{G}{k} \int^a \rho \, dh \tag{4a}$$

Substituting $\rho = nm$ and $m/k = M/R$ yields

$$n_a T_a - n_b T_b = -\frac{MG}{R} \int_b^a n \, dh \tag{5}$$

which equation can be solved for T_b and/or T_a explicitly:

$$T_b = \frac{n_a}{n_b} T_a + \frac{MG}{R} \int_b^a \frac{n}{n_b} dh \tag{6}$$

$$T_a = \frac{n_b}{n_a} T_b - \frac{MG}{R} \int_b^a \frac{n}{n_a} dh \tag{7}$$

where a and b refer to upper and lower altitude, respectively.

Equations (6) and (7) may be referred to as "single gas" equations since they are applicable to each individual number density profile. It should be remarked that the density ratios of Equations (6) and (7) can be measured directly, whereas the reference temperature T_a and T_b have to be estimated or obtained by other means. Accordingly, even if accurate density measurements for a single gas were made, a measurement of the temperature at either altitude could not be accurately obtained without the knowledge of the corresponding reference temperature.

2. Dual Gas Relation Between Number Densities and Temperature

The need for a reference temperature can be eliminated by substitution from expressions (6) and (7) to yield the following corresponding relationships:

$$T_b = \frac{1}{n_b^*/n_a^* - n_b/n_a} \frac{G}{R} \left[M^* \int_b^a \frac{n^*}{n_a^*} dh - M \int_b^a \frac{n}{n_a} dh \right] \tag{8}$$

$$T_a = \frac{1}{n_a/n_b - n_a^*/n_b^*} \frac{G}{R} \left[M^* \int_b^a \frac{n^*}{n_b^*} dh - M \int_b^a \frac{n}{n_b} dh \right] \tag{9}$$

Here, for clarity, the values designated by an asterisk refer to the heavy gas measurements, whereas the others refer to the light gas measurements. Since the measurements described in this report yield simultaneous measurements of the number densities of both the heavy and light gas with altitude, Equations (8) and (9) are applicable to

the data. Thus, Equations (8) and (9) show that a temperature determination is now made available without the necessity of invoking or knowing some reference temperature. The application of Equations (8) and (9) will be demonstrated in the next section which employs data from a hypothetical experiment to aid in the discussion.

III. ANALYSIS OF DATA FROM A HYPOTHETICAL EXPERIMENT

A. GENERAL REMARKS

In this section the usefulness of the dual gas method will be demonstrated by applying it to some numerical data. However, since no experimental data are available yet, it was necessary to generate somewhat realistic data based on atmospheric parameters discussed in the Proposed 1961 Revision of U.S. Standard Atmosphere.[11] In addition, it was assumed that a mictopause level exists at 100 km with a 10 km transition region between 95 and 105 km. For the purpose of further discussion of this hypothetical experiment, it is assumed that primary data reduction difficulties have been either eliminated or accounted for. Typical presentation of the final data could correspond to those shown in Figures 2 and 3. Figure 2 shows the "measured" relative number density-altitude behavior of helium and the ambient, whereas Figure 3 shows the analogous data in which both helium and argon are measured. Further discussion of these data can more conveniently be accomplished in two parts: (1) determination of atmospheric dynamics and (2) determination and atmospheric thermodynamics.

B. ATMOSPHERIC DYNAMICS

The data in Figures 2 and 3 can be presented to detect the beginning of diffusive separation in order to define the mictopause level and the transition region. This is shown in Figure 4. The figure

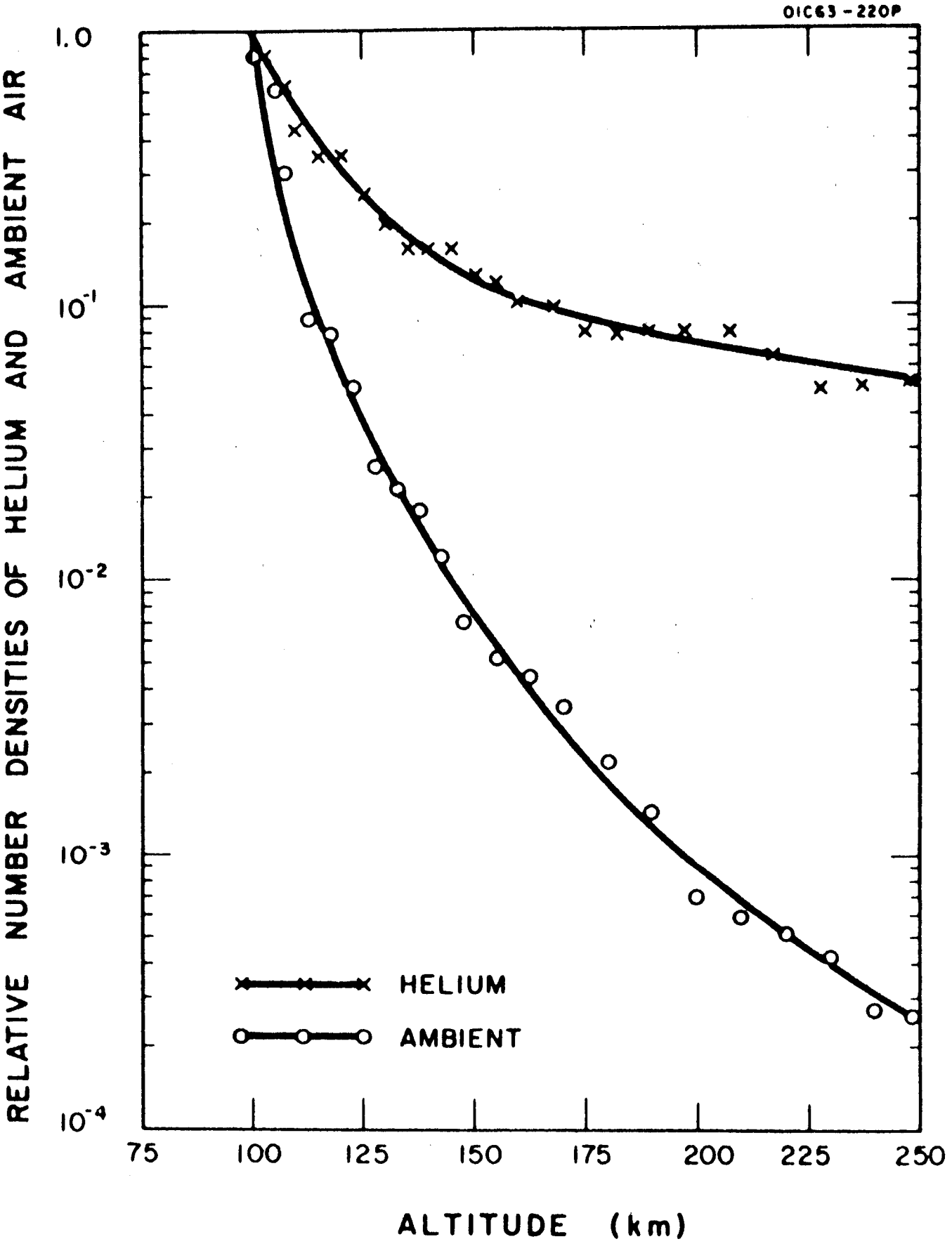

Figure 2. Experimental measurements of the relative number density of helium and ambient air between 100 and 250 km.

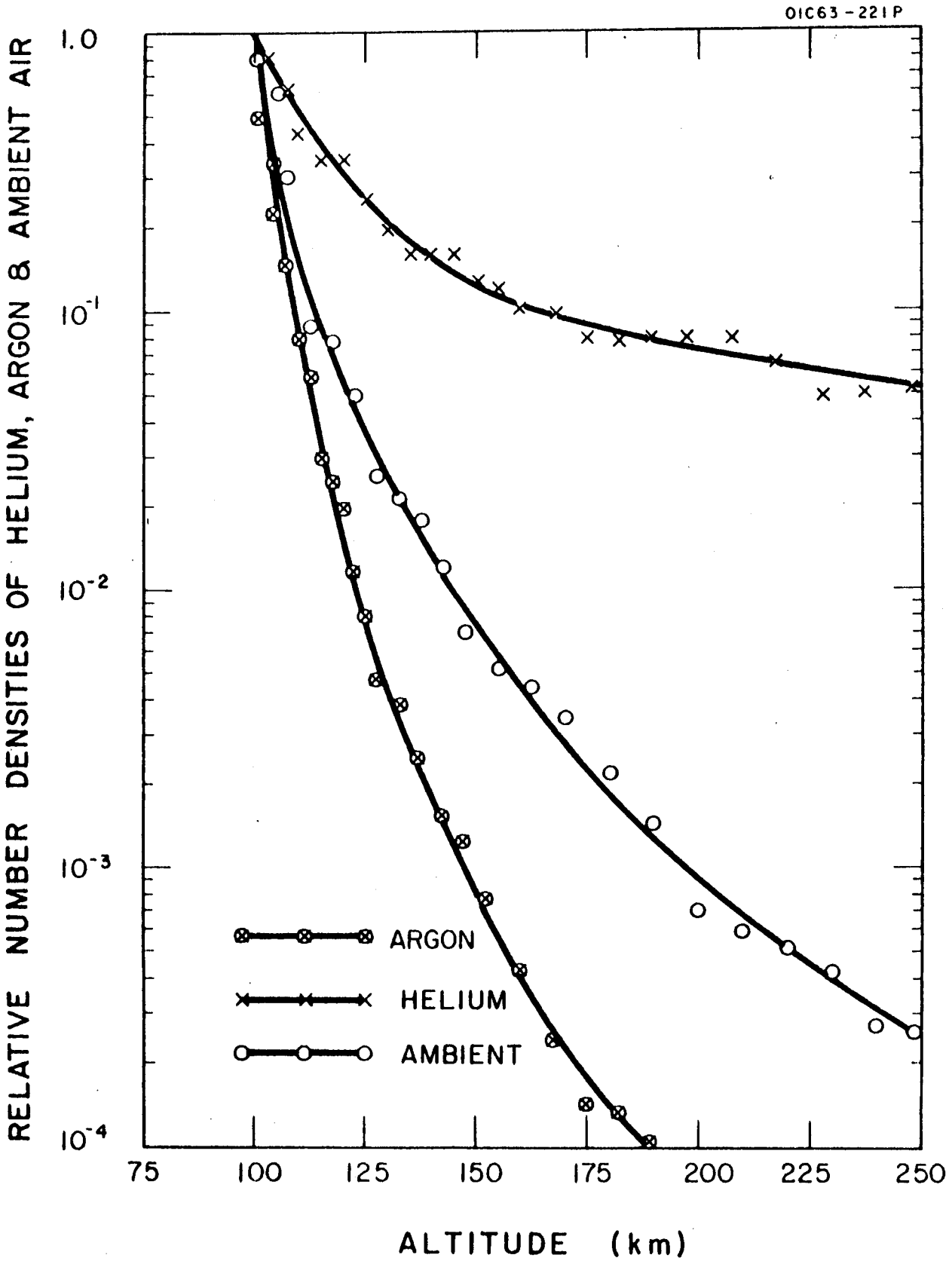

Figure 3. Experimental measurements of the relative number density of helium, argon and ambient air between 100 and 250 km.

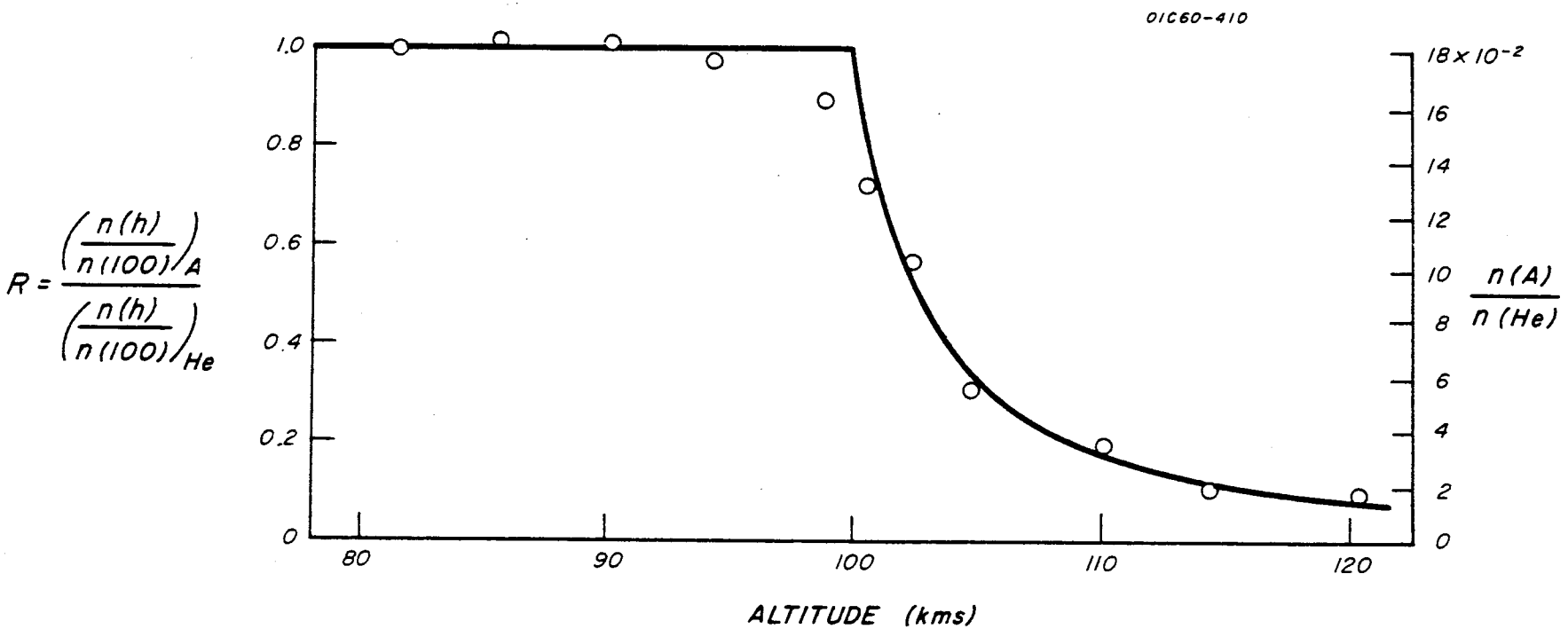

Figure 4. The diffusive separation ratio, R, as a function of altitude as derived from the data shown in Figures 2 and 3.

indicates the presence of a transition region from 95 to 105 km. Previous investigators have obtained similar information. However, the present method has the following unique advantages: (a) the mass ratio between argon and helium is 10 (as compared to only 1.5 for argon and nitrogen); (b) the noble gases do not participate in any chemical interactions; (c) the effect of ionization is negligible even at high altitudes; (d) no instrumental difficulties need be attributed to different ionization efficiencies; and finally (e) since no changes in composition of these species can occur, the atomic weights are constant throughout the entire altitude regime. Item (e) makes available an additional piece of information of considerable importance. Specifically, by determining the ratio of number density scale heights for helium and argon at various altitudes, the regions of perfect mixing, partial mixing, and complete diffusive equilibrium should be made evident. For example, for the region of perfect mixing, a ratio of 1 should prevail. This value should increase throughout the transition region until gravitational separation is complete and a value of 10 will be obtained. This behavior is shown in Figure 5. This information is of prime importance since it is required for application of the entire method to the thermodynamic characteristics of the atmosphere.

C. ATMOSPHERIC THERMODYNAMICS

The data shown in Figure 2 and 3 can be employed for the determination of T_b and/or T_a by Equations (8) and (9) for the region in which

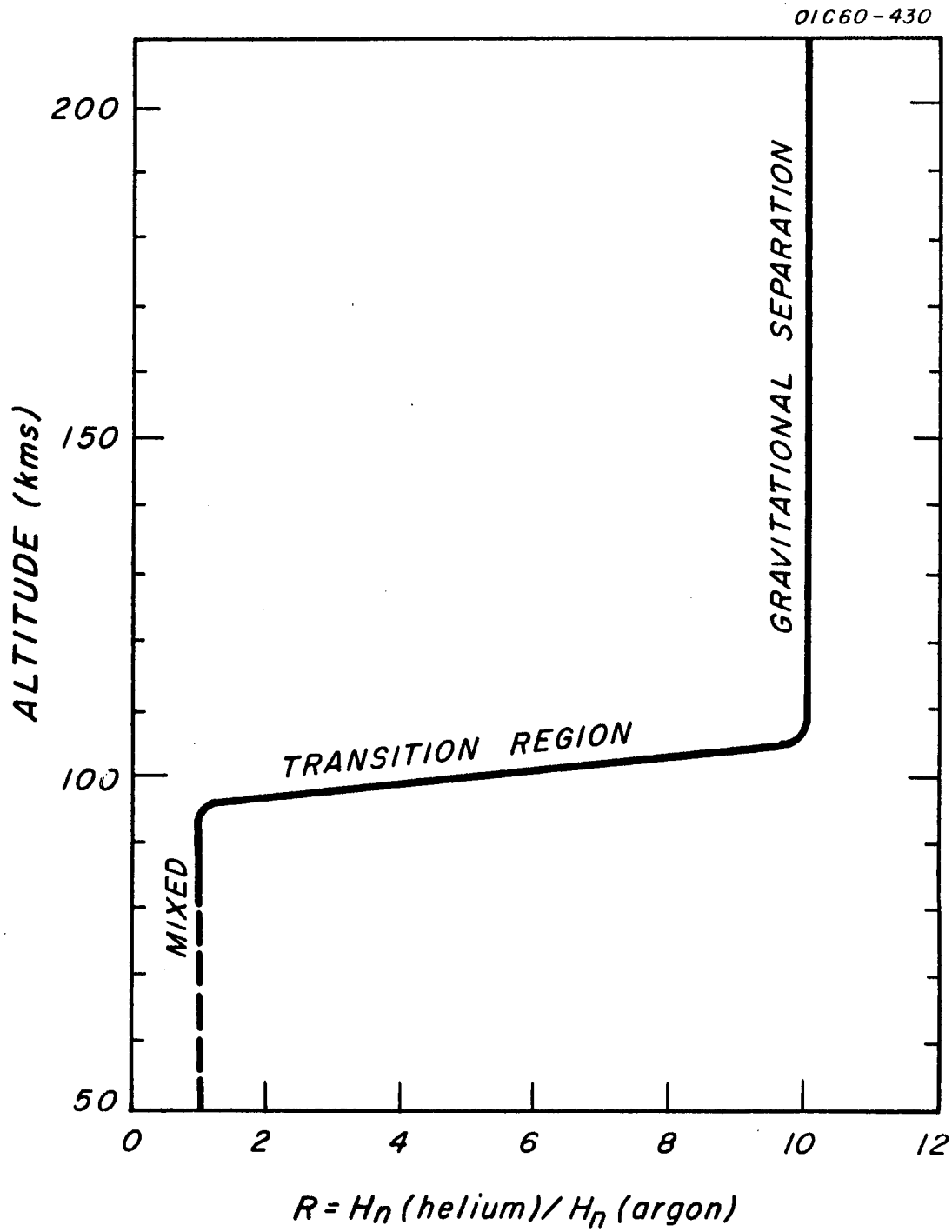

Figure 5. Number density scale heights ratio for helium-argon at different altitudes.

diffusive equilibrium prevails (see Figure 5). For example, for an Aerobee-Hi experiment the altitude region is between about 150 km and 250 km. For obtaining optimum temperature measurements, the following sequence of computation steps can be suggested: (a) calculate T_a (at 250 km) by means of Equation (9) from the measured number density profiles of helium and argon (recall that the quantities designated by an asterisk refer to heavy gas); (b) employ this T_a-value as the reference temperature in Equation (6) to calculate an accurate value of T_b for all altitudes for which good density data have been obtained; and finally (c) the employment of this T_a-value as the reference temperature T_b in Equation (7) permits an upward extension of the temperature profile for all altitudes for which reliable helium density data have been obtained. This procedure should result in the determination of an accurate temperature-altitude profile. The procedure outlined is valid but does not consider the effect of instrumental error. In the real case, of course, experimental errors are involved which a more realistic approach must recognize and take account for.

It is interesting to note that Ainsworth et al.[12] have discussed the possible existence of temperature maxima and minima in the lowest atmosphere. The helium number density profile data can also be of value in the determination of relatively small temperature perturbations in confined regions of the atmosphere. This is so because above about 150 km, the helium partial pressure is very insensitive to altitude. For example, within a 10 km range, the pressure can be considered constant.

Accordingly, any small perturbations due to local heating would be directly reflected as perturbation in the helium number density which should be more easily detected since the slope of the helium partial pressure profile is extremely small.

D. INDIRECT DETERMINATION OF THE MEAN MOLECULAR WEIGHT - ALTITUDE PROFILE

In addition to the determination of helium and argon number density explicitly, the particular mass spectrometer under consideration also measures total ion current (see Figures 2 and 3). This corresponds to the output of an ionization gauge, and can be correlated with fair accuracy to the total number density which can be used to compute the mean molecular weight, $\overline{M}$. Thus,

$$\overline{M} = \frac{R}{\overline{n}} \frac{\rho}{k}$$

where

$\overline{n}$ is the total number density.

From Equation (4):

$$\overline{M} \rho = -\frac{R}{G}\left(T \frac{d\, \ell n\, \overline{n}}{dh} + \frac{dT}{dh}\right) \tag{10}$$

The two-gas method yields the values for T, $\frac{dT}{dh}$ to substitute along with the experimental values of $\overline{n}$. Accordingly, a value for $\overline{M}$, the mean molecular weight, can be determined.

IV. SIMPLIFIED VERSION OF THE EXPERIMENT PREVIOUSLY DESCRIBED

Instead of using helium and argon density measurements, it is possible to use helium and air density measurements as long as the composition of the air does not change much. This is probably true up to altitudes of about 190 km where the mean molecular weight has dropped only about 7 percent according to measurements by Meadows and Townsend.[13] It can be expected also that the ionization gauge sensitivity stays essentially constant up to this altitude. Therefore, the total ion current readings of the helium mass spectrometer described before can be used to compute the ambient total number density. It is expected that above about 160 km, contamination of the air due to rocket outgassing becomes more and more important. Reliable total density measurements will be obtained probably between 90 and 160 km. Within this limited altitude range, the method described in this report is still applicable if the heavy gas is air (see Figure 2) instead of argon and an average value of the mean molecular weight for the particular altitude range is used. In fact, the present prototype instrument which has been developed[3] would be adequate for such an experiment.

V. SUMMARY

This report contains a description of an experimental technique for obtaining various hydrodynamic and thermodynamic properties of the upper atmosphere. This could be accomplished by employing two rocket-borne mass spectrometers capable of simultaneously measuring the number density-altitude relation of helium and ambient air in one instrument, and argon and ambient air in the other. Brief reviews were given of the instrumentation and of the theoretical analysis to be employed in the present experiment. In addition, a typical data analysis has been performed on the data from a hypothetical experiment. The analysis of the "experimental" data yielded information on the following: (1) the location and detection of the beginning of diffusive separation in the upper atmosphere; (2) a measure of the degree of diffusive separation in the transition region; (3) the location above which complete diffusive separation prevails; (4) an improved temperature-altitude profile from the beginning of diffusive separation up to extremely high altitudes; (5) determination of the temperature in the upper part of the mixed region of the atmosphere; (6) the possibility of detecting small perturbations of upper atmpspheric temperature in local regions; and (7) a determination of the variation of mean molecular weight of the ambient air in the heterosphere. It should be noted here that in the present case, the temperature is determined explicitly (not the ratio of T/M). In addition, the variation of M with altitude is determined with fair accuracy. This now makes it possible to determine those thermodynamic properties which depend upon the explicit

knowledge of T and M. These include molecular volume, mean free path, and collision frequency.

A simplified experiment is described in Section IV which requires only one mass spectrometer and can provide useful data for a limited altitude range of the Earth's atmosphere.

REFERENCES

1. S.K. Mitra, "The Upper Atmosphere," The Asiatic Society, Calcutta, 1952;
   L. Spitzer, Jr., "The Atmosphere of the Earth and Planets," ed. G.P. Kuiper, University of Chicago Press, 1952.

2. E. Meadows (Reed) and C. R. Smith, "Mass Spectrometric Investigations of the Atmosphere between 100 and 227 km," NASA Report X-613-62-82.

3. G.O. Sauermann and R.F.K. Herzog, "A Rocket-Borne Helium Mass Spectrometer," GCA Technical Report No. 61-8-N, 1961.

4. D.R. Bates and M. Nicolet, J. Atmos. Terr. Phys., 18, 65 (1960).

5. P. Mange, Ann. Geophys., 11, 153 (1955).

6. H.B. Maris, Terr. Mag. and Atmos. Elec., 34, 45 (1929).

7. P.S. Epstein, Beitr. Geophys., 35, 153 (1932).

8. W.G.L. Sutton, Proc. Roy. Soc., 182A, 48 (1943).

9. G.O. Sauermann and R.F.K. Herzog, "Helium in the Earth's Atmosphere," GCA Technical Report No. 61-6-N, 1961.

10. E.R. Manring, J.F. Bedinger, H.B. Knaflich, and R.D. Lynch, "Upper Atmospheric Wind Profiles," GCA Technical Report No. 61-1-N, 1961.

11. K. Champion and R.A. Minzner, "Proposed Revision of U.S. Standard Atmosphere 90-700 km," Interim Report of Task Group IV of Working Group of COESA, December 11, 1961.

12. J.E. Ainsworth, D.F. Fix, and H.E. LaGow, NASA TN-670, page 37, 1961.

13. E.B. Meadows and J.W. Townsend, Jr., "IGY Rocket Measurements of Arctic Atmospheric Composition Above 100 km," Space Research, ed. Kallmann Bijl, North-Holland Publishing Co., Amsterdam, 1960.

GCA Technical Report No. 62-11-N

PLANETARY AERONOMY VI:
ELECTRON TEMPERATURES IN THE IONOSPHERE

A. Dalgarno,

M. B. McElroy* and R. J. Moffett*

November 1962

Contract No. NASw-395

Prepared for

National Aeronautics and Space Administration
Headquarters
Washington 25, D. C.

GEOPHYSICS CORPORATION OF AMERICA
Bedford, Massachusetts

*Department of Applied Mathematics, The Queen's University of Belfast

Accepted for publication in April 1963 issue, Planetary and Space Science.

TABLE OF CONTENTS

ABSTRACT

Detailed calculations are described of the rate of heating of the ambient electrons arising from solar ultraviolet radiation and it is shown that the resulting difference between the electron temperature and the gas temperature at noon in a quiet ionosphere may reach a maximum value lying between 800°K and 1500°K at an altitude near 200 km but that the difference vanishes below about 120 km and above about 400 km. This is in accord with the analysis of the observational data by Bauer and Bourdeau which can therefore be explained as due to the direct action of solar ultraviolet radiation and it is unnecessary to postulate the existence of electric fields.

LEGEND FOR FIGURES

Figure 1. Noon total photoionization rates: Curve
(a) $T(\infty) = 1000^{\circ}K$
(b) $T(\infty) = 2000^{\circ}K$
(c) Watanabe and Hinteregger (1962).

Figure 2. Noon photoionization rates for $T(\infty) = 1000^{\circ}K$ for O^+, O_2^+ and N_2^+.

Figure 3. Noon photoionization rates for $T(\infty) = 2000^{\circ}K$ for O^+, O_2^+ and N_2^+.

Figure 4. Distribution of photoelectrons produced by process (1) for $T(\infty) = 1000^{\circ}K$.

Figure 5. Distribution of photoelectrons produced by process (1) for $T(\infty) = 2000^{\circ}K$.

Figure 6. Total rate of deposition of photoelectron kinetic energy (curve a) and of metastable energy (curve b) for $T(\infty) = 1000^{\circ}K$

Figure 7. Total rate of deposition of photoelectron kinetic energy (curve a) and of metastable energy (curve b) for $T(\infty) = 2000^{\circ}K$.

Figure 8. Rates of energy loss to neutral particles (solid lines) and to electrons (dashed line) for electrons of various energies above 20 eV moving in the model atmosphere with $T(\infty) = 1000^{\circ}K$.

Figure 9. Rates of energy loss to neutral particles (solid lines) and to electrons (dashed line) for electrons of various energies above 20 eV moving in the model atmosphere with $T(\infty) = 2000^{\circ}K$.

ELECTRON TEMPERATURES IN THE IONOSPHERE

A. Dalgarno,
M. B. McElroy* and R. J. Moffett*

SUMMARY

1. Introduction

Hanson and Johnson (1961) have suggested that energetic photoelectrons produced by the incident solar ultraviolet radiation may give rise to an electron temperature Te in the daytime ionosphere which is higher than the neutral particle and positive ion temperature Tg and experimental evidence supporting this view has been obtained recently by Spencer, Brace and Carignan (1962) who find that Te is much greater than Tg at altitudes between about 100 and 400 km, the maximum value of Te lying between 2400°K and 3000°K. However, because the solar photon flux adopted by Hanson and Johnson is much less than that now observed (cf. Watanabe and Hinteregger 1962), because an important process--the electron impact excitation of vibrational levels of molecular nitrogen--was omitted from consideration, and because the significance of metastable energies as a source of heating was not investigated, the conclusions of Hanson and Johnson have only qualitative significance and a re-analysis is desirable.

---

*Department of Applied Mathematics, The Queen's University of Belfast, Belfast, N. Ireland.

2. Production of Photoelectrons

2.1 Model Atmospheres

As model atmospheres we have selected two from those derived by Bates (1959) and Bates and Patterson (1961), one of which corresponds to a temperature of $1000^{o}K$ at the base of the exosphere and the other to a temperature of $2000^{o}K$. The two models probably span the possible atmospheres. The associated number densities and temperatures are reproduced in Table 1.

2.2 Solar Flux and Photoionization Rates

For the incident flux of solar photons we have adopted the values quoted by Watanabe and Hinteregger (1962) and they are reproduced in Table 2. Using a model atmosphere which is roughly a mean of the two given in Table 1, Watanabe and Hinteregger have computed the rate of production of ionization corresponding to this solar flux. We have repeated their calculations for the model atmospheres in Table 1 and a comparison of the noon ionization rates is given in Figure 1. The relative production of O^{+}, O_2^{+} and N_2^{+} ions are of interest and these are shown in Figures 2 and 3. The accuracy of the absorption and photoionization cross sections used is very uncertain and Figures 1 and 2 should be regarded as merely representative of the actual ionization rates.

Table 1

Atmospheric Temperatures and Number Densities

Altitude (Km)	$T(\infty) = 1{,}000^{\circ}K$					$T(\infty) = 2{,}000^{\circ}K$			
	$Tg(^{\circ}K)$	$n(O)$	$n(O_2)$	$n(N_2)$	n_e	$Tg(^{\circ}K)$	$n(O)$	$n(O_2)$	$n(N_2)$
500	1,000	1.03(7)	2.14(4)	6.36(5)	1.05(6)	2,000	7.14(7)	2.02(6)	3.12(7)
450	1,000	2.36(7)	1.11(5)	2.69(6)	1.24(6)	1,970	1.09(8)	4.69(6)	6.53(7)
400	1,000	5.44(7)	5.92(5)	1.16(7)	1.44(6)	1,940	1.70(8)	1.12(7)	1.40(8)
350	1,000	1.27(8)	3.24(6)	5.14(7)	1.63(6)	1,895	2.70(8)	2.77(7)	3.10(8)
300	998	3.02(8)	1.82(7)	2.33(8)	1.66(6)	1,810	4.49(8)	7.31(7)	7.30(8)
250	990	7.32(8)	1.06(8)	1.09(9)	1.17(6)	1,660	8.07(8)	2.17(8)	1.91(9)
200	952	1.89(9)	6.83(8)	5.59(9)	7.20(5)	1,390	1.72(9)	8.25(8)	6.29(9)
150	763	6.59(9)	6.63(9)	4.20(10)	4.60(5)	880	5.99(9)	6.33(9)	3.96(10)
120	380	3.40(10)	8.80(10)	4.40(11)	3.20(5)	380	3.40(10)	8.80(10)	4.40(11)

+ $1.03(7) = 1.03 \times 10^{7}\ cm^{-3}$

Table 2

Solar Spectral Intensities at Normal Incidence

λ(in Å)	Flux (in $10^8 cm^{-2} sec^{-1}$)	λ(in Å)	Flux (in $10^8 cm^{-2} sec^{-1}$)
1025.7	26	500 - 600	30
1000 - 1027	15	400 - 500	24
989.8	5	303.8	43
977.0	30	300 - 400	29
972.5	10	230 - 300	31
949.7	5	170 - 230	33
911 - 1000	37	110 - 170	3.5
850 - 911	95	80 - 110	2.4
796 - 850	25	60 - 80	1.8
700 - 796	50	30 - 60	1.5
600 - 700	47	20 - 30	0.12
584.3	29	10 - 20	0.02

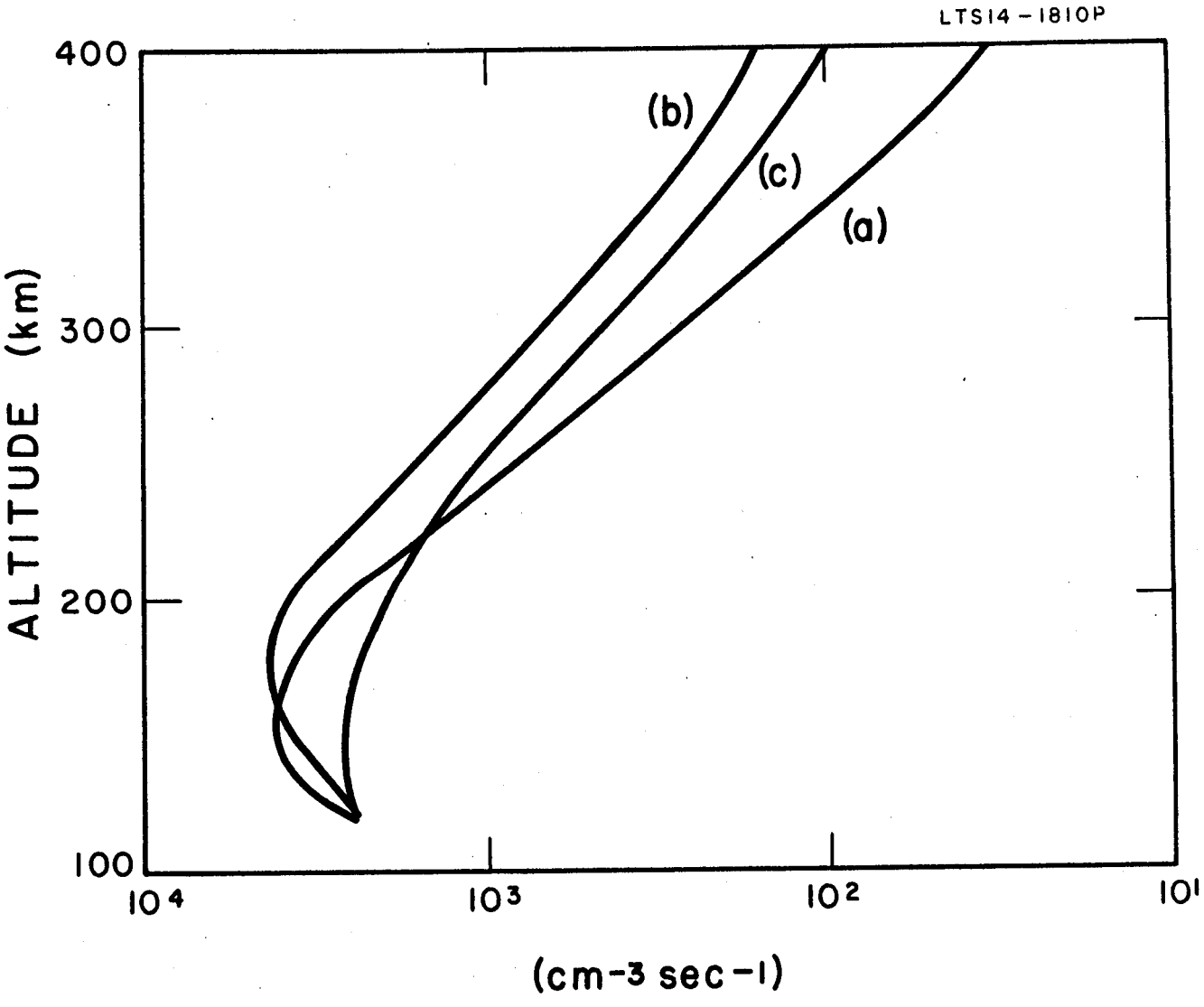

Figure 1. Noon total photoionization rates:
Curve (a) T (∞) = 1000°K
(b) T (∞) = 2000°K
(c) Watanabe and Hinteregger (1962)

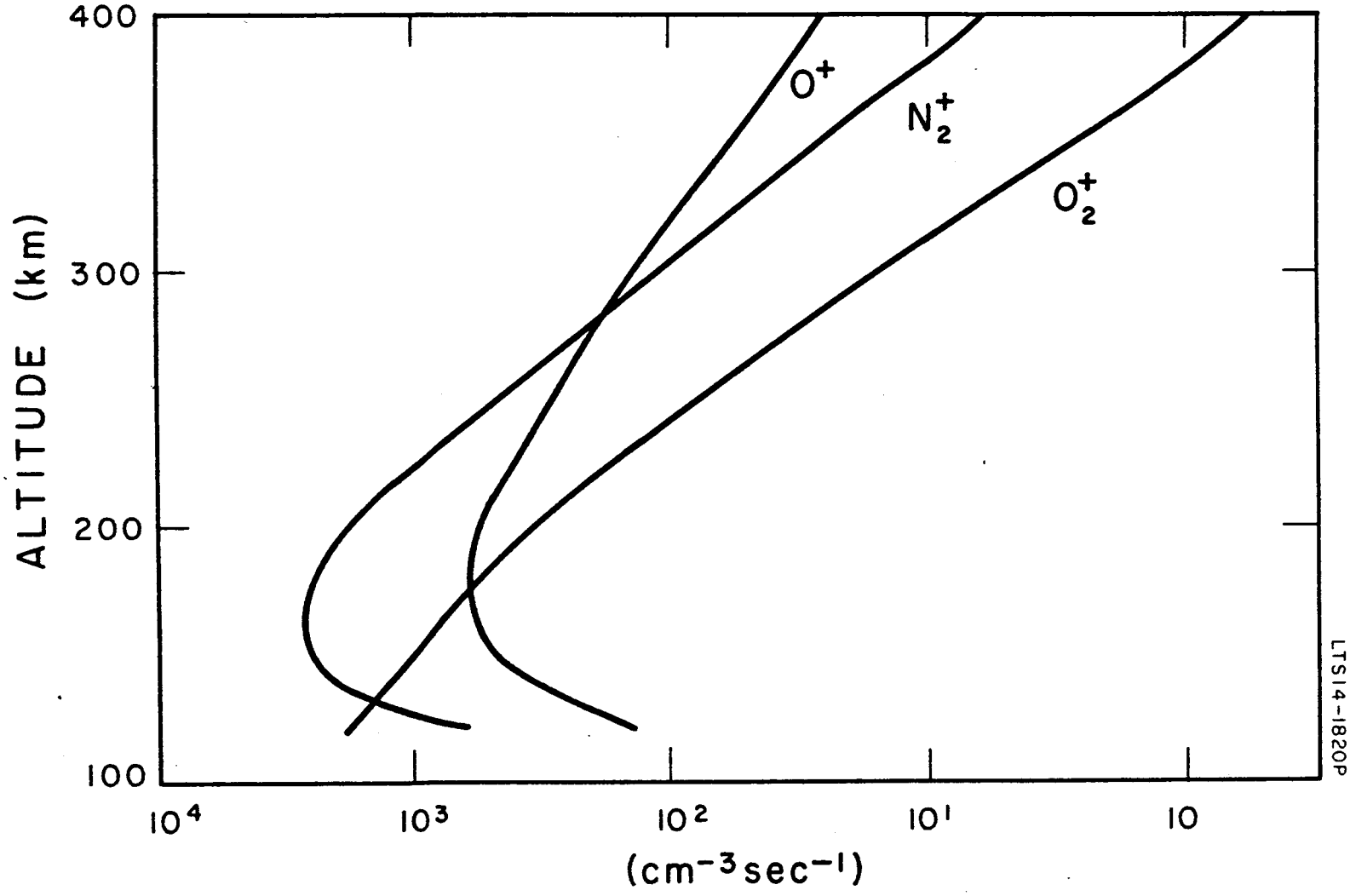

Figure 2. Noon photoionization rates for T (∞) = 1000°K for O^+, O_2^+ and N_2^+.

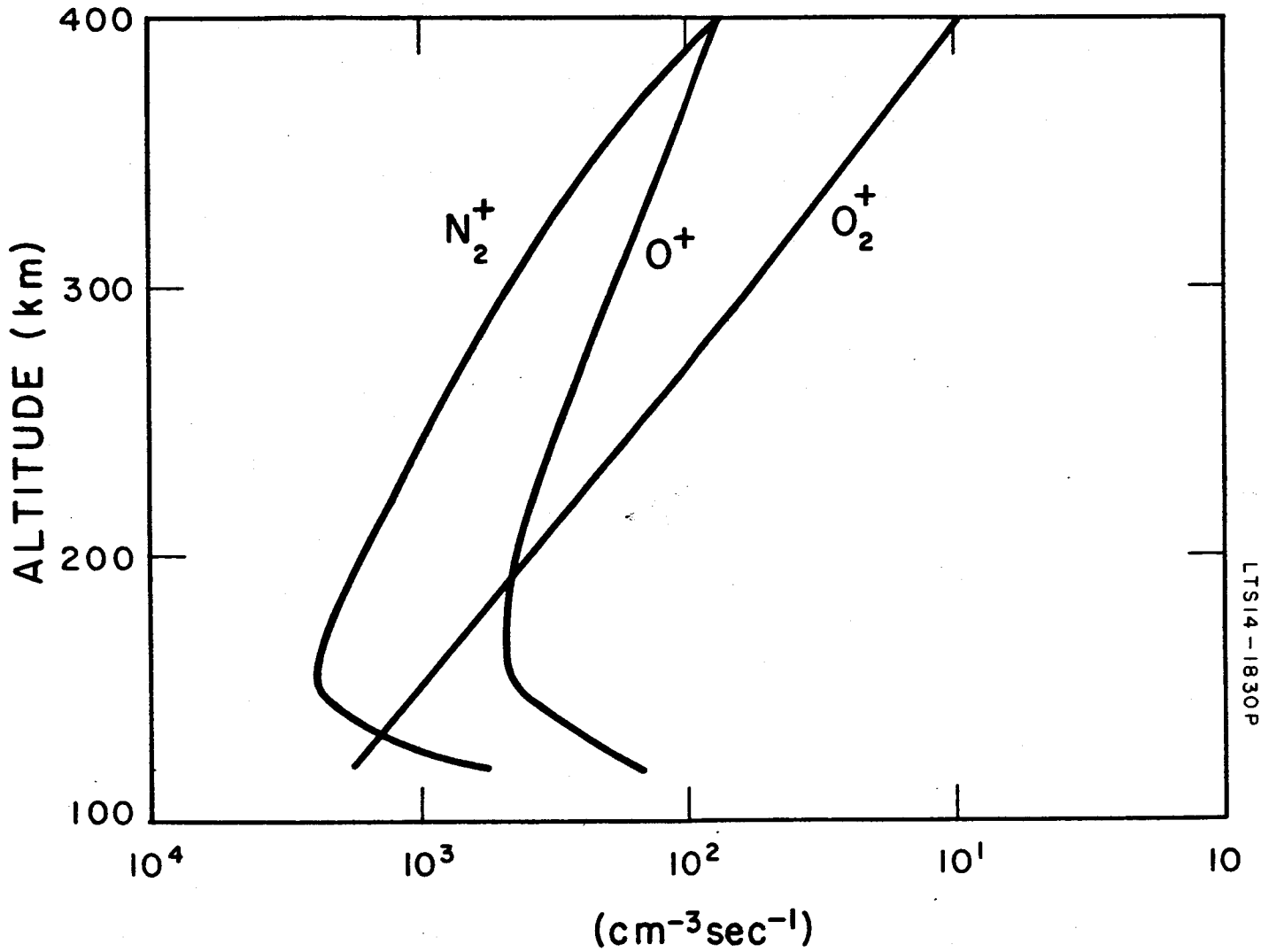

Figure 3. Noon photoionization rates for T (∞) = 2000°K for O^+, O_2^+ and N_2^+.

2.3 Equilibrium Electron Densities

Since the rates of the processes responsible for the disappearance of free electrons are still very uncertain, we have not attempted to calculate the equilibrium distributions of the electron density as functions of altitude for the assumed models but we have instead adopted the values given by Ratcliffe (1960) and listed in Table 1.

2.4 Energy Distribution of Photoelectrons

The prediction of the energy distribution of the photoelectrons is complicated by the fact that the available cross section data refer to a multiplicity of ionizing processes whereas the energy distribution depends upon the individual processes. Thus, the spectral heads for the ejection of an outer shell electron from atomic oxygen for the transitions

$$O(1s^2 2s^2 2p^4)\,^3P + h\nu \rightarrow O^+(1s^2 2s^2 2p^3)\,^4S + e \qquad (1)$$

$$O(1s^2 2s^2 2p^4)\,^3P + h\nu \rightarrow O^+(1s^2 2s^2 2p^3)\,^2D + e \qquad (2)$$

$$O(1s^2 2s^2 2p^4)\,^3P + h\nu \rightarrow O^+(1s^2 2s^2 2p^3)\,^2P + e \qquad (3)$$

are located at 910Å, 732Å and 663Å, respectively, so that a photon of wavelength, say 500Å, absorbed by atomic oxygen will produce an electron of energy 11.2eV, 7.9eV or 6.1eV depending upon which transition is involved. The internal energies of the metastable ions may still be

available as heating. Thus, the radiative lifetime of the $^2D_{3/2}$ state is 5×10^3 sec and of the $^2D_{5/2}$ state is 2×10^4 sec; and the rate coefficient for the superelastic collision

$$e + O^+(^2D) \rightarrow e + O^+(^4S) \tag{4}$$

is about 3×10^{-8} cm^3 sec^{-1} (Seaton and Osterbrock 1957). The metastable energy of the ^2D state may therefore be transferred directly to the ambient electron gas. Alternatively, the metastable ion may undergo ion-atom interchange with the atmospheric molecules, its energy thereby appearing as thermal energy of the heavy particle gas. The radiative lifetime of the $^2P_{1/2}$ state is 5 sec and of the $^2P_{3/2}$ state is 4 sec and the rate coefficients for the superelastic collisions

$$e + O^+(^2P) \rightarrow e + O^+(^2D) \tag{5}$$

$$e + O^+(^2P) \rightarrow e + O^+(^4S) \tag{6}$$

are, respectively, about 1×10^{-7} $cm^3 sec^{-1}$ and 2×10^{-8} $cm^3 sec^{-1}$ (Seaton and Osterbrock 1957). Except at low altitudes where ion-atom interchange may occur more rapidly, the ^2P state is usually deactivated by spontaneous emission, the more probable process being

$$O^+(^2P) \rightarrow O^+(^2D) + h\nu \tag{7}$$

yielding a photon of wavelength 7330 Å and leaving a metastable ^2D state, the energy of which may be transferred to the ambient electrons or to the heavy particles.

At 435 Å, the photoionizing transition

$$O(1s^2 2s^2 2p^4)\,^3P + h\nu \rightarrow O^+(1s^2 2s 2p^4)\,^4P + e \qquad (8)$$

and at 310 Å, the photoionizing transition

$$O(1s^2 2s^2 2p^4)\,^3P + h\nu \rightarrow O^+(1s^2 2s 2p^4)\,^2P + e, \qquad (9)$$

which involve the ejection of an inner shell electron, can occur (Dalgarno and Parkinson 1960). The excited state produced by (8) will subsequently decay according to

$$O^+(1s^2 2s^2 p^4)\,^4P \rightarrow O^+(1s^2 2s^2 2p^3)\,^4S + h\nu \qquad (10)$$

with the emission of a photon of wavelength 833 Å which can be absorbed by atomic oxygen yielding an electron with an energy of 1.2 eV or by molecular oxygen yielding an electron of energy 2.7 eV. The excited state produced by (9) will decay according to

$$O^+(1s^2 2s 2p^4)\,^2P \rightarrow O^+(1s^2 2s^2 2p^3)\,^2D + h\nu \qquad (11)$$

or according to

$$O^+(1s^2 2s 2p^4)\,^2P \rightarrow O^+(1s^2 2s^2 2p^3)\,^2P + h\nu \quad . \qquad (12)$$

The photons emitted in (11) and (12) have wavelengths of 581 Å and 537 Å, respectively, and can produce further ionization. As before, the metastable states in (11) and (12) may be deactivated by superelastic collisions.

Radiation of wavelengths between 310 Å and the K-shell absorption edge at about 23 Å can produce electrons with energies ranging from zero to 540 eV. These high energy electrons will in turn produce further electrons by impact ionization. For initial energies greater than perhaps 70 eV the mean number of ion pairs produced can be obtained by dividing the initial energy by 34 eV but below 70 eV the mean energy required to produce an ion pair must rise rapidly as an increasing fraction of the energy is expended in excitation processes (cf. Dalgarno and Griffing 1958). In computing the ionization rates of Figure 1, we have arbitrarily assumed that for electron energies between 20 and 70 eV, one ion pair is produced.

We shall not discuss the absorption of radiation shorter than 23 Å in detail. For our purposes it suffices to note that the solar flux of photons with wavelengths shorter than 30 Å is of the order of 0.1 erg cm^{-2} sec^{-1} and that it is largely deposited in the E-region of the ionosphere.

The photoionization pattern for the atmospheric molecules is basically similar to but, because of the vibrational structure, more complex than that of atomic oxygen.

The transformation of this essentially qualitative discussion into a quantitative prediction of the energy distribution of the photoelectrons must be somewhat arbitrary. For the photoionization cross sections, we have used the values listed by Watanabe and Hinteregger (1962); and we have assumed that whenever the photon energy is such that a multiplicity of transitions can occur, the probability of a particular transition is proportional to the statistical weight of the product positive ion state. The transitions which have been taken into account are given in Table 3.

The resulting distributions with altitude of the rates of production of photoelectrons of various energies arising from the transition (1) are illustrated in Figures 4 and 5 for the two model atmospheres. Similar curves may be constructed for the other photoionizing processes. The total rates of deposition of photoelectron kinetic energy are given in Figures 6 and 7 which also show the distributions with altitude of the rates of deposition of energy retained initially in the metastable states $O^+(^2D)$ and $O_2^+(^4\pi_u)$. Part of the energy will subsequently be converted into radiation and the remainder into heat, the division depending upon the collision processes by which the fast electrons are slowed down.

Table 3

Transitions Taken Into Account in Deriving the Energy Distribution of Photoelectrons

Atomic Oxygen Transitions

Electron removed	Resulting state of O^+	Threshold energy in eV
2p	^4S	13.6
2p	^2D	16.9
2p	^2P	18.7
2s	^4P	28.5
2s	^2P	40.0

Molecular Oxygen Transitions

Electron removed	Resulting state of O_2^+	Threshold energy in eV
$\pi_g 2p$	$^2\pi_g$	12.1
$\pi_u 2p$	$^4\pi_u$	16.2
$\pi_u 2p$	$^2\pi_u$	17.0
$\sigma_g 2p$	$^4\Sigma_g^-$	18.2
$\sigma_u 2s$	$^2\pi_u$	~ 28
$\sigma_g 2s$	$^2\pi_g$	~ 40

Molecular nitrogen transitions

Electron removed	Resulting state of N_2^+	Threshold energy in eV
$\sigma_g 2p$	$^2\Sigma_g^+$	15.6
$\pi_u 2p$	$^2\pi_u$	16.7
$\sigma_u 2s$	$^2\Sigma_u^+$	18.8
$\sigma_g 2s$	$^2\Sigma_g^+$	~ 35

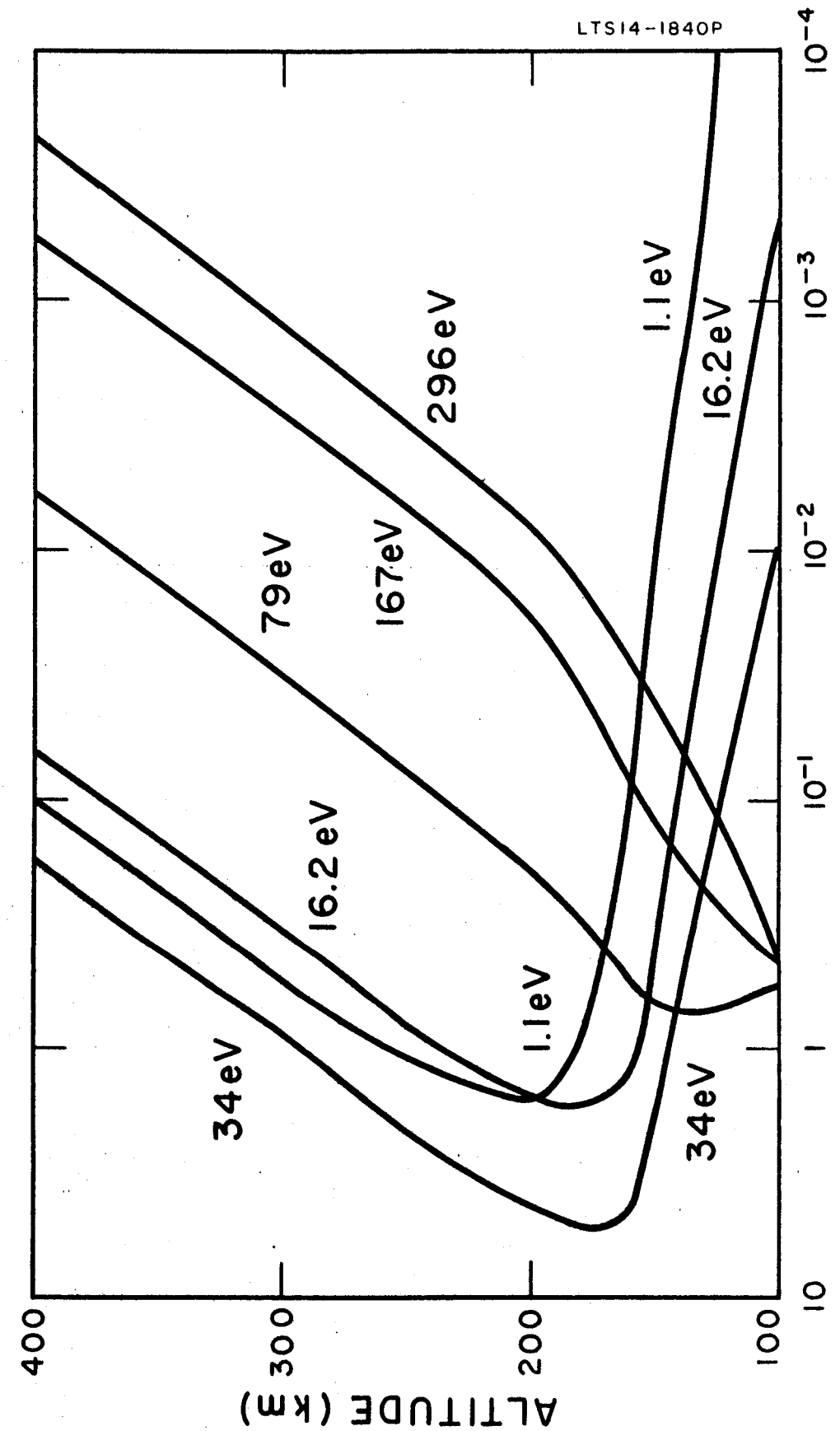

Figure 4. Distribution of photoelectrons produced by process (1) for T (∞) = 1000^{0}K.

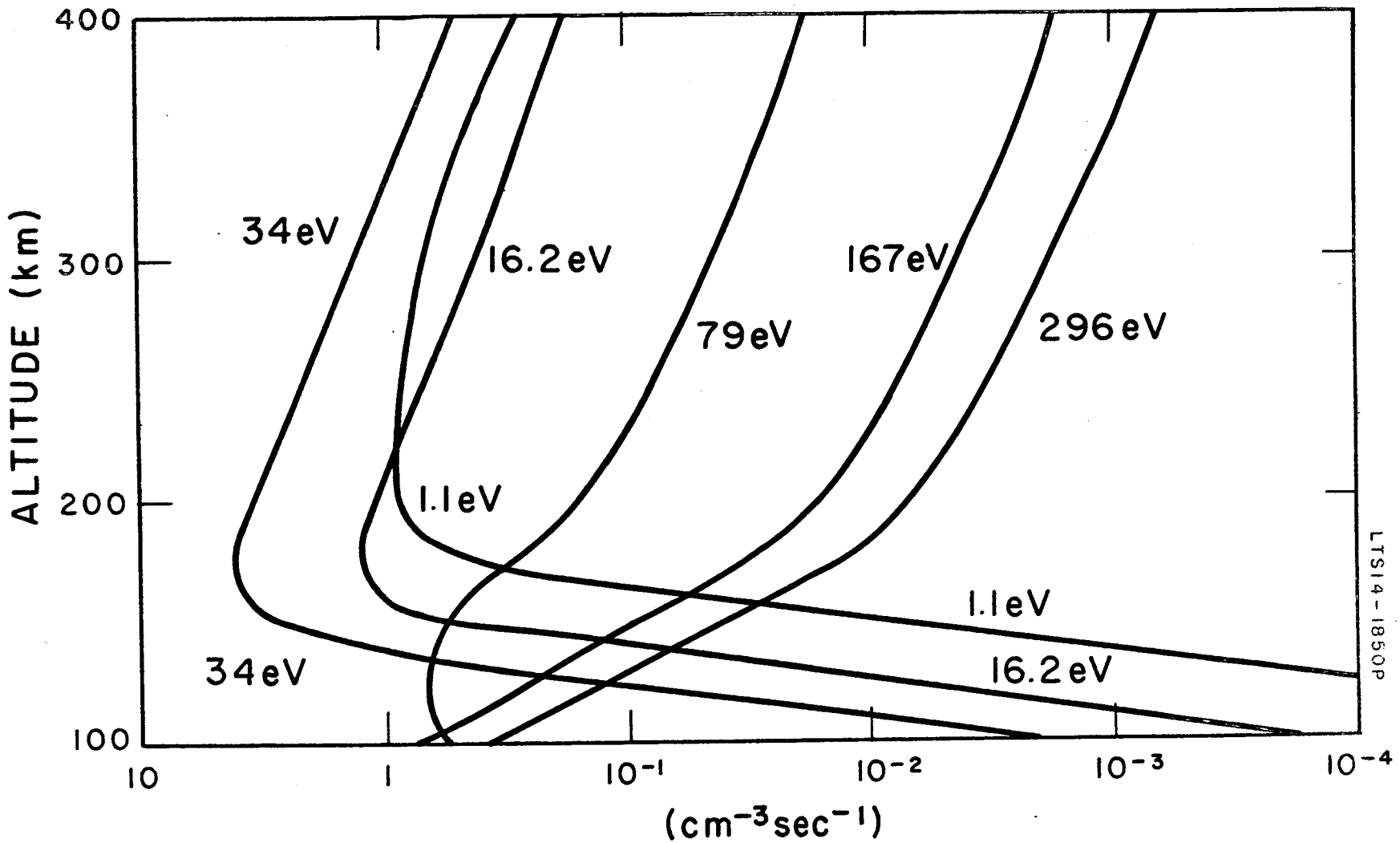

Figure 5. Distribution of photoelectrons produced by process (1) for T (∞) = 2000°K.

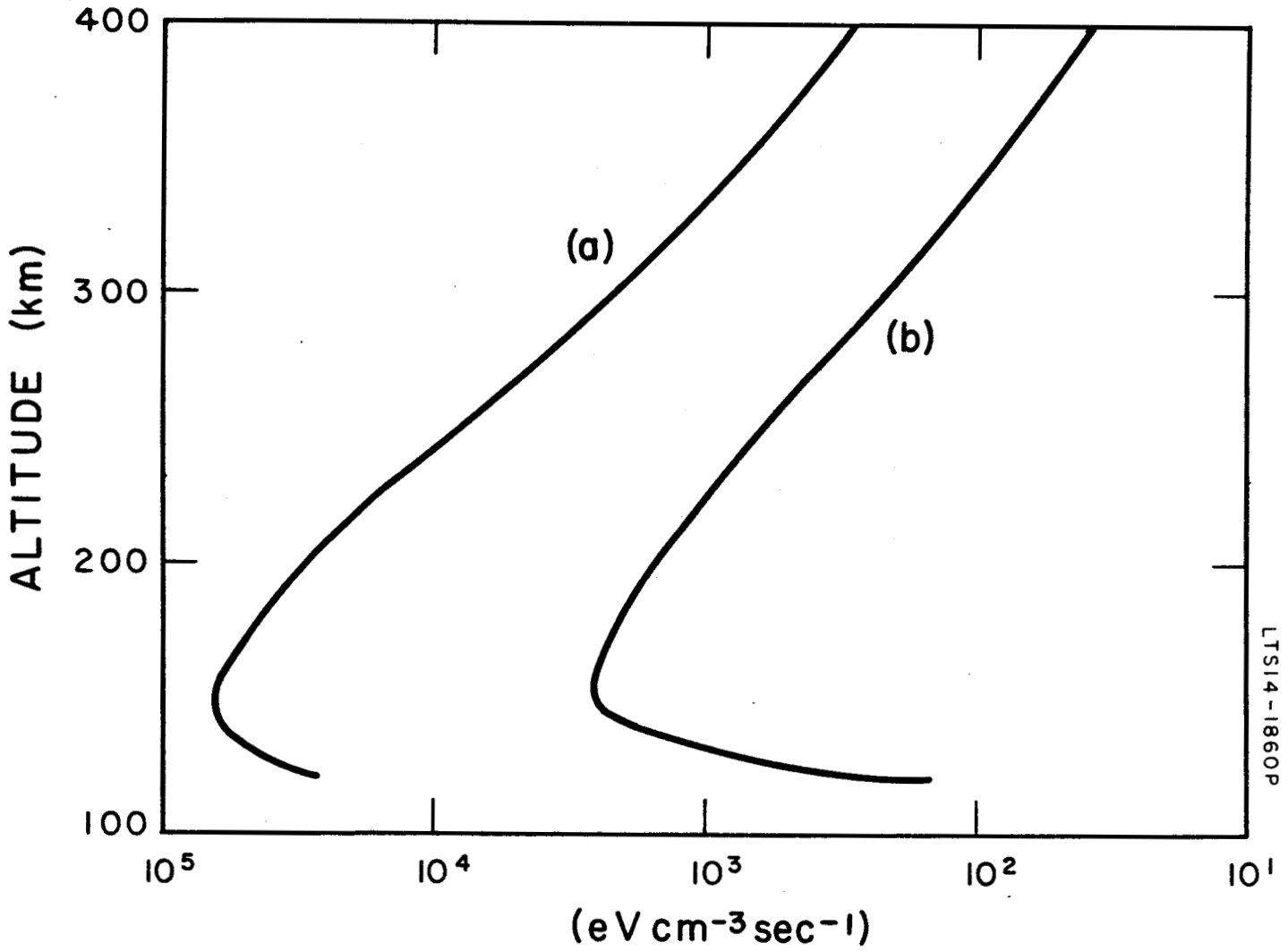

Figure 6. Total rate of deposition of photoelectron kinetic energy (curve a) and of metastable energy (curve b) for T (∞) = 1000°K.

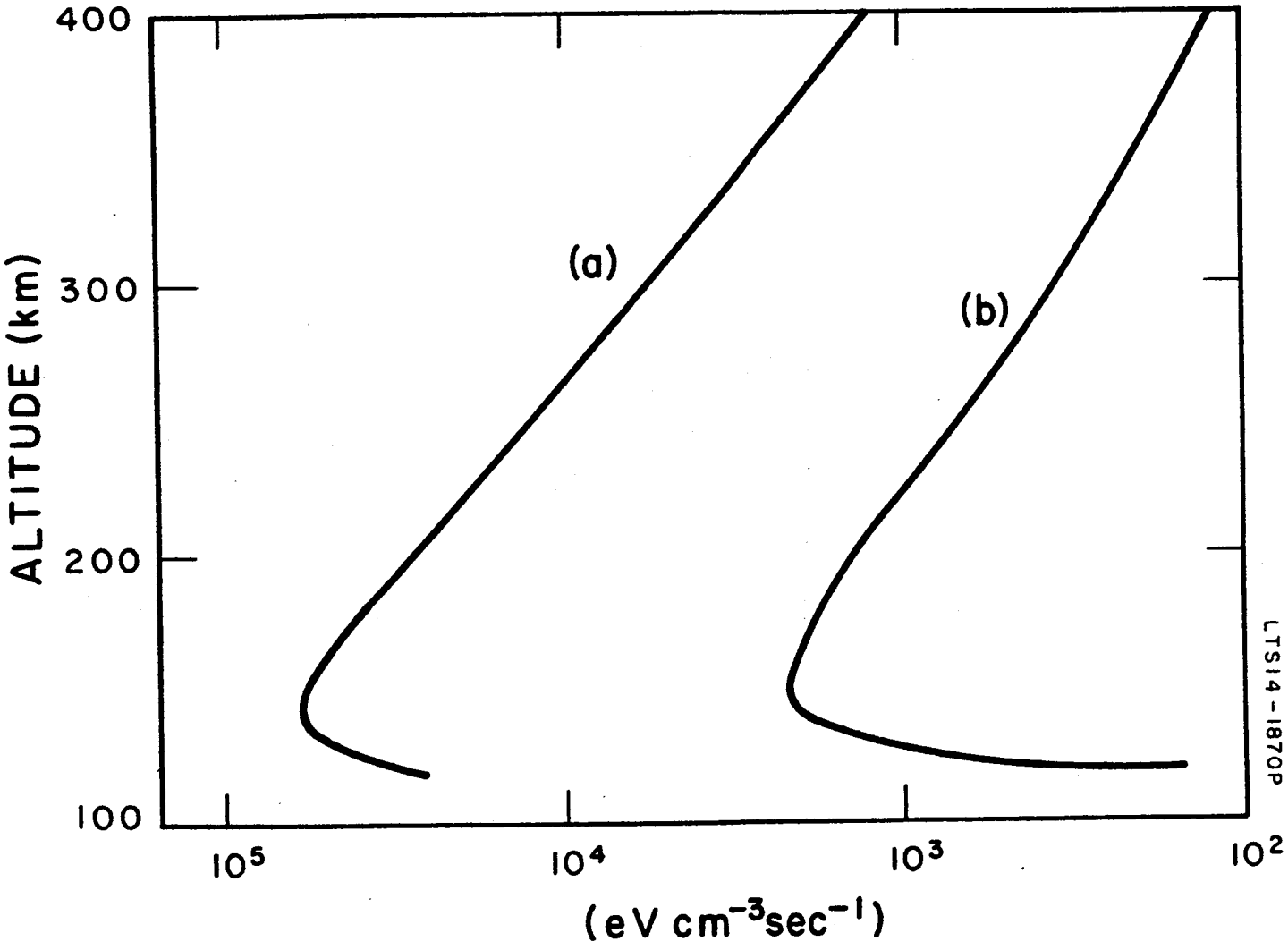

Figure 7. Total rate of deposition of photoelectron kinetic energy (curve a) and of metastable energy (curve b) for T (∞) = 2000°K.

3. Energy Loss Processes

We shall not present here a detailed discussion of the energy loss processes through which a fast electron is slowed.

3.1 Critical Altitudes and Energies

The results of the comparisons of the efficiencies of energy loss to the neutral particles and to the electrons are summarized in Table 4 which gives for various electron energies the critical altitudes for the two model atmospheres above which loss to the electrons is the more probable and below which loss to the neutral particles is the more probable; it is being assumed that vibrational energy of N_2 is converted to thermal energy of the neutral particle gas. If we assume that vibrational energy of N_2 is converted to thermal energy of the electron gas, the critical altitudes are unchanged for $E \geq 5$ eV but do not exist for lower energies, all of the electron kinetic energy below 5 eV being transferred to the ambient electrons.

We may summarize the results also by introducing critical energies E_c which are such that for $E > E_c$, E_c is transferred to the electron gas and for $E < E_c$, E is transferred to the electron gas. The critical energies are shown in Figures 8 and 9 for the two model atmospheres corresponding to the alternative assumptions that vibrational energy of N_2 is converted to thermal energy of the neutral particle gas and that it is converted to thermal energy of the electron gas.

Table 4

Critical Altitudes

$T(\infty) = 1{,}000^{\circ}K$		$T(\infty) = 2{,}000^{\circ}K$	
Energy (eV)	h_c (km)	Energy (eV)	h_c (km)
40	500	18	500
20	370	14	408
10	286	10	332
8	260	8	276
7	236	7	252
6	178	6	176
5	170	5	170
4	220	4	230
3	224	3	240
2	204	2	210
1.5	152	1.5	150

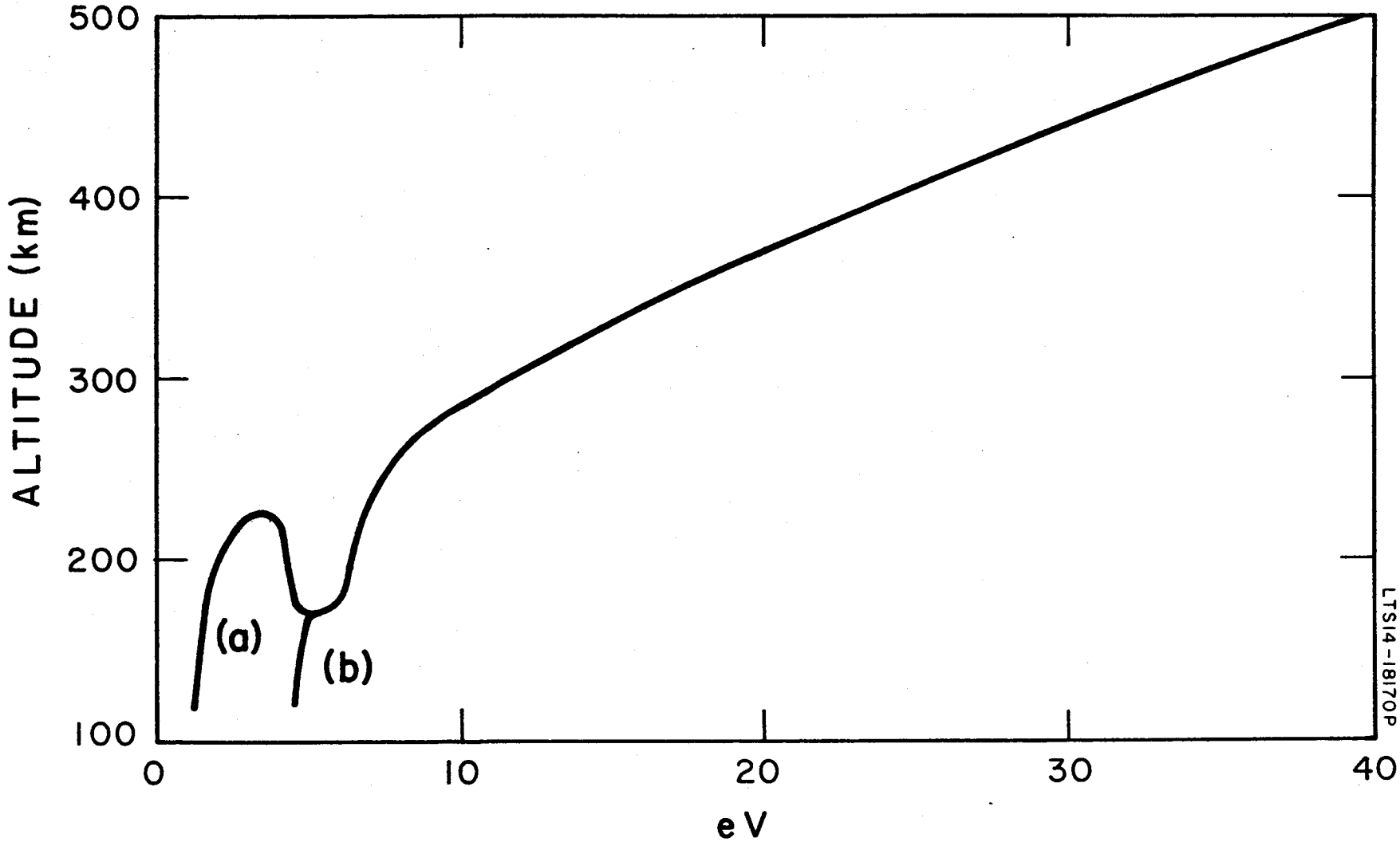

Figure 8 . Critical energies for the model atmosphere with T (∞) = 1000°K, assuming that the vibrational energy of N_2 is converted to thermal energy of (a) the neutral particles and (b) the electron gas.

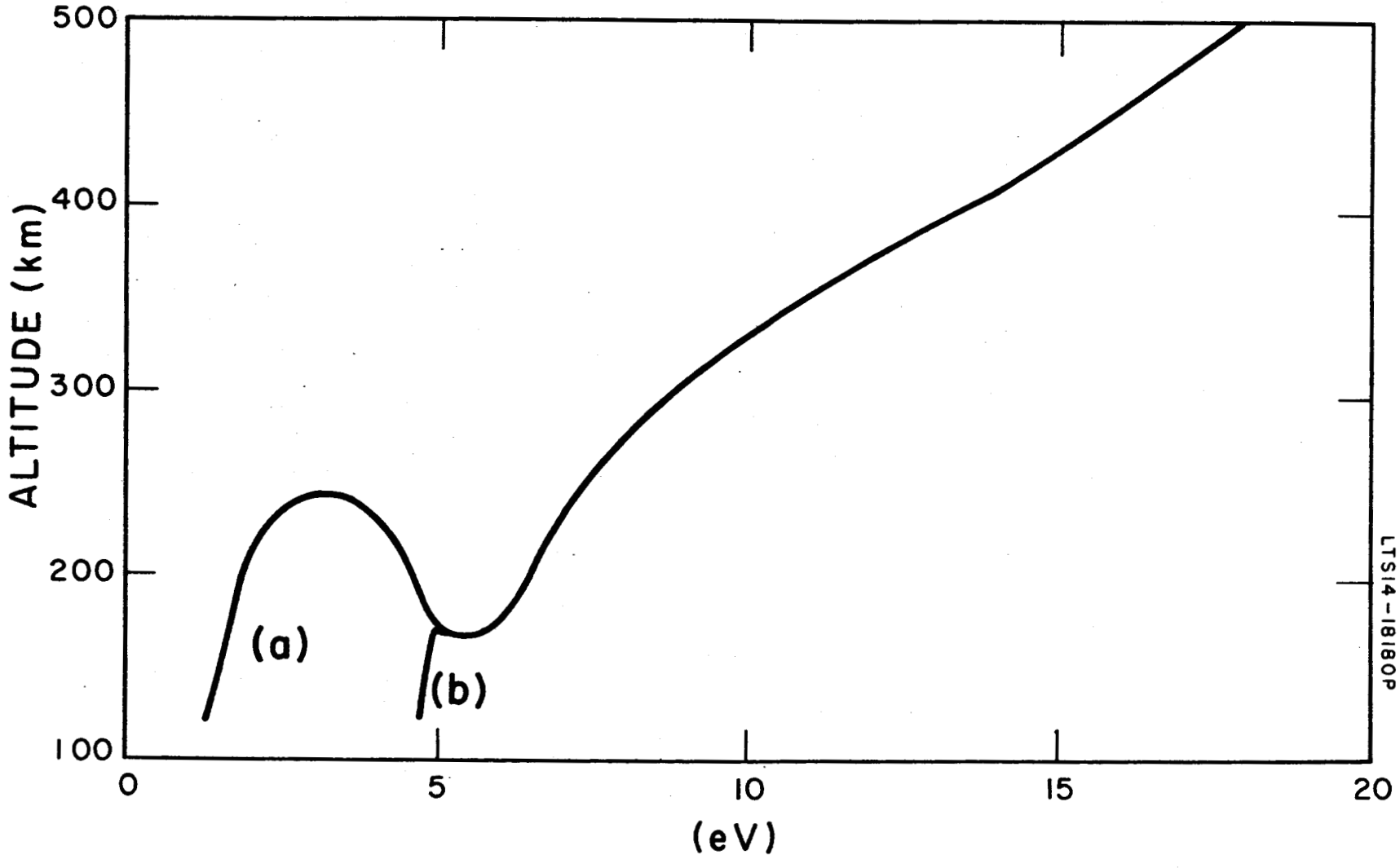

Figure 9 . Critical energies for the model atmosphere with T (∞) = 2000°K, assuming that vibrational energy of N_2 is converted to thermal energy of (a) the neutral particles and (b) the electron gas.

4. Heat Fluxes and Electron Temperatures

Combining the predicted initial energy distribution of the photoelectrons with the critical altitudes and energies yields the distribution of energy which is transferred to the ambient electrons. The results are shown in Figures 10 and 11, there being four distributions for each atmosphere depending upon the ultimate fate of the energies initially stored as metastable energy and as vibrational energy.

Equating the heat fluxes to the rate of cooling of the electron gas to the heavy particles leads to the electron temperatures of Figure 12.

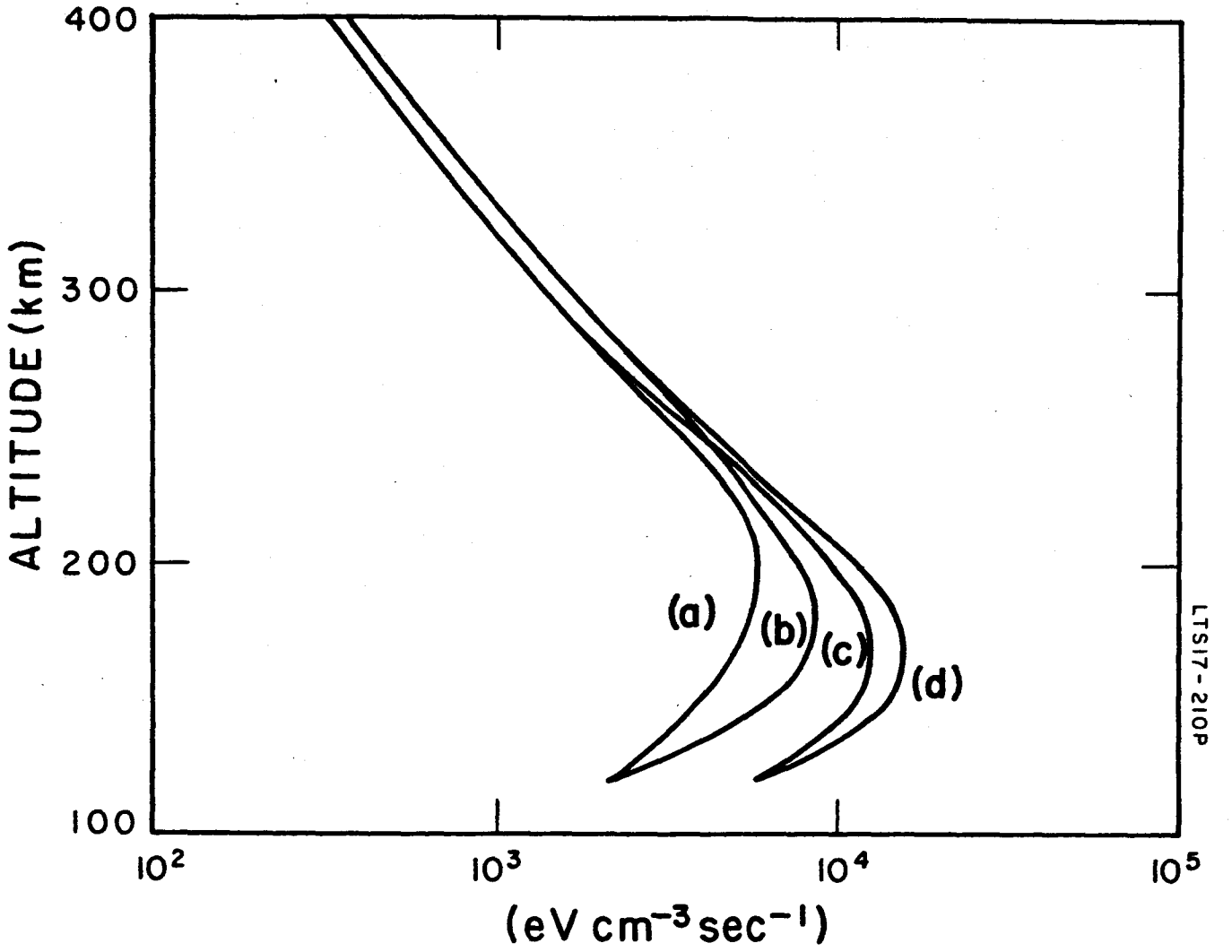

Figure 10. Heat fluxes to the ambient electrons for the atmosphere with T (∞) = 1000°K:
curve (a) excluding metastable energy and excluding vibrational energy;
curve (b) including metastable energy but excluding vibrational energy;
curve (c) excluding metastable energy but including vibrational energy;
curve (d) including metastable energy and including vibrational energy.

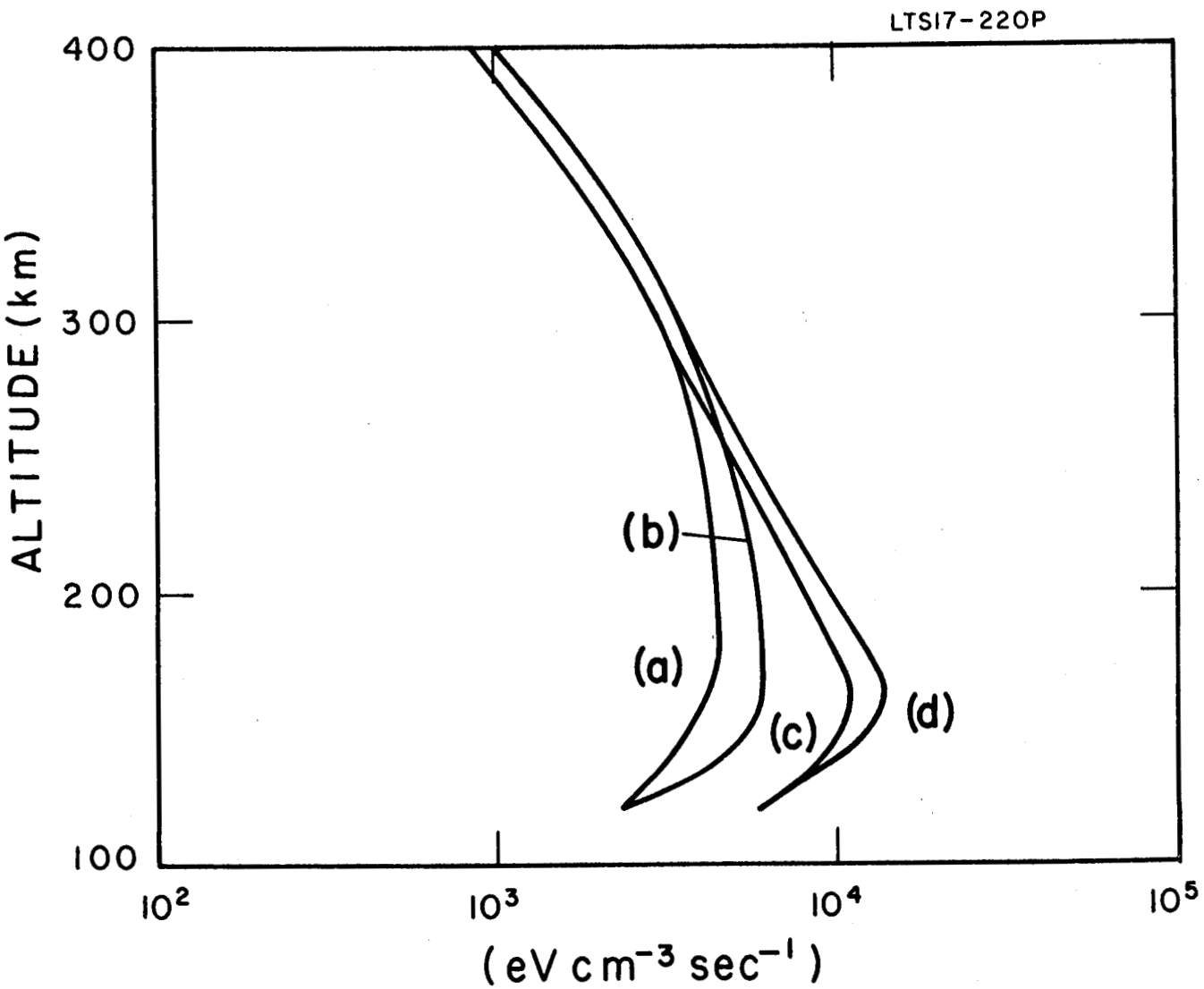

Figure 11. Heat fluxes to the ambient electrons for the atmosphere with T (∞) = 2000°K. The labelling of the four curves is as for Figure 10.

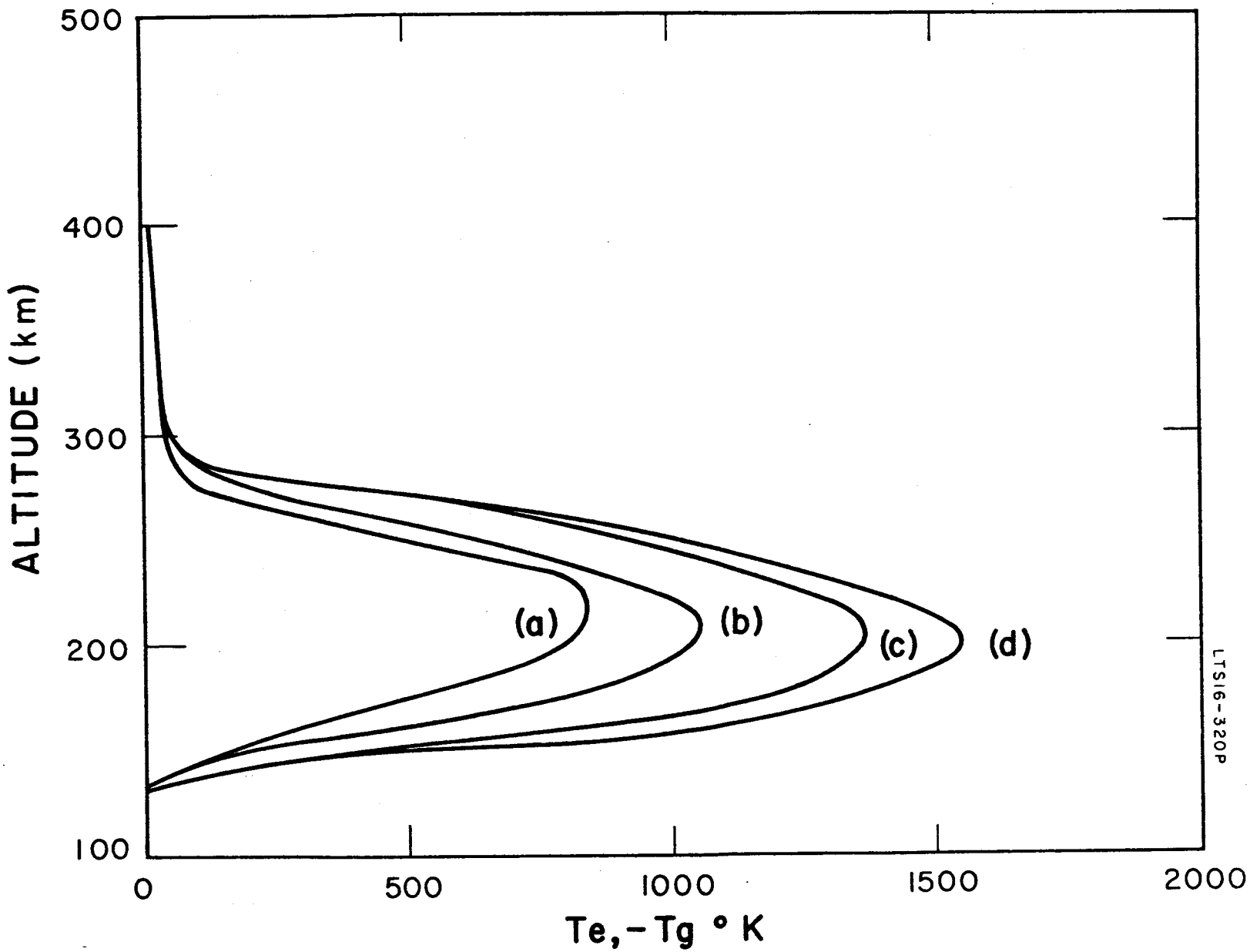

Figure 12. Difference between electron and gas temperatures with altitude for the atmosphere with T (∞) = 1000°K, and the heat inputs for Cases (a) through (d) as shown in Figure 10.

5. Discussion

The observational evidence concerning electron temperatures in the ionosphere has been reviewed recently by Bauer and Bourdeau (1962). They conclude that except at sunrise the electron and neutral particle temperatures in a quiet ionosphere are equal up to altitudes of 200 km and at altitudes above the F2 peak. In the lower F region, the difference between the electron temperature and the heavy particle temperature attains a maximum value of about $1000^{\circ}K$ at an altitude near 250 km.

In view of the several uncertainties in the theoretical analysis, the agreement between the theoretical predictions and the observations is very satisfactory. Indeed, the observed magnitude of the maximum temperature difference is closely equal to that predicted for the case when vibrational energy of molecular nitrogen is not transferred to the electron gas. The predicted location of the maximum is about 30 km lower than that observed but this small discrepancy can plausibly be attributed to an underestimate of the cooling rate, especially in view of recent work by Phelps (1962, private communication) indicating that the cross section for low energy excitation of the first vibrational level of molecular nitrogen is quite large. Thus, the observational data on electron temperatures in a quiet ionosphere can be explained as due to the direct action of solar ultraviolet radiation and it is unnecessary to postulate the existence of electric fields.

At sunrise and during disturbed conditions the observational results indicate greater departures from temperature equilibrium (cf. Bauer and Bourdeau 1962) and work is in progress to analyze these phenomena.

REFERENCES

Bates, D.R., 1959, Proc. Roy. Soc., A253, 451.

Bates, D.R. and Patterson, T.N.L., 1961, Planetary Space Sci., 5, 328.

Bauer, S.J. and Bourdeau, R.E., 1962, J. Atmos. Sci., 19, 218.

Dalgarno, A. and Griffing, W.G., 1958, Proc. Roy. Soc., A248, 415.

Dalgarno, A. and Parkinson, D., 1960, J. Atmos. Terr. Phys., 18, 335.

Hanson, W.B. and Johnson, F.S., 1961, Mémoires Soc. R. Liège Serie 5, 4, 390.

Phelps, A.V., 1962, Private Communication.

Ratcliffe, J.A., 1960, Physics of the Upper Atmosphere (Academic Press).

Seaton, M.J. and Osterbrock, D.E., 1957, Astrophys. J., 125, 66.

Spencer, N.W., Brace, L.H. and Carignan, G.R., 1962, J. Geophys. Res., 67, 157.

Watanabe, K. and Hinteregger, H.E., 1962, J. Geophys. Res., 67, 999.

GCA Technical Report No. 62-14-N

PLANETARY AERONOMY VII:
THE SOLAR FLUX INCIDENT AT THE TOP OF THE ATMOSPHERES OF EARTH AND NEIGHBORING PLANETS FOR THE SPECTRAL REGION 50 A TO 3000 A

E. D. Schultz and A. C. Holland

November 1962

Contract No. NASw-395

Prepared for

National Aeronautics and Space Administration
Headquarters
Washington 25, D. C.

GEOPHYSICS CORPORATION OF AMERICA
Bedford, Massachusetts

LIST OF FIGURES

LIST OF TABLES

THE SOLAR FLUX INCIDENT AT THE TOP OF THE ATMOSPHERES OF EARTH AND NEIGHBORING PLANETS FOR THE SPECTRAL REGION 50 A TO 3000 A*

E. D. Schultz and A. C. Holland

SUMMARY**

Most planetary atmospheric gases strongly absorb radiation below 3000 A. These absorptions often result in photoionization and/or photodissociation; so although the total flux below 3000 A is small, its effect on the aeronomic properties of the upper atmosphere such as chemical composition, atmospheric thermodynamics, atmospheric dynamics, terrestrial gas reflectivities, etc. is large. Accordingly, the distribution and absolute intensity of the solar flux for wavelengths below 3000 A is an important aeronomic parameter for systematic studies of planetary aeronomy such as are being performed at GCA under the present contract.

As a first step, the solar flux incident at the top of the Earth's atmosphere has been compiled for the spectral region 50 A to 3000 A.[1]* The compilation was based essentially on the work of K. Watanabe,[2] H. E. Hinteregger,[3] C. R. Detwiler et al.,[4] and F. S. Johnson.[5]

Between 50 A and 1850 A, the major emission lines were distinguished from the continuum and are presented separately. The continuum and weak lines are lumped together. The emission lines published by Watanabe[2]

---

*This work was partially supported under Contract No. AF33(657)-9199.

**The figures and tables referred to in this Summary text may be found in GCA TR 62-14-N and are not reproduced here.

and by Detwiler et al.[4] were modified to reflect the most recent measurements by Hinteregger.[3] Beyond 1850 A, emission lines could not be resolved from the continuum. Below 283 A, the absence of emission lines merely reflects the lack of experimental data.

In the near ultraviolet, the data published by Johnson[5] and by Detwiler and co-workers[4] agree down to 2400 A; but at shorter wavelengths, they differ by a factor that reaches 2.0 at 2200 A. The two sets were joined at 2600 A using the method outlined in Table 1. In the far ultraviolet, the discrepancy between Detwiler and Watanabe was not consistent, and the two sets of data were arbitrarily joined at 1600 A. The top of Earth atmosphere solar photon flux from 50 A to 3000 A are reproduced from the original work[1] in Figures 1 through 5 to serve as a basis for calculating similar data for other planets. Tabulated values of how the tables and graphs were generated are given in Tables 1 and 2.

In all of the figures, the pure experimental data are plotted in two clear and unambiguous presentations of the tabulation to provide a convenient comparison of the contribution of major emission lines with the contribution of the continuum and weak lines. As indicated in the tabulation, some of the individual emission lines contain contributions from the same and/or other elements or unresolved multiplets.

To obtain the flux values at the top of the atmospheres of neighboring planets, intensity dilution factors are easily determined using an

inverse square relation based on mean radius vector magnitudes. These data appear in Table 3. For convenient reference the flux data for Mercury, Venus, Mars and Jupiter have been computed and are included with values for Earth in Tables 4 and 5. The previously discussed tabulated data for Earth were used as a base to generate the entire model of the solar photon flux from 50 A to 3000 A for the top of the atmospheres of Venus and Mars.

It should be emphasized that the intensity dilution factors are average values. Variation in these factors due to orbital eccentricities alone are shown in Table 6 for the cases of Venus, Earth and Mars. Furthermore, the variation in the factor for Earth reflects itself in additional variance in the factors for other planets, since the original intensity data were obtained at Earth for an assumed radius vector of 1 A.U. However, for present purposes, the simplifying assumption of zero eccentricity of Earth's orbit is justified since the experimental errors and/or the real time variation of flux may exceed variations due to the Earth's orbit eccentricity.

Inasmuch as the eccentricity of Venus' orbit is less than that for Earth, we may also consider that variance as negligible. In the case of Mars, however, such an approximation cannot be made. When the eccentricities for Earth and Mars are coupled, the resulting variation in the dilution factor for the latter can reach as high as 45 percent.

Figure 6 is a plot of the magnitude of the radius vector of Mars for the decade 1960 - 1970. Figures 7 through 16 can be conveniently employed for the solar flux incident in the top of the atmospheres of Venus and Mars.

Additional variations due to other factors such as the variance of solar activity throughout the eleven-year cycle and the solar flares and prominences are present during which strong UV and X radiation have been observed. However, at present these factors cannot be taken into account in any meaningful manner.

Finally, a comparison of the different sources of data was not attempted here; discussions of individual methods and experimental errors can be obtained at the sources. It is important to emphasize the limitations of this presentation, but at the same time recognize its value for certain investigations. While the numerical values in the model may change as more experimental measurements are made, the essential format of the model should remain.

GCA Technical Report No. 62-15-N*

PLANETARY AERONOMY VIII:
A CONGERIES OF ABSORPTION CROSS SECTIONS
FOR WAVELENGTHS LESS THAN 3000 Å

E. D. Schultz, A. C. Holland
and F. F. Marmo

November 1962

Contract No. NASw-395

Prepared for

National Aeronautics and Space Administration
Headquarters
Washington 25, D. C.

GEOPHYSICS CORPORATION OF AMERICA
Bedford, Massachusetts

*This work was partially supported by ASD Contract No. AF33(657)-9199, BPSN Nr: 6799 760B 4122, and also appears as an ASD Technical Report.

TABLE OF CONTENTS

TABLE OF CONTENTS (continued)

LIST OF TABLES

Absorption Coefficients

LIST OF FIGURES

Absorption Coefficients and Cross Sections

A CONGERIES OF ABSORPTION CROSS SECTIONS FOR WAVELENGTHS LESS THAN 3000 Å

E. D. Schultz, A. C. Holland
and F. F. Marmo

I. INTRODUCTION

The absorption of solar vacuum ultraviolet radiation by atmospheric gases is of primary importance in any comprehensive study of planetary aeronomy. Absorption cross section measurements have been made by numerous investigators, but their results are scattered throughout the literature. Some general surveys of these studies do exist (see, for example, References 3, 19, and 27); however, a detailed and up-to-date collection of absorption cross sections in the vacuum ultraviolet will serve as a ready aid for investigating atmospheric problems.

The purpose of this report is to begin such a compilation of experimental data. To obtain this presentation, the literature was searched for current experimental data and reviews of investigations in this area. In a few cases, data were obtained through private communication with particular investigators. Available absorption curves and tabulations, in the spectral region from 100 Å to 3000 Å, of various authors were collected and identified. In each case where tabulated values of absorption coefficients or cross sections were available, plots in this report were constructed by connecting points with straight line segments. Where curves but not tabulations were available, the curves were reproduced either directly or by linearizing semi-log figures. Table 1 is a block summary of authors whose studies are included in this compilation. In

Tables 2 through 23 appear the pure experimental data. Figure 1 is a graphical summary of the respective spectral regions studied--all which appear in Figures 2 through 31 and which were reproduced without attempted interpretation.

Two lists of references follow the discussion. The Direct List includes those authors whose articles have been consulted for this study and/or whose data have been plotted in the absorption cross section figures. The Indirect List includes authors whose works have been cited herein but were not directly consulted.

Included among the gases which are known or suspected to be present in the Earth and/or other planetary atmospheres are:

Oxygen	Argon
Ozone	Nitric Oxide
Carbon Dioxide	Nitrous Oxide
Carbon Monoxide	Nitrogen Dioxide
Water Vapor	Ammonia
Nitrogen	Methane

An accompanying brief discussion of the absorption characteristics together with a historical sketch of each gas considered appear below. Where extracts were published in a format similar to the intended pattern of this report, the authors are quoted directly. In this respect, it is emphasized that our purpose is to accumulate existing information in this area and to present a fairly complete package for convenient reference and availability in the present systematic study of planetary aeronomy and for future applications. The contents will be updated and/or extended as more refined data are made available.

GCA Technical Report No. 63-2-N

PLANETARY AERONOMY X:

ATOMIC POLARIZABILITIES AND SHIELDING FACTORS

A. Dalgarno

February 1963

Prepared for

National Aeronautics and Space Administration
Headquarters
Washington 25, D. C.

This contract was partially supported under Contract No. NASw-395

*This review will be published in "Advances in Physics" edited by B. H. Flowers.

GEOPHYSICS CORPORATION OF AMERICA
Bedford, Massachusetts

TABLE OF CONTENTS

Table of Contents (Continued)

ATOMIC POLARIZABILITIES AND SHIELDING FACTORS

A. Dalgarno

SUMMARY

1. INTRODUCTION

Atomic polarizabilities describe the changes in the charge distribution of an atom when it interacts with an electric field and because of its close relationship to dielectric constants, the study of dipole polarizabilities has a lengthy history. Interest in atomic shielding factors is of more recent origin and was stimulated by attempts to determine nuclear quadrupole moments from observations of hyperfine structure. To a first approximation, atomic hyperfine structure is due to the interaction between the nucleus and the valence electrons, and the inner closed shells of electrons act merely to screen the nuclear charge and so to modify the electrostatic field in which the valence electrons move. However, another type of shielding occurs because the valence electrons distort the spherical symmetry of the closed shells and the distorted shells then interact with the nucleus. Alternatively, the nuclear multipole moments induce equivalent moments in the charge distribution of the closed shells and these moments then interact with the valence electrons.

2. ABSTRACT OF RESULTS

Although they refer to different phenomena, polarizabilities and shielding factors are examined together in this report since the mathematical procedures for calculating them are very similar and a larger body of experimental data becomes available for assessing the accuracy of the methods used. A detailed discussion is given of the methods of calculating atomic polarizabilities and shielding factors and the relationships between them are demonstrated. The formulation of the uncoupled Hartree-Fock approximation is presented and it is shown that the methods are all approximate versions of it. A more accurace procedure, the coupled Hartree-Fock approximation, is described. Comprehensive tables of dipole and quadrupole polarizabilities and of quadrupole shielding factors are included together with an assessment of the probable accuracy.

A cursory examination of the Table of Contents makes evident that the nature and extent of the present report does not make it feasible to include any more detail than that given in the previous paragraph.

SECTION II — EXPERIMENTAL

SUMMARIES OF WORK ACCOMPLISHED UNDER CONTRACT NO. NASw-395 AND PREVIOUSLY PUBLISHED AS GCA TECHNICAL REPORT NUMBERS 62-4-N, 62-8-N, 62-9-N AND 63-1-N

In this section, rather comprehensive summaries of previously published GCA Technical Reports are given. Included in these summaries are the pertinent tables, figures, and data. Brief analyses are also given so that the report is able to stand on its own. To indicate the detail and scope of work covered in the original reports, in each case the summaries are preceded by (1) the original Title Page, (2) the original Table of Contents, and (3) miscellaneous items such as abstracts, lists of figures, etc.

GCA Technical Report No. 62-4-N

PLANETARY AERONOMY I:

ABSORPTION AND PHOTOIONIZATION COEFFICIENTS OF PROPYLENE AND BUTENE-1 IN THE VACUUM ULTRAVIOLET

J.A.R.Samson, F.F. Marmo, and
K. Watanabe

April 1962

Contract No. NASw-395

Prepared for

NATIONAL AERONAUTICS AND SPACE ADMINISTRATION
HEADQUARTERS
WASHINGTON 25, D. C.

GEOPHYSICS CORPORATION OF AMERICA
Bedford, Massachusetts

Published in The Journal of Chemical Physics, Vol. 36, No. 3, pp. 783-786, February 1, 1962.

TABLE OF CONTENTS

ABSORPTION AND PHOTOIONIZATION COEFFICIENTS OF PROPYLENE AND BUTENE-1 IN THE VACUUM ULTRAVIOLET

J.A.R. Samson, F.F. Marmo and K. Watanabe

SUMMARY

I. INTRODUCTION

A continuing program is being conducted to measure the absorption and photoionization coefficients of gases and vapors. The results are applied to planetary atmospheres; suitable fillings for photon counters; and a search for suitable gases which ionize at longer wavelengths than nitric oxide, thereby extending the usable range of absolute measurements.

A detailed analysis of the absorption and photoionization of propylene and butene-1 in the region 1000-2000 A is given in this report.

The absorption spectrum of propylene and butene-1 below 2000 A has been studied by several investigators;[1-6] comparisons of previous to the present work will be made in the appropriate places in the text below.

In the present study the total absorption coefficient of propylene and butene-1 vapor in the region 1050-2000 A and the photoionization coefficient in the region 1050 A to the onset of ionization were measured by means of photoelectric methods. From these measurements two Rydberg series were identified in propylene along with some vibrational structure. Further, ionization potentials were obtained directly for the two vapors and found to be in good agreement with previously published data.[4]

II. EXPERIMENTAL

Measurements of absorption coefficients and photoionization yields were made by methods described previously.[7,8] Data for the total absorption coefficients were obtained with six pressures ranging from 0.04 to 0.2 mm Hg, and for photoionization absorption coefficients with three pressures from 0.5 to 2 mm Hg. The absorption coefficient, k in cm^{-1}, was defined as previously[7] by the equation $I = I_o \exp(-kx)$, where I_o and I are the incident and transmitted light intensities, respectively, and x, in cm, is the absorbing path length of the vapor expressed at NTP. The photoionization coefficient is defined as the product of the ionization yield and the total absorption coefficient. Absolute yields were obtained by comparison of the ionization current of the investigated vapors to that of nitric oxide. Nitric oxide yields were calibrated against a thermocouple in 1954.[9] These yields have recently been revised[10] and are the ones used in this present work.

III. RESULTS AND DISCUSSION

Mean absorption coefficients of propylene and butene-1 in the spectral region 1050-2000 A are summarized in Figures 1 through 4, which were made by drawing smooth curves through points for about three hundred wavelengths. The experimental uncertainty in the mean k-value is estimated to be about 10% for nearly all wavelengths, pressure measurements being the main source of error.

A. PROPYLENE

1. Region 1500 - 2000 A

Figure 1 gives the total absorption coefficients of propylene between 1500 - 2000 A. A broad absorption band with a maximum at 1720 A is the most prominent feature in this region. Unlike the absorption spectrum of ethylene, which has quite discrete structure, propylene exhibits rather diffuse bands. However, some structure is evident to the short-wavelength side of the absorption band and is possibly due to strong vibrational bands superimposed on the main transition. The average separation of these bands is 1360 cm^{-1} which is of the same order as the separation of the vibrational bands found in ethylene in this region by Price and Tutte;[3] namely, 1370 cm^{-1}. Price and Tutte attribute this vibration in ethylene as being due to the totally symmetrical valence frequency of the double bond.

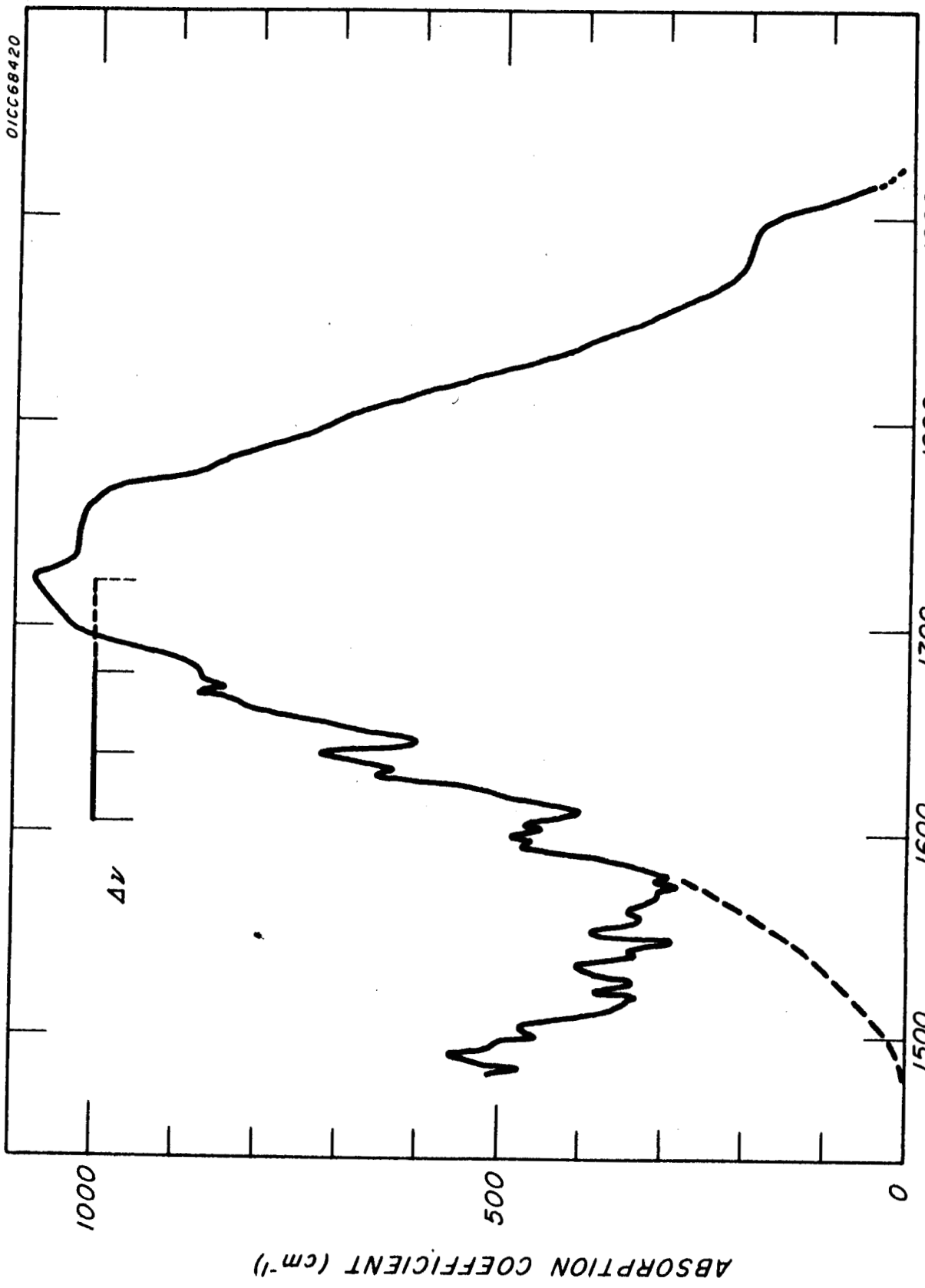

Figure 1. Total absorption coefficients of propylene between 1500 - 2000 A.

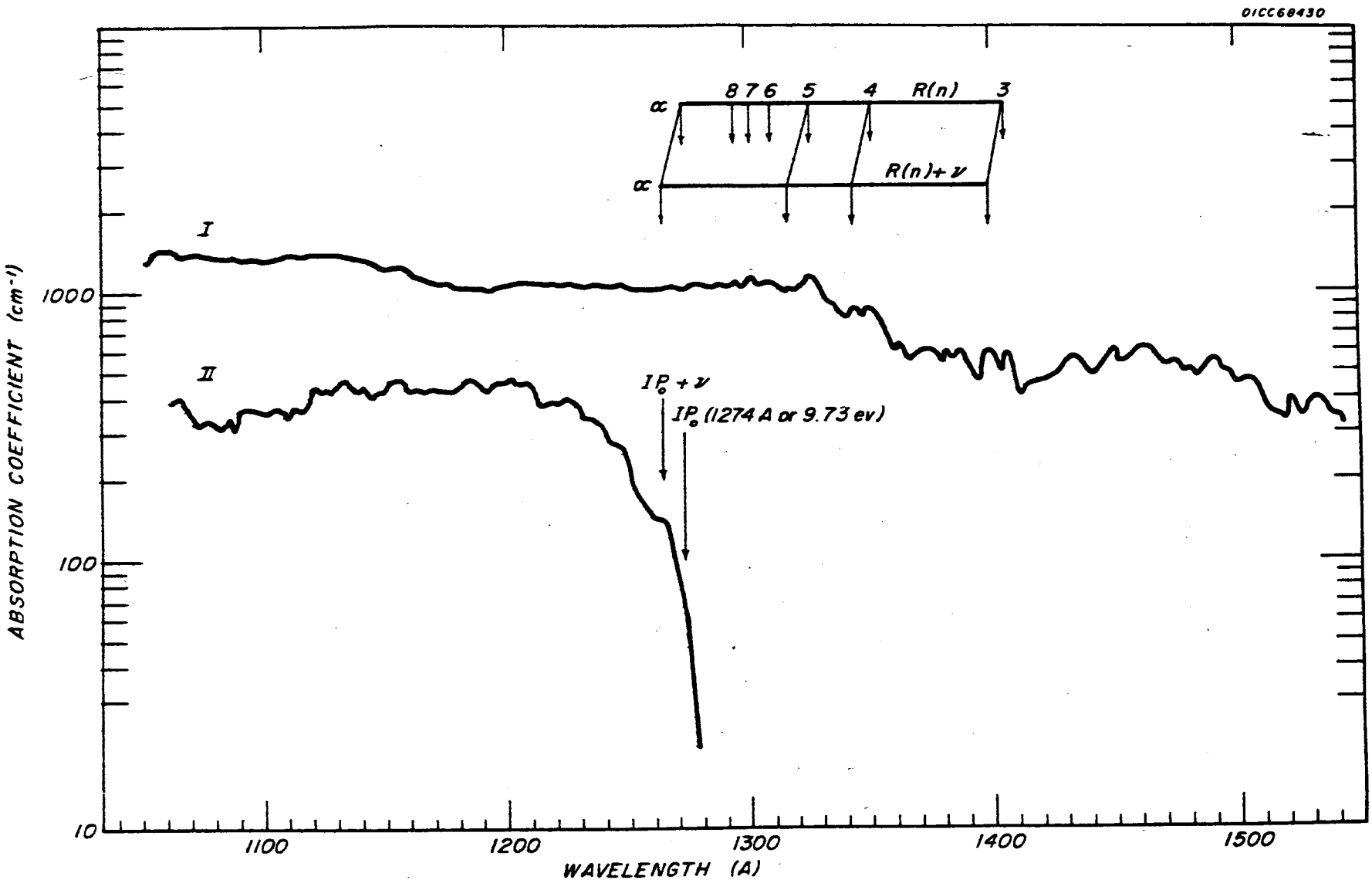

Figure 2. Total absorption coefficients (curve I) and photoionization coefficients (curve II of propylene between 1050 - 1550 A.

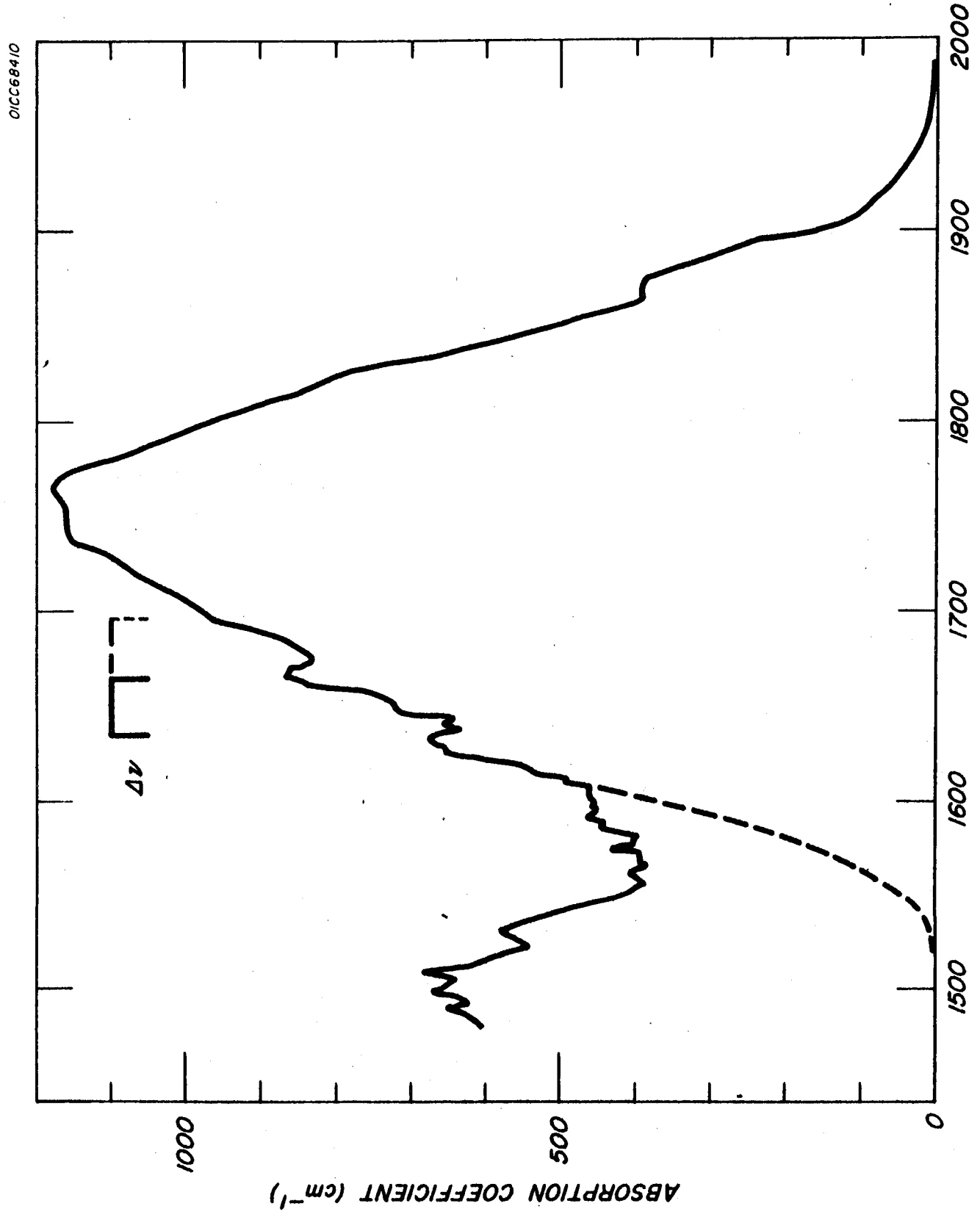

Figure 3. Total absorption coefficients of butene-1 between 1500 - 2000 A.

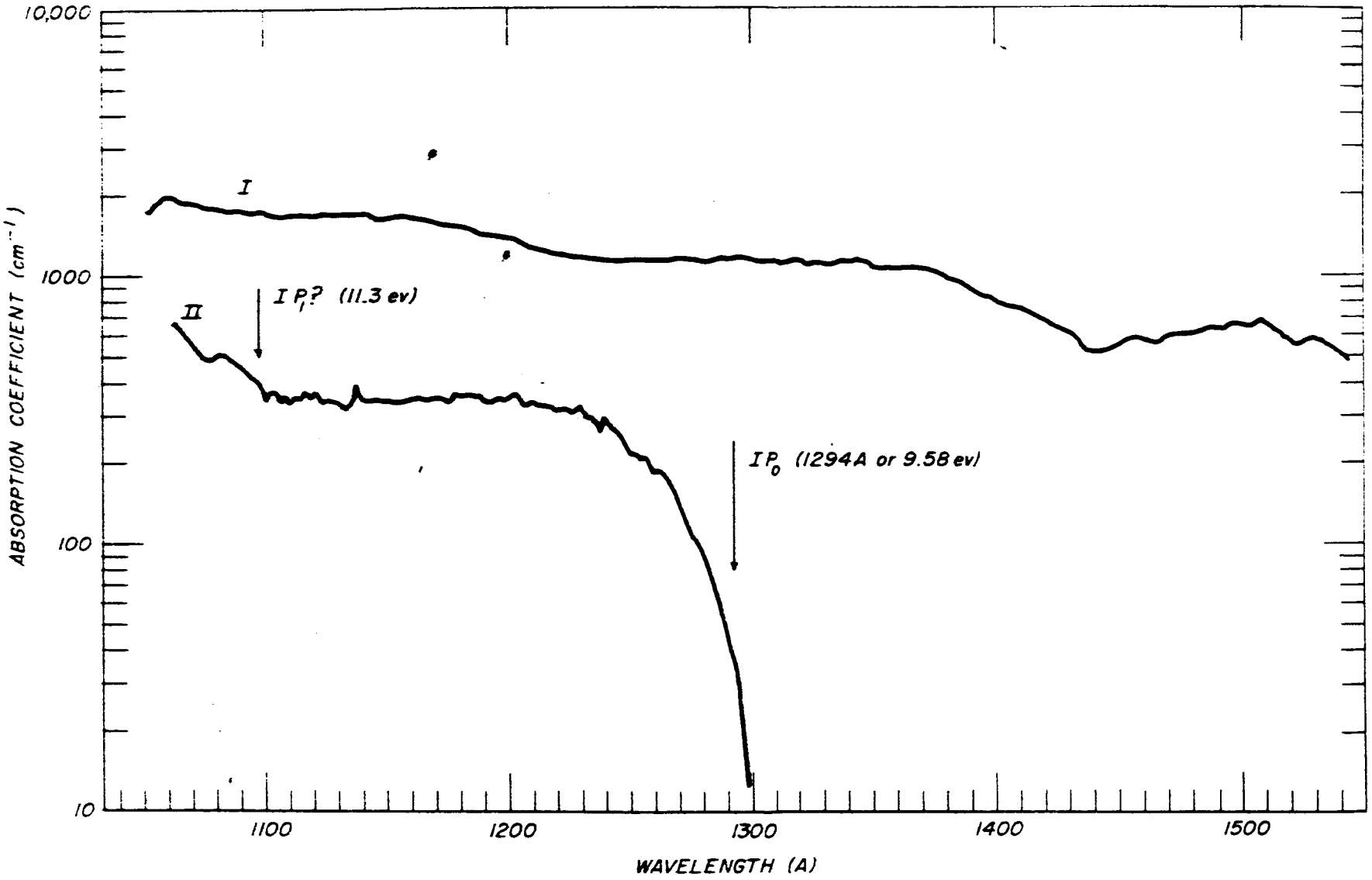

Figure 4. Total absorption coefficients (curve I) and photoionization coefficients (curve II) of butene-1 between 1050 - 1550 A.

The oscillator strength f for this absorption band was calculated from the relation $f = 4.31 \times 10^{-9} \int \epsilon d\nu$, where $\epsilon = k/0.1028$.[11] The limits of the integral for the above band are somewhat uncertain to the short-wavelength side of the band; however, the dotted curve in Fig. 1 approximates the band limit. Taking the area under this curve, one gets $f = 0.32$.

2. Region 1050 - 1500 A

To wavelengths shorter than 1300 A, the absorption spectrum (curve I, Figure 2) is essentially continuous. However, between 1300 - 1550 A, considerable structure can be seen. Although this structure is more diffuse than in ethylene, two Rydberg series can be identified with the help of the photoionization absorption coefficient curve (II). This curve gives an onset for ionization at 1274 A (9.73 ev), while a second break in the curve is indicative of another ionization potential due to a transition into a vibrational state of the ion, $\Delta\nu = 527$ cm^{-1}, at 1265.5 A (9.80 ev). This vibration probably represents a twisting vibration about C = C bond in analogy with the almost certain identification of this vibration in ethylene.[3] Using these ionization potentials as a guide and from the doublet nature of some of the bands in curve I, two series were identified and found to fit the following Rydberg formulas:

$$R(n): \quad \nu = 78586 - R/(n+0.85)^2 \quad n = 3, 4 \ldots , \qquad (1)$$

$$R(n) + \Delta\nu: \quad \nu = 79051 - R/(n+0.85)^2 \quad n = 3, 4 \ldots , \qquad (2)$$

where R is the Rydberg constant, R(n) a Rydberg series, and R(n) + $\Delta\nu$ a doublet member of the R(n) series. The position of these Rydberg bands are shown in Figure 2. The calculated series limits of 78586 cm^{-1} (9.74 ev) and 79051 cm^{-1} (9.80 ev) agree well with the ionization potentials obtained from the photoionization experiments.

The structure of curve II compares favorably with that published by Steiner et al.[5] In particular, they obtain an ionization potential at 9.73 $\pm$ 0.02 ev and a break in their ionization efficiency curve occurs at the same position we have assigned to the R + ν series limit at 9.80 ev. The observed ionization potential at 9.73 ev agrees with previously published data using photoionization methods.[4]

Price and Tutte[3] did not publish a Rydberg series in propylene; however, from the structure of their spectrum, they do estimate a series limit at 9.6 ev in good agreement with the first series limit of 9.74 ev found in this work. Electron impact techniques yield, in general, slightly higher ionization potentials than photoionization methods, and in propylene these values vary from 9.81 to 10 ev.[12]

Theoretical values at 10.14 and 9.96 ev for the first ionization potential of propylene have been calculated by Higuchi[13] and Streitwieser,[14] respectively. Walsh[15] has estimated that a second ionization potential, corresponding to the removal of a σ CC electron, should occur around 12.0 ev. This occurs at shorter wavelengths than

reported here and no evidence of its presence is apparent from curve II; however, due to the lowering of the ionization potentials by alkyl substitution, it may be apparent in butene.

B. BUTENE-1

1. Region 1500 - 2000 A

Butene-1 has a very similar absorption spectrum to that of propylene; however, as can be seen from Figure 3, the discrete structure is much more diffuse. The maximum of the main absorption band at 1760 A shows a shift towards the red as compared to propylene. This shift was also observed by Carr and Stücklen[1] as the number of alkyl groups around the double bond increased.

An f-value of 0.36 was obtained assuming the band followed the dotted curve in Figure 3. This value compares favorably with that of 0.39 obtained by Gary and Pickett.[2]

2. Region 1050 - 1500 A

In Figure 4, curve I, some absorption bands can be seen between 1300 and 1550 A; however, they are far too diffuse and unresolved to observe any Rydberg series. The absorption spectrum is otherwise continuous down to the limit of observation at 1050 A.

Curve II in Figure 4 represents the photoionization absorption coefficient of butene-1. Ionization begins at about 1297 A, rises

sharply, and has a point of inflection at 1294 A or 9.58 ev representing the first ionization potential of the molecule. The region between 1297 and 1294 A represents the Boltzmann energy distribution in the molecule at room temperature. The ionization potential at 9.58 ev is in good agreement with previously published data using photoionization methods,[4,5] and is, in general, slightly lower than values obtained by electron impact techniques, which vary from 9.76 to 10.00 ev.[12] Franklin calculated the ionization potential of butene-1 using a semi-empirical relation and obtained a value of 9.7 ev.[16] As mentioned in the discussion on propylene, Walsh[15] estimated a higher ionization potential in propylene at around 12 ev. Due to the lowering of the ionization potential by alkyl substitution one might expect a higher ionization potential in butene-1 at somewhat less than 12.0 ev. From curve II, Figure 4, an abrupt increase in the ionization cross section at 11.3 ev suggests a higher ionization potential and may be due to the removal of the σ CC electron as suggested by Walsh.

REFERENCES

1. Carr, E. P. and Stücklen, H., J. Chem. Phys. 4, 760 (1936).

2. Gary, J. T. and Pickett, L. W., J. Chem. Phys. 22, 599 (1954).

3. Price, W. C. and Tutte, W. T., Proc. Roy. Soc. (London) A174, 207 (1940).

4. Watanabe, K., J. Chem. Phys. 26, 542 (1957).

5. Steiner, B., Giese, C. F., and Inghram, M. G., J. Chem. Phys. 34, 189 (1961).

6. Schoen, R. E. and Weissler, G. L., University of Southern California, Los Angeles (private communication).

7. Watanabe, K., Inn, E. C. Y., and Zelikoff,M., J. Chem. Phys. 21, 1026 (1953).

8. Watanabe, K., Marmo, F. F., and Inn, E. C. Y., Phys. Rev. 91, 1155 (1953).

9. Watanabe, K., J. Chem. Phys. 22, 1564 (1954).

10. Watanabe, K., (unpublished material).

11. MacColl, A., Quart. Rev. (London) 1, 16 (1947).

12. Kiser, R. W., "Tables of Ionization Potentials," Tech. Rept. TID-6142 (1960), U. S. Atomic Energy Commission.

13. Higuchi, J., J. Chem. Phys. 32, 636 (1960).

14. Streitwieser, A., J. Am. Chem. Soc. 82, 4123 (1960).

15. Walsh, A. D., Trans. Faraday Soc. 42, 779 (1946).

16. Franklin, J. L., J. Chem. Phys 22, 1304 (1954).

GCA Technical Report No. 62-8-N

PLANETARY AERONOMY IV:

THE DUOPLASMATRON AS A VACUUM ULTRAVIOLET LIGHT SOURCE

J.A.R. Samson and H. J. Liebl

August 1962

Contract No. NASw-395

Prepared for

National Aeronautics and Space Administration
Headquarters
Washington 25, D. C.

GEOPHYSICS CORPORATION OF AMERICA
Bedford, Massachusetts

Published in Review of Scientific Instruments, Vol. 33, No. 12, pp. 1340 - 1343, December 1962.

TABLE OF CONTENTS

LIST OF FIGURES

THE DUOPLASMATRON AS A VACUUM ULTRAVIOLET LIGHT SOURCE*

J.A.R. Samson

I. INTRODUCTION

The Duoplasmatron was developed about twelve years ago as a highly efficient source of protons. After its publication[1] in 1956, a number of variations were designed and used as ion or electron sources for such applications as accelerator ion sources and ion propulsion devices.[2,3,4] A further application was suggested by Herzog;[5] namely, that the highly concentrated plasma of a Duoplasmatron possibly would emit intense vacuum ultraviolet radiation.

In the spectral region below 1000 A conventional light sources are of the high voltage pulsed type with their inherent disadvantages that they radiate electrical noise and are difficult to operate at a constant light intensity output. Thus, it is desirable to look for a light source which emits radiation below 1000 A of comparable intensity to the high voltage pulsed type but which operates from a D.C. supply. The hot filament type of light source falls into this category with the exception of light intensity. It was felt, therefore, that with the combination of hot filament and axial magnetic field as found in the Duoplasmatron that the light intensity would be comparable with the high voltage pulsed light sources.

---

*The content of this report has been submitted for publication to the "Review of Scientific Instruments," and is included in this report in its entirety.

A preliminary measurement of the total intensity between 1050 A and 1350 A was made using a nitric oxide ion chamber with a Duoplasmatron which was currently being used as an ion source. The source had an anode opening of 0.008 inches. Using hydrogen in the Duoplasmatron with an arc current of 300 mA, a flux of approximately 10^{12} photons/sec/cm^2 was measured at a distance of 25 cm from the anode opening for the 1216 A Lyman-alpha line. This is based on the assumption that 50% of the ion chamber response was due to the 1216 A line--an assumption which is normally true for a hot filament-type hydrogen lamp. Subsequently, a Duoplasmatron light source was designed, built, and tested.

The principle of the Duoplasmatron can briefly be described as follows: A low pressure arc discharge in hydrogen, typically 20 to 100 microns pressure, is constricted by a funnel-shaped baffle placed between the electron emitting cathode (hot filament) and the anode. A strong axial magnetic field of approximately 2000 oersteds is developed between the baffle and the anode by a pole piece arrangement similar to those used as magnetic lenses in electron microscopes; this further constricts the discharge to a narrow plasma beam along the axis. If the anode has a central opening, a very intense ion or electron beam can be extracted from the plasma. Any gas can be used to produce the ions provided the gas does not poison the filament.

II. DESIGN CONSIDERATIONS

In the Duoplasmatron the plasma density on the axis near the anode increases quickly with the magnetic field strength, and after passing a flat maximum slightly decreases. In practice, this means one has to operate the Duoplasmatron above a minimum magnetic field strength to provide a maximum plasma density on the axis. In conventional Duoplasmatrons the magnetic field is generated by a solenoid of 2000 to 7000 amp turns, providing a magnetic field of the order of 2000 oersteds between the pole pieces. However, it would appear that a permanent magnet of equivalent strength would be equally as efficient as a solenoid and at the same time have the following advantages: (a) no power supply for the magnetic field is needed; (b) since the heat generated in the solenoid is of the same order as the heat generated by the arc, then for a given cooling rate a higher arc current can be drawn if the solenoid is replaced by a permanent magnet; (c) since the baffle electrode, which forms one pole of the magnetic field, operates at a different electrical potential than the anode, which forms the other magnetic pole, it is necessary in the case of a solenoid to have an additional air gap in the path of the magnetic flux through the iron enclosure to provide electrical insulation. For a given magnetic field strength this requires additional magnetic induction. This is avoided if one chooses ceramic permanent magnetic material, which is electrically insulating. (d) There are ceramic magnets on the market which have an exceptionally high coercive force, typically around 2000 oersteds.[6] That means the required

magnetic length is relatively small; therefore, less iron is needed and since the ceramic material itself is much lighter than copper, the whole assembly becomes considerably shorter and lighter than an equivalent design employing a magnet coil.

III. CONSTRUCTION

A sectional view of the Duoplasmatron is shown in Figure 1. The magnetic field is provided by three rings of highly-oriented barium ferrite permanent magnetic material (Indox V) which are magnetized in the direction of their axis. This provides a field of 7000 oersteds between the baffle aperture and the slit holder. The magnetic flux goes from one pole of the magnet through the source flange and the slit holder over the gap, through the wall of the baffle electrode, and then through the cover plate to the other pole of the magnet. The slit--the two halves of which are screwed to the slit holder--is held by the strong magnetic field between the apex of the baffle electrode and the slit holder which slides in the source flange. This way the slit can easily be pulled out and inspected. The magnetic field presses the slit against the anode which is an air-cooled disc of copper. The cooling disc, a ceramic spacer ring and the baffle electrode--onto which is screwed a stainless steel retainer ring--are sealed to the source flange with six screws simultaneously, having indium or gold O-rings between each other. The baffle electrode is closed by a feed-through cap, which carries the gas inlet tube and two ceramic terminal bushings which hold two studs between which the filament is mounted. The filament is platinum mesh wire, which is dipped in a suspension of barium carbonate and activated in a hydrogen atmosphere. A cooling fan, mounted on the cover plate, blows air through twelve holes in the cover plate, along the baffle electrode, through twelve holes in the cooling disc, and finally out through twelve channels in the source flange.

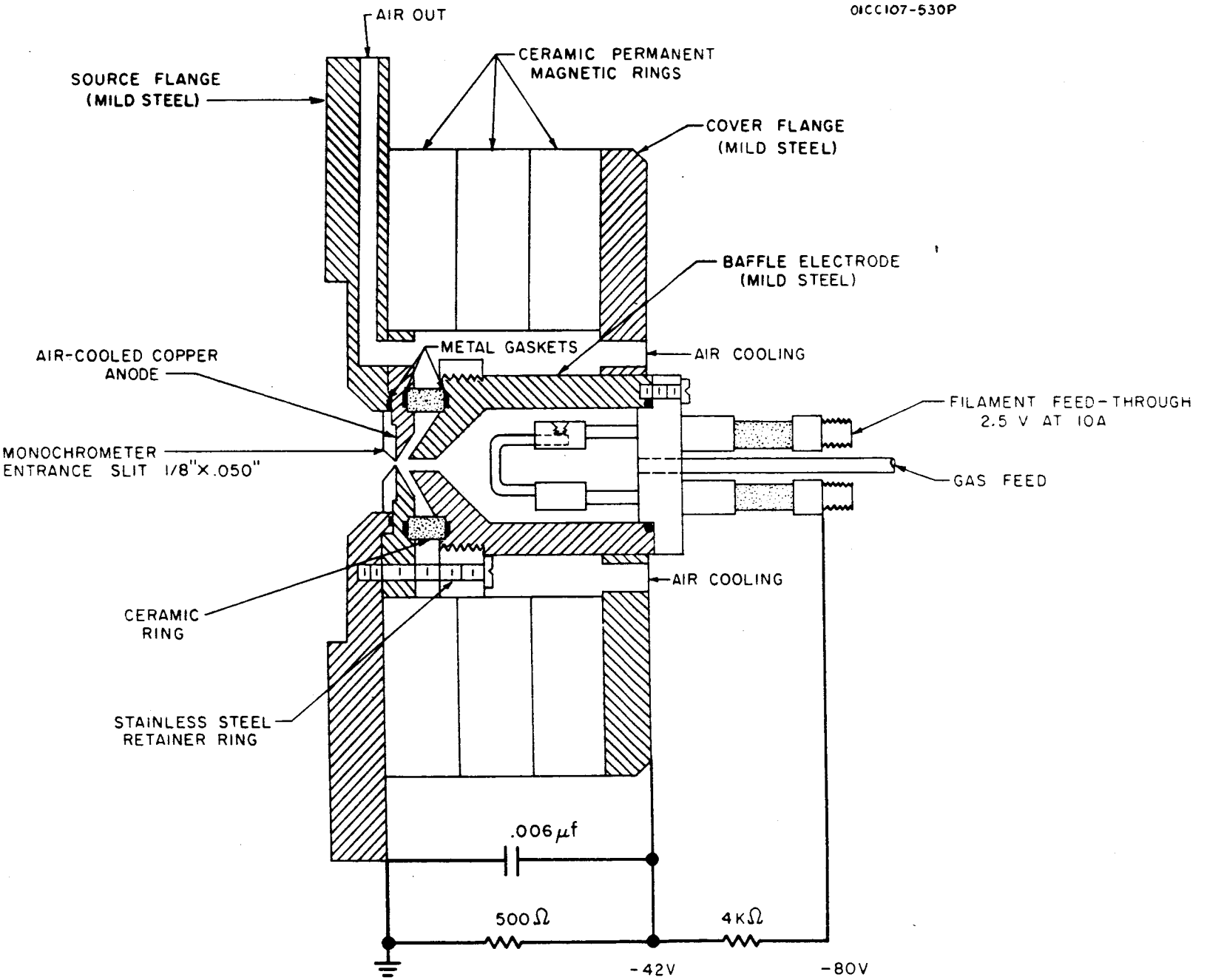

Figure 1. Duoplasmatron light source. The voltage distribution shown is typical under discharge conditions in hydrogen.

SCALE = 1 in.

The circuit diagram for the arc power supply is shown in Figure 2. The supply is current stabilized by simply inserting an amperite ballast tube in series with the load. Figure 3 shows the current-voltage characteristics of a typical tube. The power supply was constructed with ten amperite 3-38 A ballast tubes in parallel in order to provide current stabilization for 0.3 amps to 3 amps by switching in the number of tubes required to provide the desired arc current.

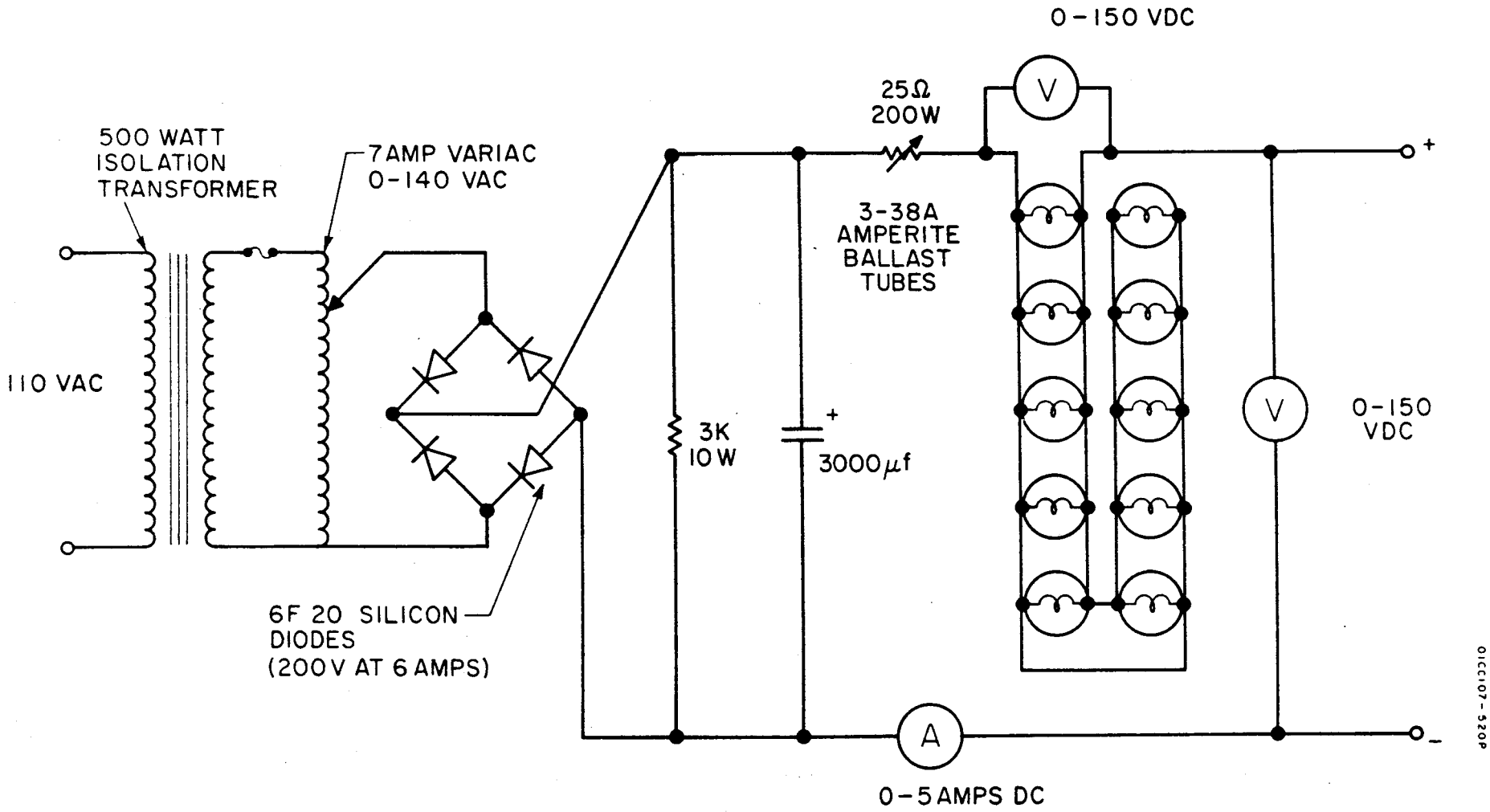

Figure 2. Current regulated power supply from 0.3 to 3 amps.

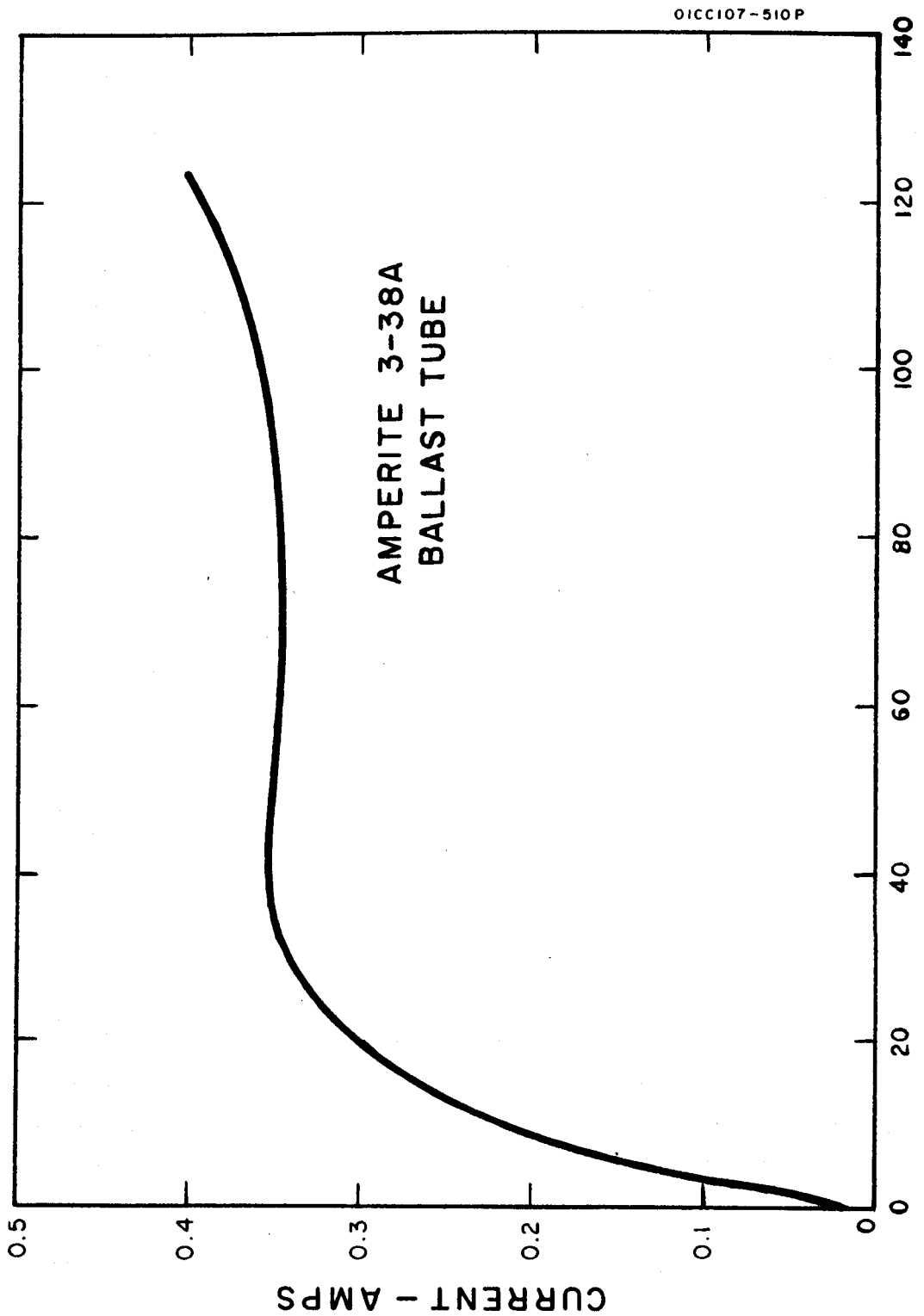

Figure 3. Current-voltage characteristic of an amperite 3-38A ballast tube.

IV. RESULTS

The Duoplasmatron, as shown in Figure 1, has been operated successfully both as an ion source and as a vacuum ultraviolet light source. The extractor aperture of the Duoplasmatron ion source was replaced by a slit assembly 1/8 inch high by 50 microns wide. The slit-assembly constituted the entrance slit of a 1/2 M Seya-type vacuum monochromator having a reciprocal dispersion of 16 A/mm. Under such conditions a wavelength resolution of approximately 2 A was obtained. No windows were used between the light source and the monochromator since no suitable materials exist which will transmit radiation below 1050 A (the short wavelength transmission limit of lithium fluoride). However, due to the low operating pressure of the Duoplasmatron and the small slit area, a pressure of 1×10^{-4} torr was maintained in the monochromator chamber without the use of a differential pumping chamber between the light source and monochromator. When the discharge was started, the pressure in the monochromator decreased by a factor of two or three. This, apparently, is due to the intense ionization in the vicinity of the entrance slit impeding the flow of neutral gas through the slit into the monochromator. The entrance slit is at a positive potential relative to the baffle in the Duoplasmatron.

The ultraviolet detector was an EMI 9514B photomultiplier tube sensitized to vacuum ultraviolet radiation by coating its envelope with sodium salicylate. The quantum efficiency of this scintillator has been

measured from 2000 A down to 800 A and found to be constant.[7] Although it is probable that the constancy of the quantum yield of sodium salicylate continues in the region of our measurements down to 550 A, one must be careful in comparing the relative intensity of two lines rather widely separated as the efficiency of diffraction gratings in the vacuum ultraviolet region of the spectrum is not constant with wavelength.[8]

Figure 4 shows the spectrum of hydrogen between 1800 A and 900 A. It is a typical hydrogen spectrum with the molecular continuum to longer wavelengths of 1650 A and the many-lined molecular spectrum to shorter wavelengths with the atomic lines of the Lyman series, alpha and beta, at 1215.7 A and 1025.7 A, respectively. However, it does differ from the spectrum produced in a hydrogen glow discharge (cold cathode type) in that the atomic resonance line at 1215.7 A is several times more intense than the most intense molecular line, usually 1608 A. As the arc current was varied from 0 to 0.9 amps, the light intensity increased almost linearly--the molecular lines increasing at a somewhat slower rate than the atomic lines. This result can be correlated with the analysis of the beam composition as a function of arc current as reported by Moak et al.[3] who found a rather linear and more rapid increase in the atomic ion content than in the molecular ion content.

An argon spectrum from 550 A to 1100 A is shown in Figure 5. The arc current was 1.5 amps with 30 volts between anode and filament. As the arc current increased from zero, the radiation from excited neutral

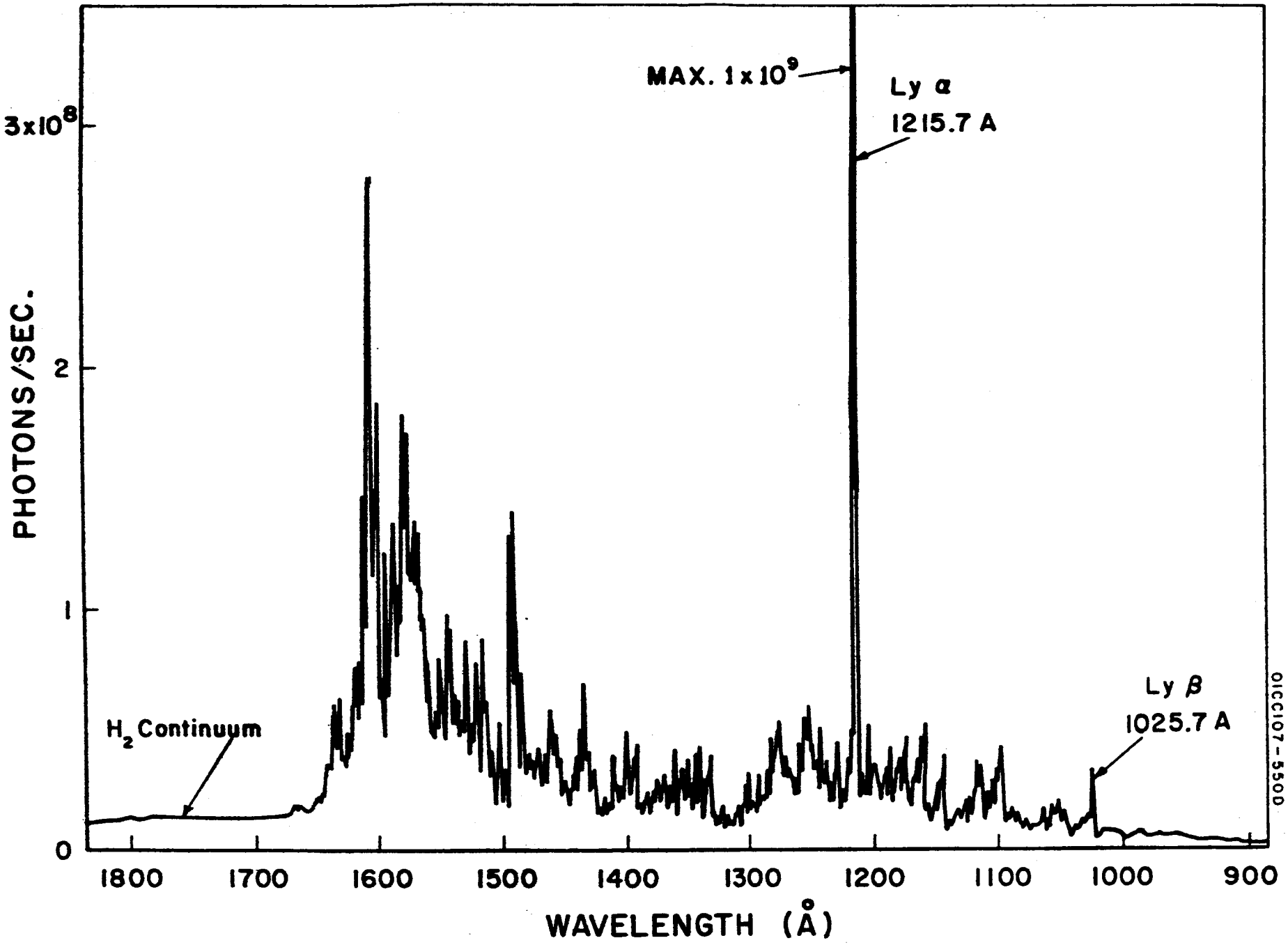

Figure 4. Hydrogen spectrum taken with an arc current of 0.9 amp. wavelength resolution is approximately 2 angstroms.

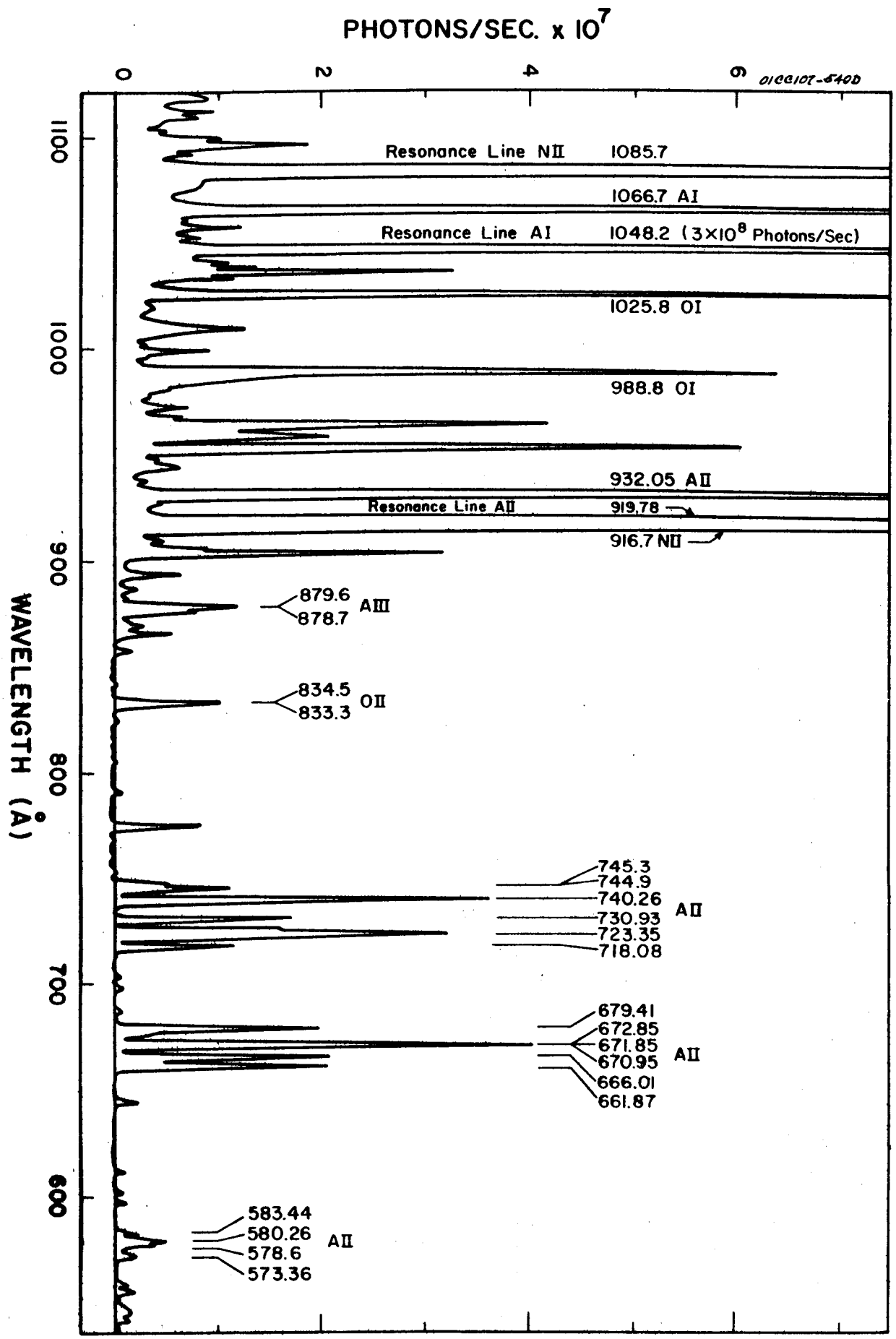

Figure 5. Argon spectrum taken with an arc current of 1.5 amp.

atoms increased to a maximum around 1 amp and then remained constant or even decreased slightly as the arc current increased further; however, the radiation from the singly and doubly ionized atoms continued to increase. At 3 amps the 879.6 A and 878.7 A lines of AIII were a factor of five more intense than shown in Figure 5, whereas the AII series increased by only a factor of two. The presence of an air leak was indicated by radiation from atomic nitrogen and oxygen.

That the magnetic field confines the discharge to a very intense radiating plasma along the axis is evidenced by the fact that if the ceramic magnets are removed one by one, the light intensity decreases rapidly to the point of essentially zero light intensity at zero magnetic field.

The Duoplasmatron is suitable as a D.C. light source producing considerable intensity in the spectral region below 1000 A; however, the results presented here, in argon, are somewhat less intense than those of a 6 kv, 60 pps spark discharge. By increasing the arc discharge current, it appears possible to increase the intensity of the radiation to the point where it is comparable to that of the high voltage pulsed discharge.

REFERENCES

1. Ardenne, M. V., Tabellen der Elektronenplysik, Ionenphysik and Ubermikroskopie, Deutschen Verlag der Wissenschafter, Berlin, Vol. I, p. 544 (1956).

2. Froehlich, H., Nukleonik, 1, 183 (1959).

3. Moak, C. D. et al., Rev. Sci. Instr., 30, 694 (1959).

4. Burton, B. S., Jr., "The Duoplasmatron," Presented at ARS Conference on Electrostatic Propulsion (November 1960).

5. Herzog, R.F.K., Private Communication (January 1962).

6. In the present construction, Indox V was used which was produced by Indiana Steel Products, Valparaiso, Indiana.

7. Johnson, F. S., Watanabe, K. and Tousey, R., J. Opt. Soc. Am., 41, 702 (1951).

8. Samson, J.A.R., J. Opt. Soc. Am., 52, 525 (1962).

GCA Technical Report No. 62-9-N

PLANETARY AERONOMY V:
VACUUM ULTRAVIOLET LIGHT SOURCES

J.A.R. Samson

August 1962

Contract No. NASw-395

Prepared for

National Aeronautics and Space Administration
Headquarters
Washington 25, D. C.

GEOPHYSICS CORPORATION OF AMERICA
Bedford, Massachusetts

TABLE OF CONTENTS

LIST OF FIGURES

VACUUM ULTRAVIOLET LIGHT SOURCES

J.A.R. Samson

SUMMARY

I. INTRODUCTION

For high resolution spectroscopy, it is essential to use a light source which produces a continuous spectrum in the wavelength region of interest. Unfortunately, in the region below 2000 A, there are few light sources which produce an intense continuum. Although this is unimportant when photographic techniques are used as detectors, it is very important when photoelectric devices are used. In this discussion, we are interested in photoelectric detectors since they provide a higher degree of accuracy in the measurement of absorption cross sections. Further, the intensity of radiation is often the important factor in photoionization measurements.

Although a continuous light source is often desirable, much valuable work can be achieved with a line spectrum especially at the important solar emission lines; viz., the 1215.7 H I, 584 He I, and the 304 He II lines. A line spectrum is often more intense than a continuum; and further, it is not always necessary to have a high resolution spectrometer to produce highly monochromatic lines since the separation of the lines may be one or two Angstroms. For instance, a glow discharge in helium produces the intense 584 A line of He I quite isolated from any neighboring lines. Therefore, a resolution of several Angstroms can still

produce pure 584 A radiation. It is also easier to assess the amount of scattered light present in a line spectrum than in a continuous spectrum and therefore easier to make corrections for it.

Due to the great variety of experiments in vacuum ultraviolet radiation physics, no single light source would satisfy all experimental requirements nor would it cover the wavelength range of, say, 100 A to 2000 A.

The intent of this present work was to study the production of vacuum ultraviolet radiation by a variety of methods and compare the relative intensity of the radiation on the same spectrometer with a standard slit width and grating. The spectrometer used was a McPherson No. 235 ½ M Seya monochromator with a 1200 L/mm grating blazed for normal incidence at 1500 A. At the Seya angle of incidence, 35°, this represents a blaze at about 1300 A. The entrance and exit slits were 50 microns wide with the exit slit 6 mm high. A resolution of two Angstroms was realized under the above conditions.

II. CONTINUUM LIGHT SOURCES

A. HYDROGEN CONTINUUM

The hydrogen continuum is best produced in a D.C. glow discharge tube, preferably with a platinized capillary to enhance the recombination of atomic hydrogen. A hydrogen pressure of ½ mm Hg is normal to produce a relatively strong continua. As the pressure decreases, the intensity of the molecular radiation decreases whereas the intensities of the atomic lines increase.

Figure 1 shows the measured hydrogen continuum from 1675 A to 2300 A obtained from a D.C. glow discharge operated with a current of 300 mA at 200 watts. Superimposed on the continuum are the second order lines of the intense line spectrum above 1050 A. A lithium fluoride window was used in order to remove second order lines due to radiation of shorter wavelength than 1050 A, the transmission limit of lithium fluoride. Thus, a smooth continuum is produced from 1675 A to 2100 A. To extend the usefulness of the continuum to longer wavelengths, quartz or sapphire windows should be used since their transmission limits are 1800 A and 1400 A, respectively. The dashed line in Figure 1 represents the continuum in the absence of the second order lines. Below 2000 A the peak radiant flux of the continuum is 1.6×10^7 photons/sec. For comparison, the intensity of the Lyman-alpha line, 1215.7 A, and the molecular band at 1608 A is given in Figure 1. However, the relative intensities of these lines and the continuum vary with pressure.

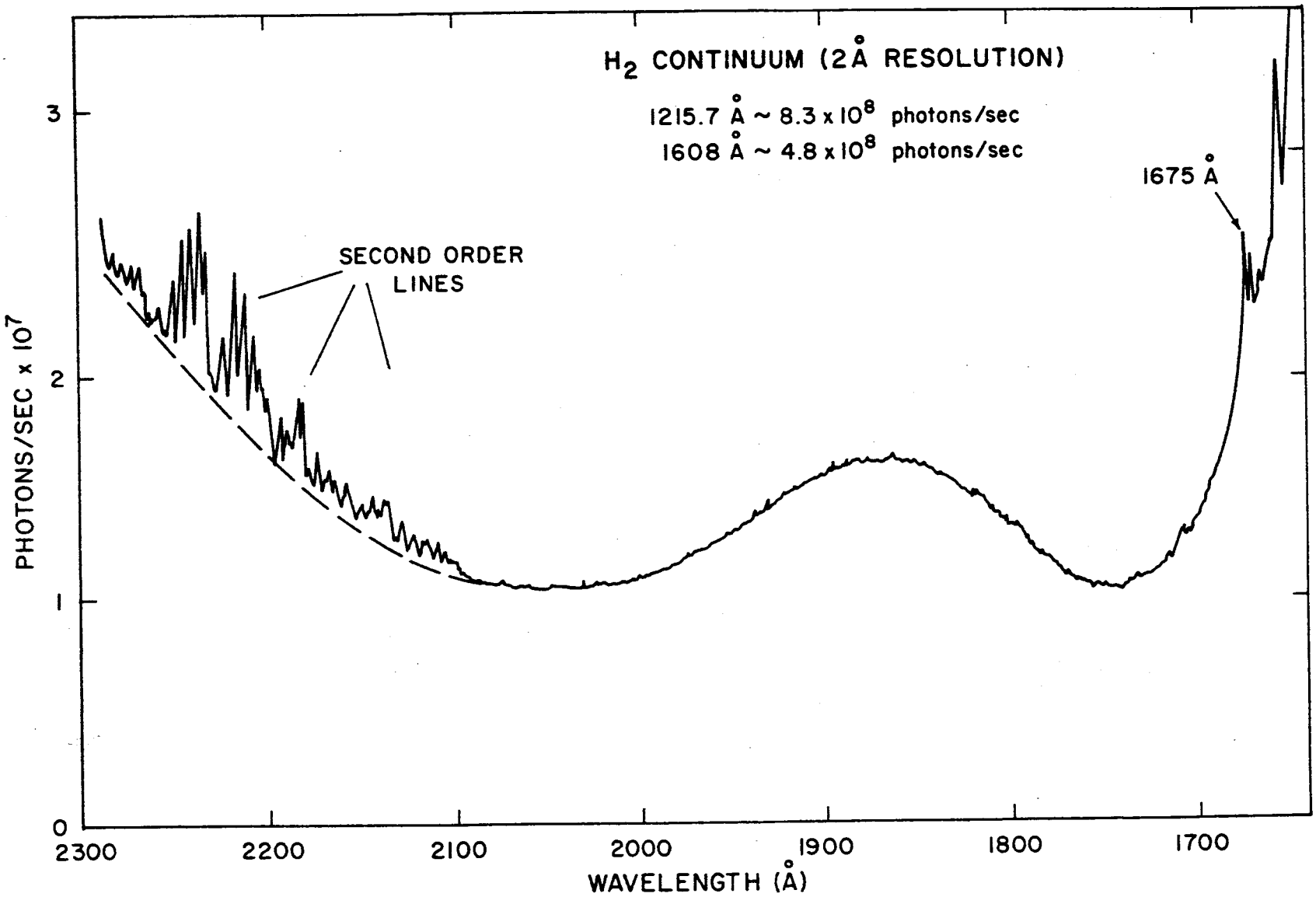

Figure 1. The hydrogen continuum transmitted through a lithium fluoride window. The dashed line indicates the H_2 continuum when the second order lines are removed.

B. RARE GAS CONTINUA

Several rare gas continua have been produced by Tanaka et al.[1] covering the range 600 A to 2000 A. No estimates of the absolute intensities are available, however, since the method of detection was by photographic techniques.

Recently, Huffman et al.[2,3] at the Air Force Cambridge Research Laboratory successfully produced a relatively strong continuum using a condensed repetitive spark in purified helium. Other examples of rare gas (xenon, krypton, and argon) continua[4] are shown in Figure 2.

In the present investigation, the absolute flux produced by the Jarrell-Ash xenon lamp was measured under the standard conditions described in the original report and found to be 1.5×10^7 photons/sec at the peak of the continuum around 1670 A.

C. LYMAN CONTINUUM

The conventional source of continua below 1000 A is the Lyman flash tube.[5] This is essentially an impulsive discharge from a capacitor through a narrow bore capillary, with an external gap in series to give a high breakdown voltage. As the power is increased, the continuum extends to shorter wavelengths. Photographically, it has been observed down to about 200 A. Photoelectrically, the continuum is useful from the visible only down to approximately 1000 A. A comparison of various types of flash tubes has been given by Parkinson and Reeves.[6]

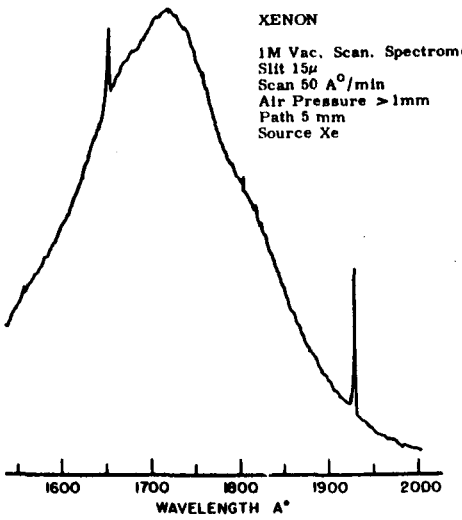

USEFUL RANGE 1600 - 1950 A
WITH LITTLE LINE EMISSION
Catalog No. 45-503

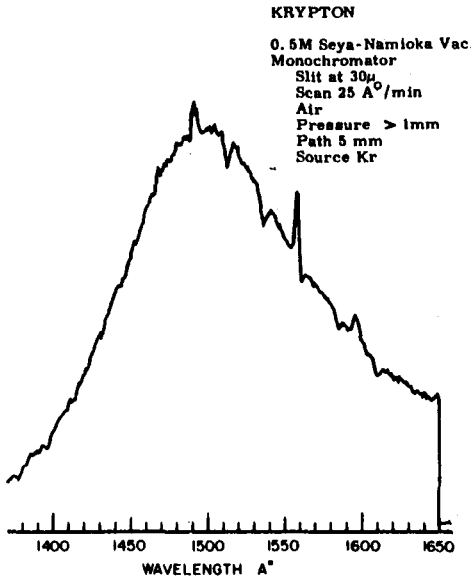

USEFUL RANGE 1300 - 1650 A
WITH LITTLE LINE EMISSION
Catalog No. 45-502

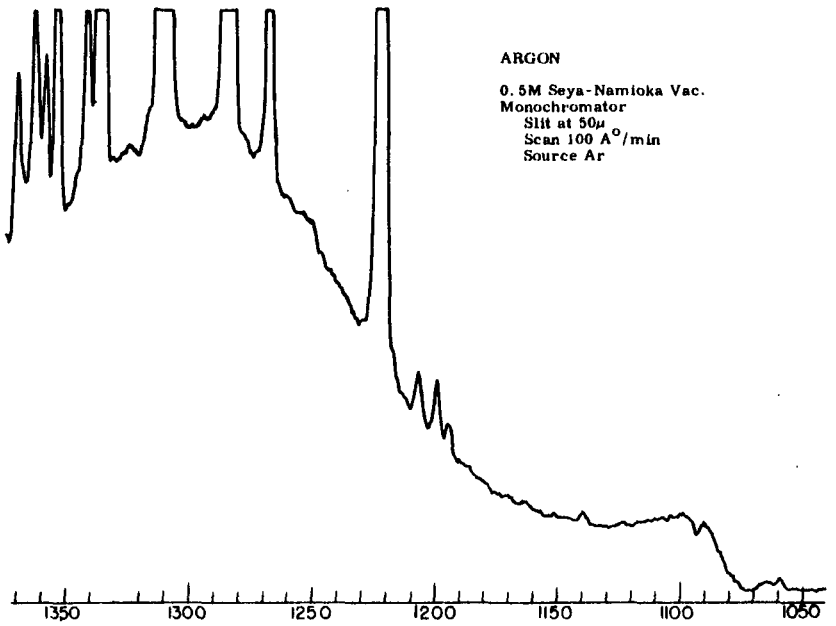

USEFUL RANGE 1090 - 1300 A
RATHER SEVERE LINE EMISSION
BUT STILL USEFUL
Catalog No. 45-501

Figure 2. Rare gas continua produced by xenon, krypton, and argon at approximately 150 mm Hg pressure in LiF sealed lamps. The absolute flux at the peak of the xenon continuum is about 1.5×10^7 photons/sec.

A typical spectrum obtained with a Garton-type[7] flash tube is shown in Figure 3 for one, two, and four discharges, each discharge lasting about a microsecond. The spectrum was obtained on a 2 M vacuum spectrograph (McPherson No. 240) with a 600 L/mm grating blazed for 1500 A. The entrance slit was 100 μ wide.

A usable continuum extends from the visible to below 1200 A even for a single discharge. Below 1200 A the continuum is superimposed with an intense line spectrum. However, the continuum is observed to go down to about 500 A, at which point the absorption of the He ionization continuum starts and the grating efficiency for normal incidence is close to zero. In the original negative, with four discharges, lines are observed down to 300 A. It is interesting to note that there is sufficient neutral helium in the Pyrex tube of the flash tube to produce a Rydberg series in absorption of the 584.3 A He I series illustrating the usefulness of the continuum for absorption studies even in this short wavelength region. The presence of such highly ionized species as O V and O VI demonstrates the high temperatures achieved in the flash tube.

In Figure 4, oscilloscope traces of the discharge current and light intensity (555 A) as a function of time are shown. The sweep time is 2 μ sec/large division. From the light output oscillogram, it can be seen that 70 percent of the light intensity takes place within 2 μ sec.

The flash tube appears to be an excellent source of continuum radiation from the visible down to approximately 1000 A. The short

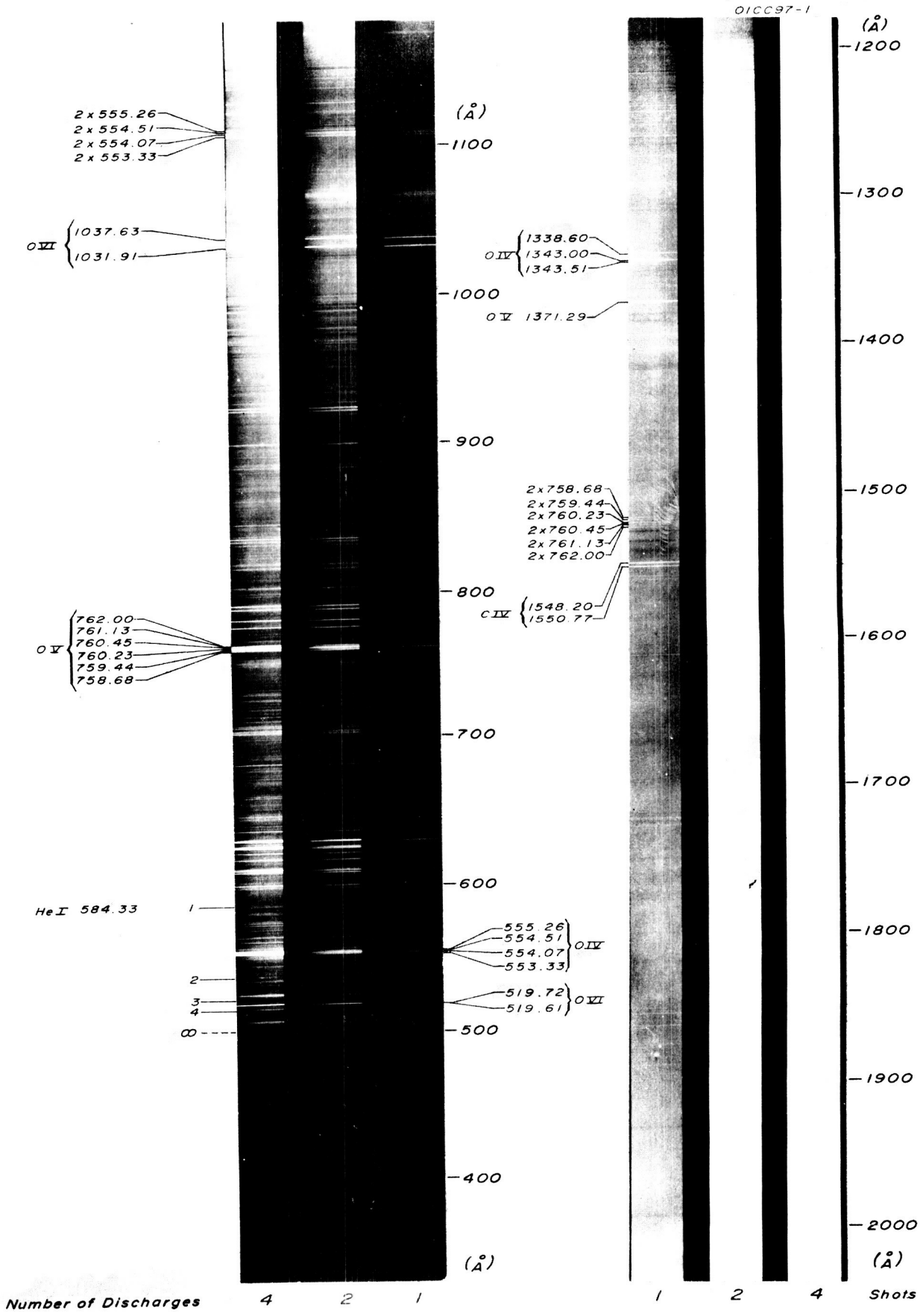

Figure 3. Flash tube spectrum of helium between 500 and 2000 Å. Exposures for one, two, and four discharges are shown. The line spectrum is due to impurities; namely, oxygen.

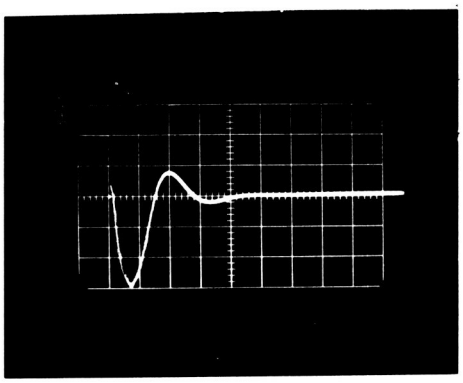

DISCHARGE CURRENT
VS.
TIME

(2 μ sec/major division)

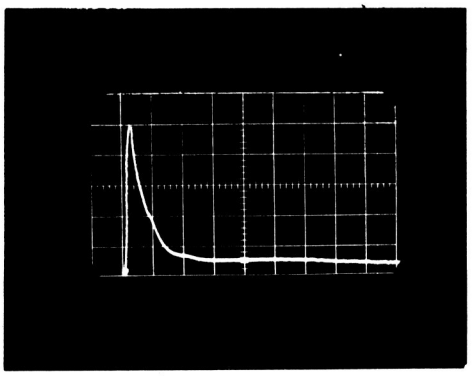

LIGHT OUTPUT (555 A)
VS.
TIME

(2 μ sec/major division

Figure 4. Oscillograms of the current and light output of the flash tube.

duration of the light pulse and the ability to trigger the discharge at any precisely required time makes this type of light source particularly suitable for absorption studies in such transient phenomena as found in shock tube research and possibly in measuring reaction rates greater than 1 μ sec.

III. LINE EMISSION LIGHT SOURCES

A. D.C. COLD CATHODE DISCHARGE

In a cold cathode gas discharge, several hundred volts must be applied to the electrodes; then when a free electron exists in the tube, it will be accelerated until it accumulates sufficient energy to cause ionization in the gas. This process multiplies and a Townsend avalanche is formed. In order for the discharge to be self-sustaining, the positive ions must receive enough energy to produce secondary electrons when they impinge on the cathode. Thus, in the glow discharge region, much higher voltages are required to sustain a discharge than in the arc region where the electrons are produced by temperature emission from a hot cathode--the cathode being heated either by ion bombardment or by an electric current as in a hot filament.

A common design for a cold cathode discharge tube is to use a water-cooled quartz or Pyrex capillary sealed into a hollow cathode and anode by O-rings. However, the present cold cathode discharge tube was based on a design by W. Hunter[8] of the Naval Research Laboratories. It differs from the more conventional type in that it uses a water-cooled cathode and allows the quartz capillary to run hot rather than cooling the capillary with a water jacket. The main advantage of this feature is that there is no danger of water entering the vacuum system should the capillary break. Figure 5 shows the general structure of the D.C. cold cathode discharge lamp. This type of light source is very suitable

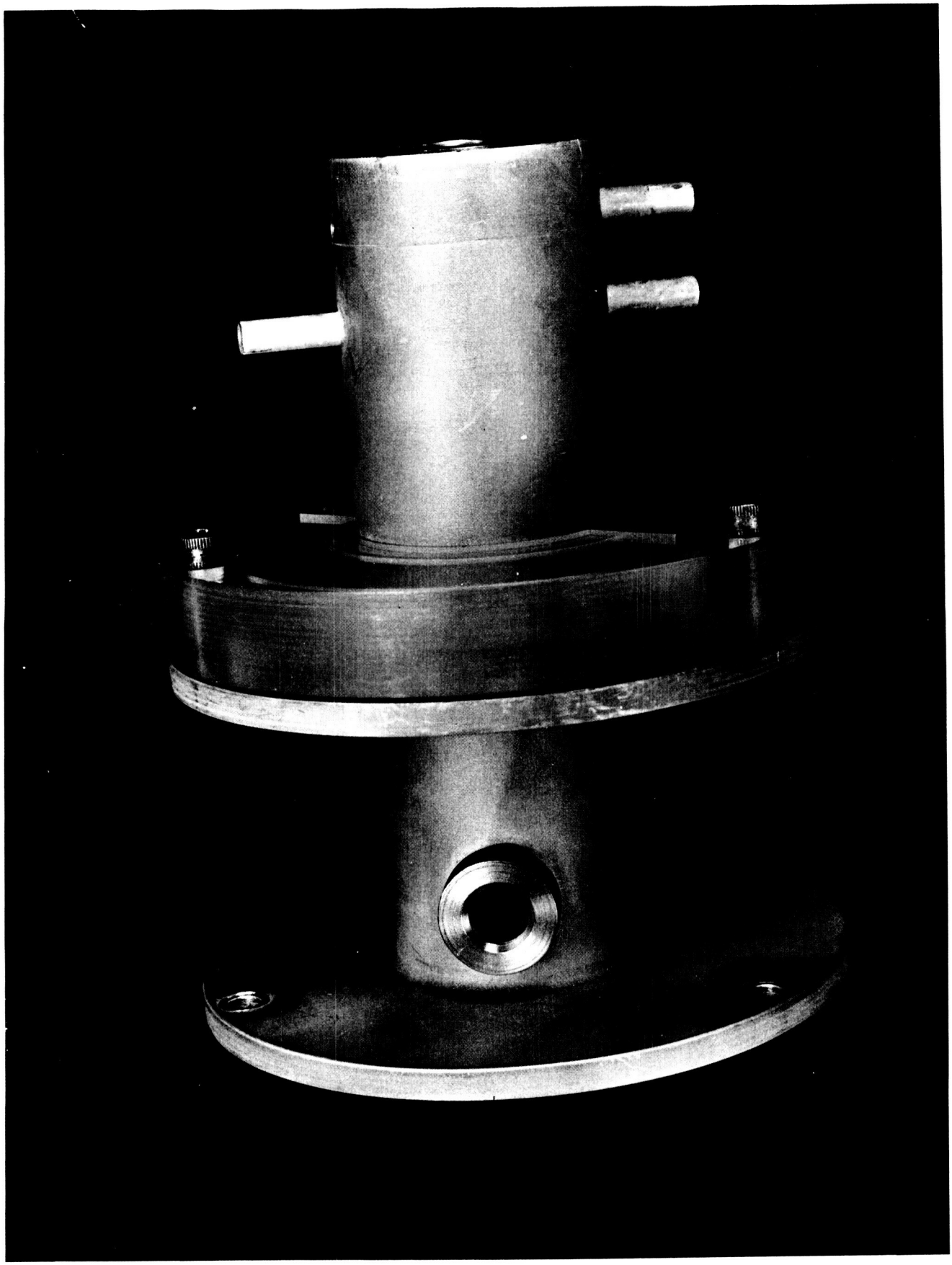

Figure 5. Complete discharge lamp.

in exciting molecular lines and the resonance lines of atoms. The molecular lines can be enhanced if the capillary interior is slightly metallized. However, it is not so suitable in producing radiation from the more highly ionized atoms. Since the source of radiation below 1000 A is due mainly to highly ionized atoms, the usefulness of the glow-discharge lamp is mainly above 1000 A with the exception of the He I 584 A, Ne I 735.8 A, and Ne I 743.7 A resonance lines.

Figure 6 shows a typical hydrogen spectrum recorded by the EMI 9514B photomultiplier sensitized to vacuum UV radiation by coating with sodium salicylate. The spectrum is mainly due to molecular hydrogen; however, the resonance lines, Lyman-α and β, can be seen. The actual spectral energy distribution shown here is, of course, dependent on the individual grating used.[9] The absolute flux at Lyman-α was measured with a nitric oxide ionization chamber; and since the quantum yield of sodium salicylate is relatively constant[10] between 1000 and 2000 A, the photomultiplier trace gives the absolute flux of the radiation emanating from the exit slit. The spectral response above 1300 A is well known and is not reproduced here. The spectrum was taken with 50 micron slits on a ½ M Seya Monochromator (McPherson 235). A resolution of about 2 A is realized.

Using exactly the same parameters for the monochromator, the helium glow-discharge spectrum was investigated and compared to the intensity of the hydrogen spectrum. The spectrum is shown in Figure 7.

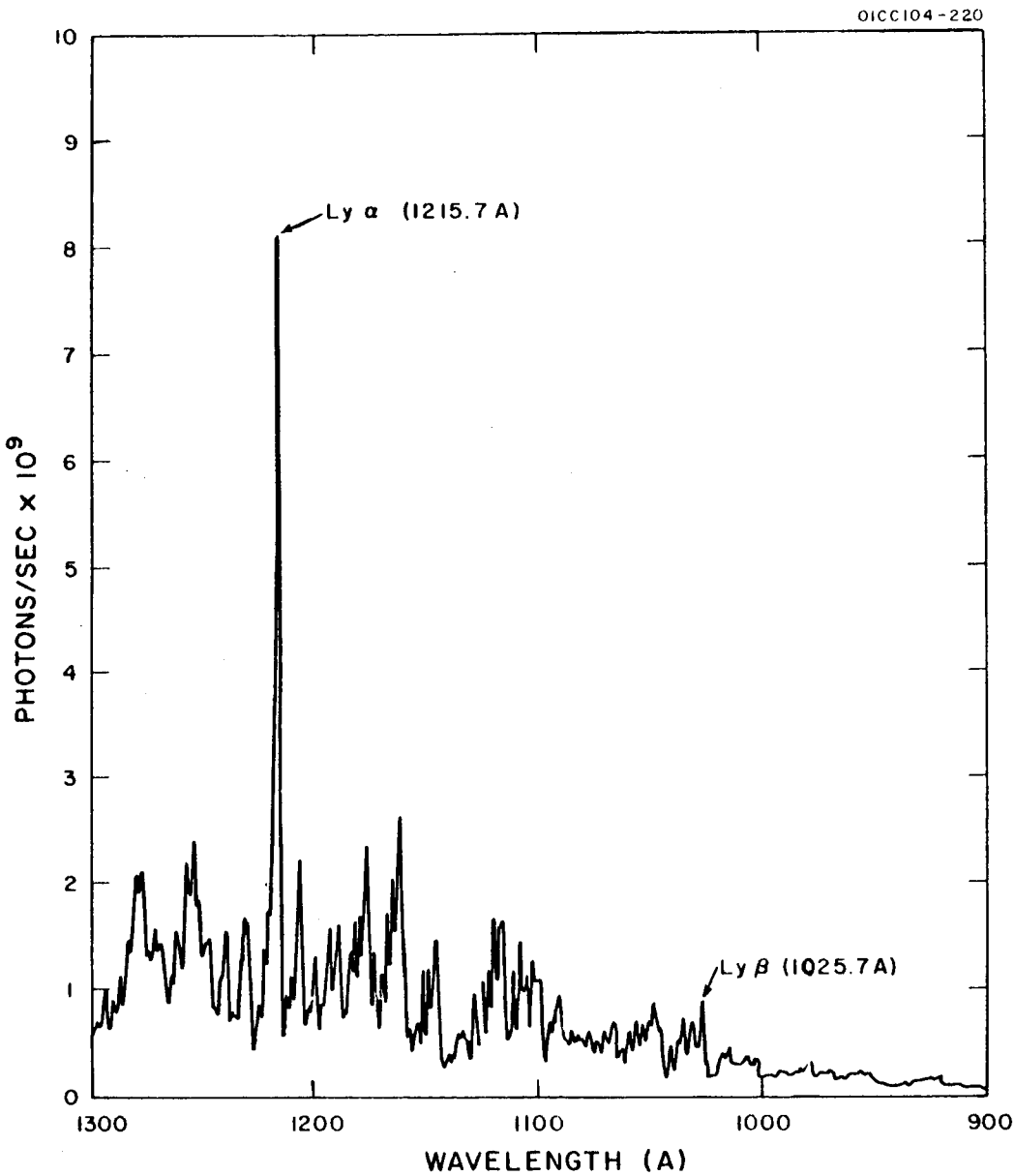

Figure 6. Hydrogen Spectrum between 900 A and 1300 A. The important solar emission lines of Lyman-α (1215.7 A) and Lyman-β (1025.7 A) are shown.

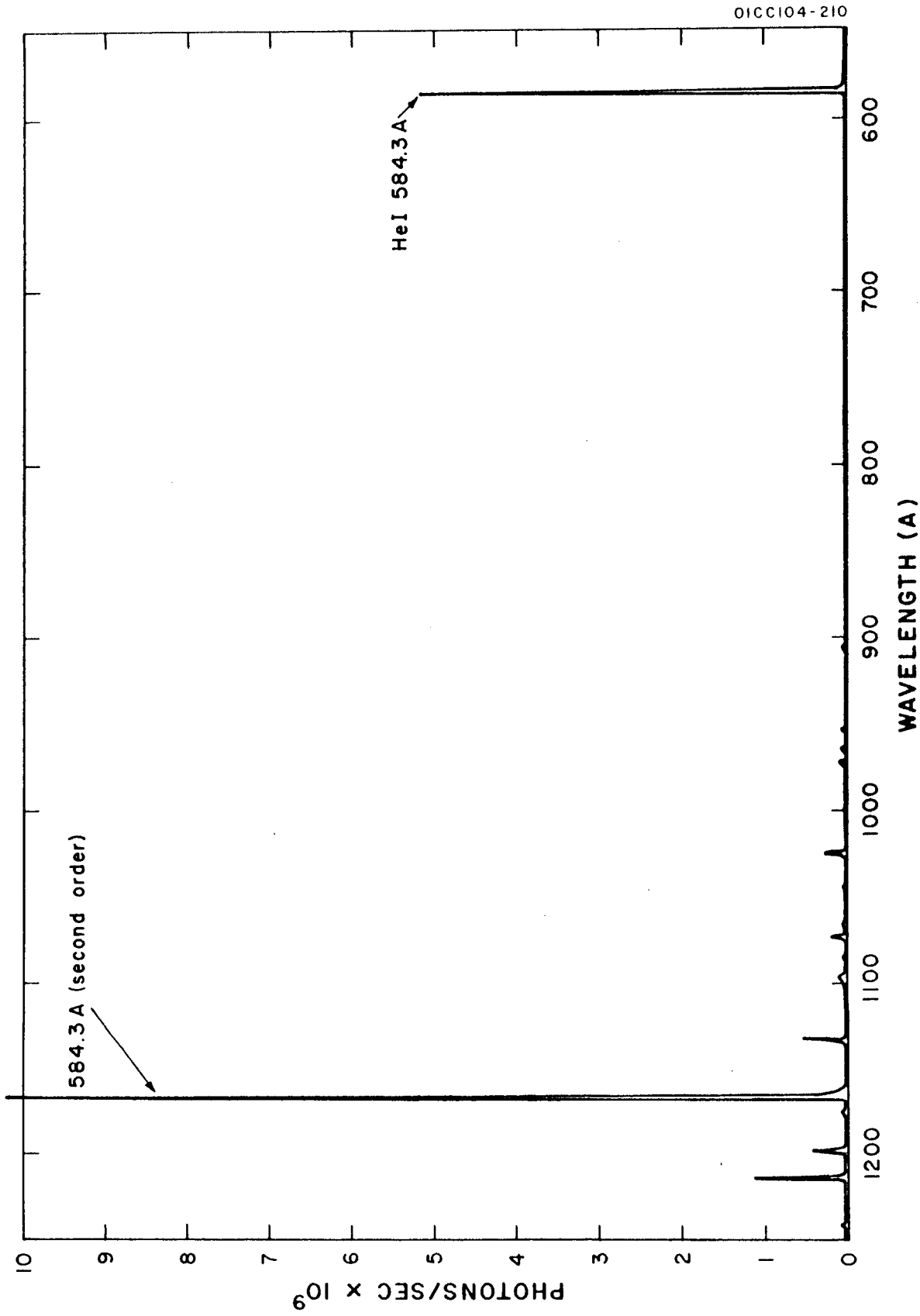

Figure 7. Glow-Discharge Spectrum in Helium between 550 A and 1200 A Showing Both First and Second Order of He I (584.3 A).

Its usefulness is in producing the He I resonance line at 584.3 A with considerable intensity. The second order 584 A line is more intense than the first order, indicating that this grating is more efficiently blazed in the region of 1200 A than to shorter wavelengths. The grating was blazed for 1500 A at normal incidence; but for a few weak impurity lines, the helium spectrum below 1300 A is concentrated solely in the 584.3 A line. The absolute photon flux at 584.3 A was obtained by assuming that the quantum yield of sodium salicylate remained constant down to 584 A.[10]

An argon spectrum was investigated and found to produce--in addition to the A I resonance lines at 1048 A and 1066 A--many lines of shorter wavelength down to 500 A. In fact, the spectrum below 1000 A is very similar to that produced by the Duoplasmatron, shown in Part C of this section. However, the intensities were at least an order of magnitude lower than that produced by the Duoplasmatron. Typical values of the radiant flux are given below for a 270 watt glow discharge in argon operated at 300 mA.

Wavelength (Å)	Origin	Flux in Photons/Sec
1066	A I	3.60×10^8
1048	A I	6.30
920	A II	0.52
671	A II	0.03
573	A II	0.003

It would appear, therefore, that the glow-discharge lamp is admirably suited to produce the profuse hydrogen line spectrum from 900 to 1675 A, the hydrogen continuum above 1675 A, and atomic resonance lines including the He I resonance line at 584.3 A and the Ne I lines at 735.8 A and 743.7 A. For other line radiation below 1000 A, another type of light source must be used.

B. HOT FILAMENT ARC DISCHARGE

The use of hot filaments to provide the free electrons necessary to sustain a discharge in hydrogen and other gases has been described in the literature.[11,12] The main advantage in using a hot filament to produce an arc discharge appears to be due to the fact that a discharge current of several amperes can be created by low voltages, typically 50 to 100 V. Thus, the need for a high voltage power supply is eliminated. On the other hand, a prime disadvantage is the need to renew the filaments periodically due to a decrease in their electron emission. However, with some experience this does not present a major obstacle.

The one comparison--between the hot filament arc discharge and other types of discharges--that has rarely been expressed, is that of light intensity in the vacuum ultraviolet region and of the origin of the radiation; viz., molecular, atomic, neutral or ionized atoms. However, this is done in the present work which compares the intensity and type of spectrum produced by discharges excited by different methods.

The arc discharge described here is based on the design used by P. Hartman.[12,13] Although the arc discharge produces a strong hydrogen molecular spectrum, the atomic resonance line is by far the most intense line. Using the standard ½ M Seya Monochromator with 50 micron slits, the 1216 A line produced 10^{10} photons/sec, which is at least 50 percent of the total radiation between 1350 A and 1050 A. Further, the higher members of the Lyman series of atomic hydrogen, beta and gamma, appeared clearly above the weaker molecular bands.

By using a mixture of hydrogen and helium in the discharge--approximately 25 percent hydrogen--the radiation becomes nearly monochromatic in the Lyman-alpha line at 1216 A. Actually, the intensity of the atomic lines in the pure hydrogen discharge did not change appreciably when helium was added; however, the intensities of the molecular lines were greatly reduced. Figure 8 shows the Lyman series of atomic hydrogen when a hydrogen-helium mixture was used in the arc discharge.

When a discharge in argon was studied, the argon resonance line at 1048 A and the 1066.7 A line appeared with good intensity although about an order of magnitude less intense than the hydrogen 1216 A line. The resonance line of ionized argon at 919.8 A also appeared along with many weaker lines to shorter wavelengths. Unfortunately, with argon this particular lamp would not operate properly, but presumably the argon lines appeared down to about 500 A as they do in the glow discharge. If the argon lines are of usable intensity, then

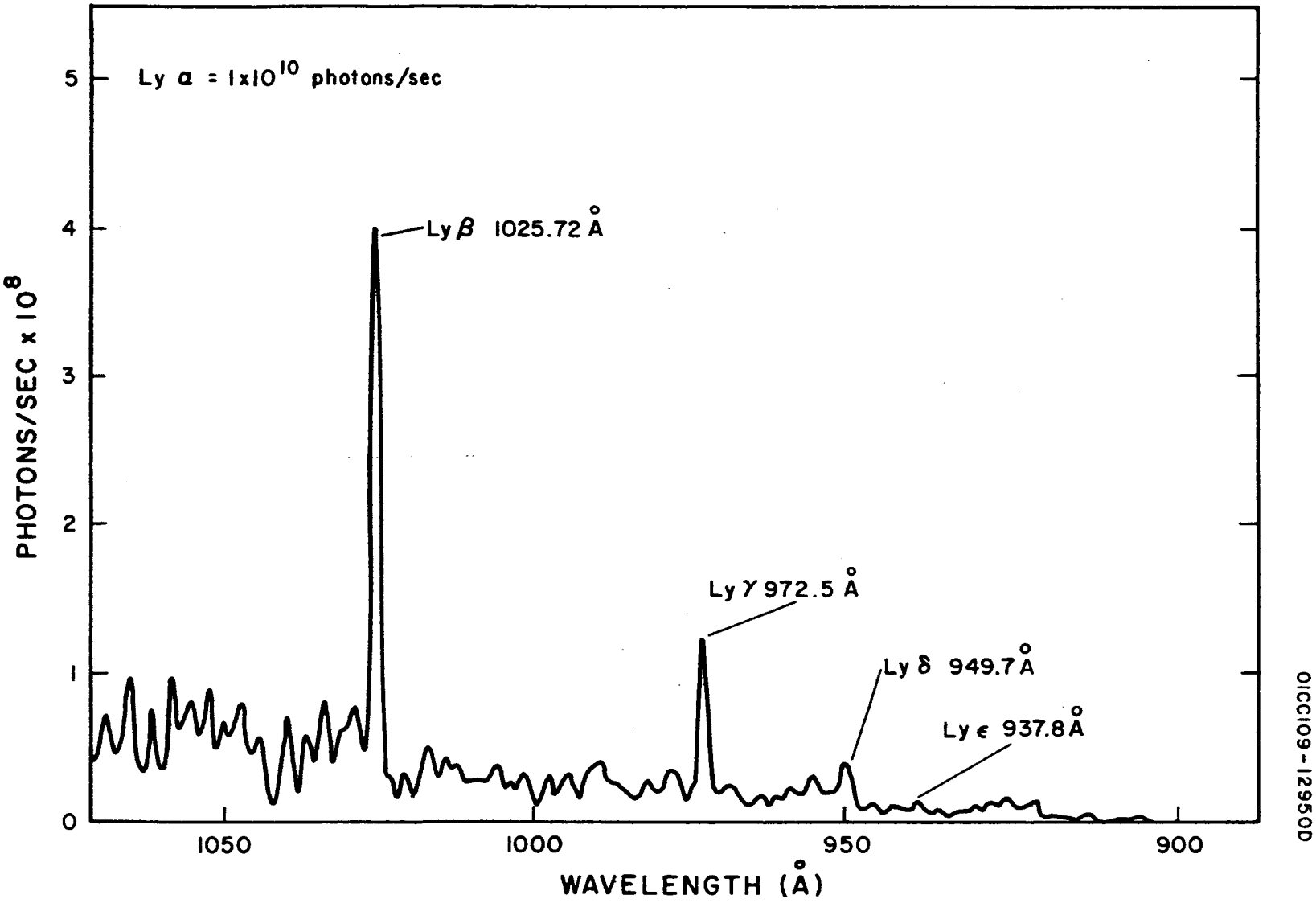

Figure 8. Lyman series of atomic hydrogen obtained in an H_2-He mixture with the hot filament discharge lamp. The intensity of the Lyman-alpha line is given at the top of the figure.

this is one of the major advantages of the hot filament arc discharge. Normally, to produce radiation below 1000 A of usable intensity, one must use a high voltage spark discharge. The disadvantage of the spark discharge is that high frequency electrical noise is radiated and this is very hard to shield against.

The hot filament arc discharge in hydrogen produces an over-all, more intense spectrum than the cold cathode discharge. The intensity ratio is only a factor of two or three; however, the ratio of atomic to molecular line intensities is much greater for the hot filament arc discharge. In both types of discharge using a hydrogen-helium mixture, nearly monochromatic radiation at 1216 A is produced.

C. THE DUOPLASMATRON

The Duoplasmatron was developed about twelve years ago as a highly efficient source of protons. After its publication[14] in 1956, a number of variations were designed and used as ion or electron sources for such applications as accelerator ion sources and ion propulsion devices.[15-17] A further application was suggested by Herzog;[18] namely, that the highly concentrated plasma of a Duoplasmatron possibly would emit intense vacuum ultraviolet radiation.

In the spectral region below 1000 A conventional light sources are of the high voltage pulsed type with their inherent disadvantages that they radiate electrical noise and are difficult to operate at a

constant light intensity output. Thus, it is desirable to look for a light source which emits radiation below 1000 A of comparable intensity to the high voltage pulsed type but which operates from a D.C. supply. The hot filament type of light source falls into this category with the exception of light intensity. It was felt, therefore, that with the combination of hot filament and axial magnetic field as found in the Duoplasmatron that the light intensity would be comparable with the high voltage pulsed light sources.

A preliminary measurement of the total intensity between 1050 A and 1350 A was made using a nitric oxide ion chamber with a Duoplasmatron which was currently being used as an ion source. The source had an anode opening of 0.008 inches. Using hydrogen in the Duoplasmatron with an arc current of 300 mA, an intensity of approximately 10^{12} photons/sec/cm^2 was measured at a distance of 25 cm from the anode opening for the 1216 A Lyman-alpha line. This is based on the assumption that 50 percent of the ion chamber response was due to the 1216 A line--an assumption which is normally true for a hot filament-type hydrogen lamp. Subsequently, a Duoplasmatron light source was designed, built, and tested. The design considerations, construction, and operating principles have been discussed in detail in the original report and are not repeated here in this Summary.

1. Brief Description and Results

The Duoplasmatron, as shown in Figure 9, has been operated successfully both as an ion source and as a vacuum ultraviolet light

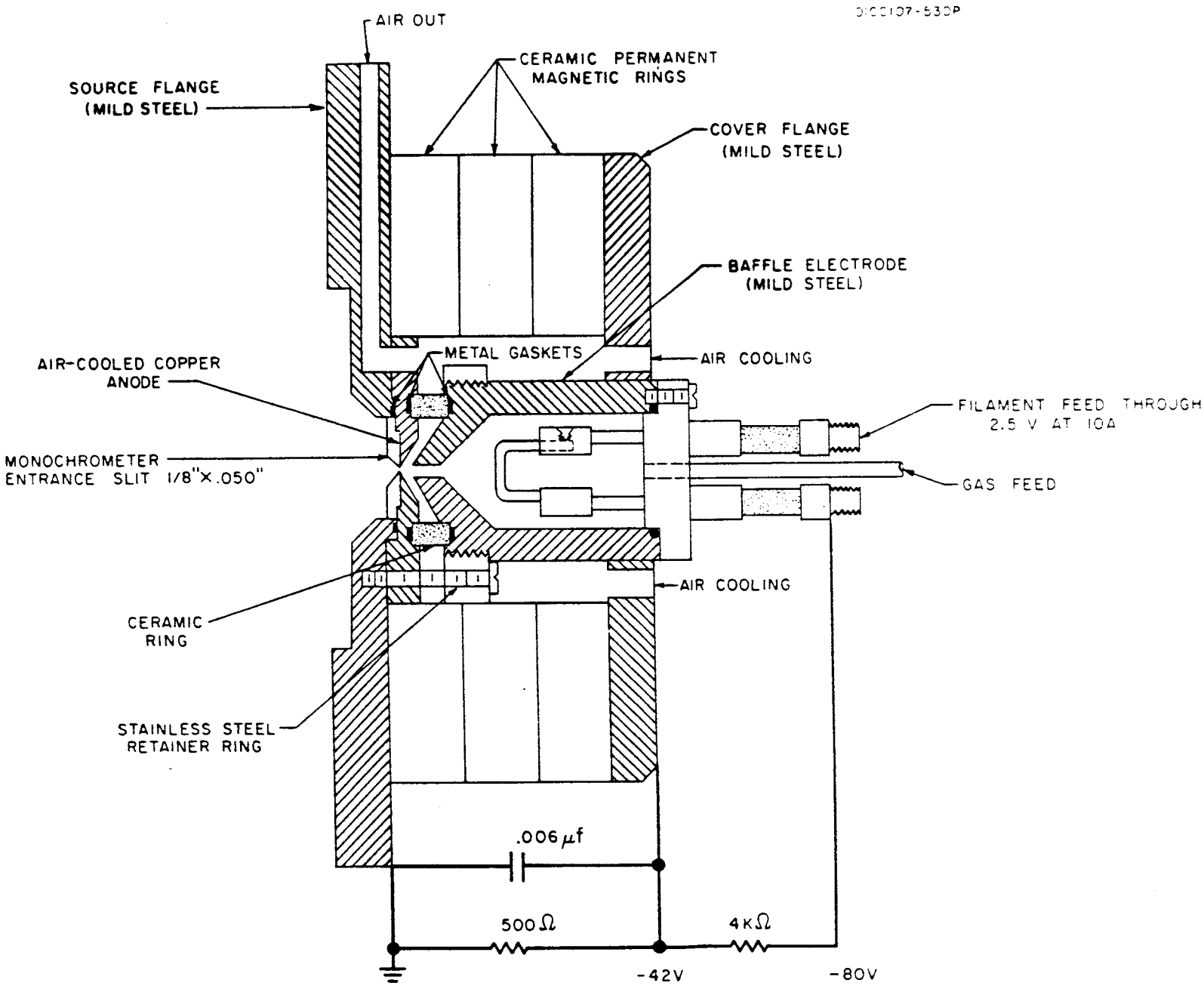

Figure 9. Duoplasmatron light source. The voltage distribution shown is typical under discharge conditions in hydrogen.

SCALE = 1/n

source. The extractor aperture of the Duoplasmatron ion source was replaced by a slit assembly 1/8 inch high by 50 microns wide. The slit-assembly constituted the entrance slit of a 1/2 M Seya-type vacuum monochromator having a reciprocal dispersion of 16 A/mm. Under such conditions a wavelength resolution of approximately 2 A was obtained. No windows were used between the light source and the monochromator since no suitable materials exist which will transmit radiation below 1050 A (the short wavelength transmission limit of lithium fluoride). However, due to the low operating pressure of the Duoplasmatron and the small slit area, a pressure of 1×10^{-4} torr was maintained in the monochromator chamber without the use of a differential pumping chamber between the light source and monochromator. When the discharge was started, the pressure in the monochromator decreased by a factor of two or three. This, apparently, is due to the intense ionization in the vicinity of the entrance slit impeding the flow of neutral gas through the slit into the monochromator. The entrance slit is at a positive potential relative to the baffle in the Duoplasmatron.

The ultraviolet detector was an EMI 9514B photomultiplier tube sensitized to vacuum ultraviolet radiation by coating its envelope with sodium salicylate. The quantum efficiency of this scintillator has been measured from 2000 A down to 800 A and found to be constant.[10] Although it is probable that the constancy of the quantum yield of sodium salicylate continues in the region of our measurements down to 550 A, one must be careful in comparing the relative intensity of two lines rather

widely separated as the efficiency of diffraction gratings in the vacuum ultraviolet region of the spectrum is not constant with wavelength.[9]

Figure 10 shows the spectrum of hydrogen between 1800 A and 900 A. It is a typical hydrogen spectrum with the molecular continuum at longer wavelengths than 1650 A and the many-lined molecular spectrum at shorter wavelengths than 1650 A, which include the atomic lines of the Lyman series, alpha and beta, at 1215.7 A and 1025.7 A, respectively. However, it does differ from the spectrum produced in a hydrogen glow-discharge (cold cathode type) in that the atomic resonance line at 1215.7 A is several times more intense than the most intense molecular line, usually 1608 A. As the arc current was varied from 0 to 0.9 amps, the light intensity increased almost linearly--the molecular lines increasing at a somewhat slower rate than the atomic lines. This result can be correlated with the analysis of the beam composition as a function of arc current as reported by Moak et al.[15] who found a rather linear and more rapid increase in the atomic ion content than in the molecular ion content.

An argon spectrum from 550 A to 1100 A is shown in Figure 11. The arc current was 1.5 amps with 30 volts between anode and filament. As the arc current increased from zero, the radiation from excited neutral atoms increased to a maximum around 1 amp and then remained constant or even decreased slightly as the arc current increased further; however, the radiation from the singly and doubly ionized atoms continued to increase. At 3 amps the 879.6 A and 878.7 A lines of A III were a

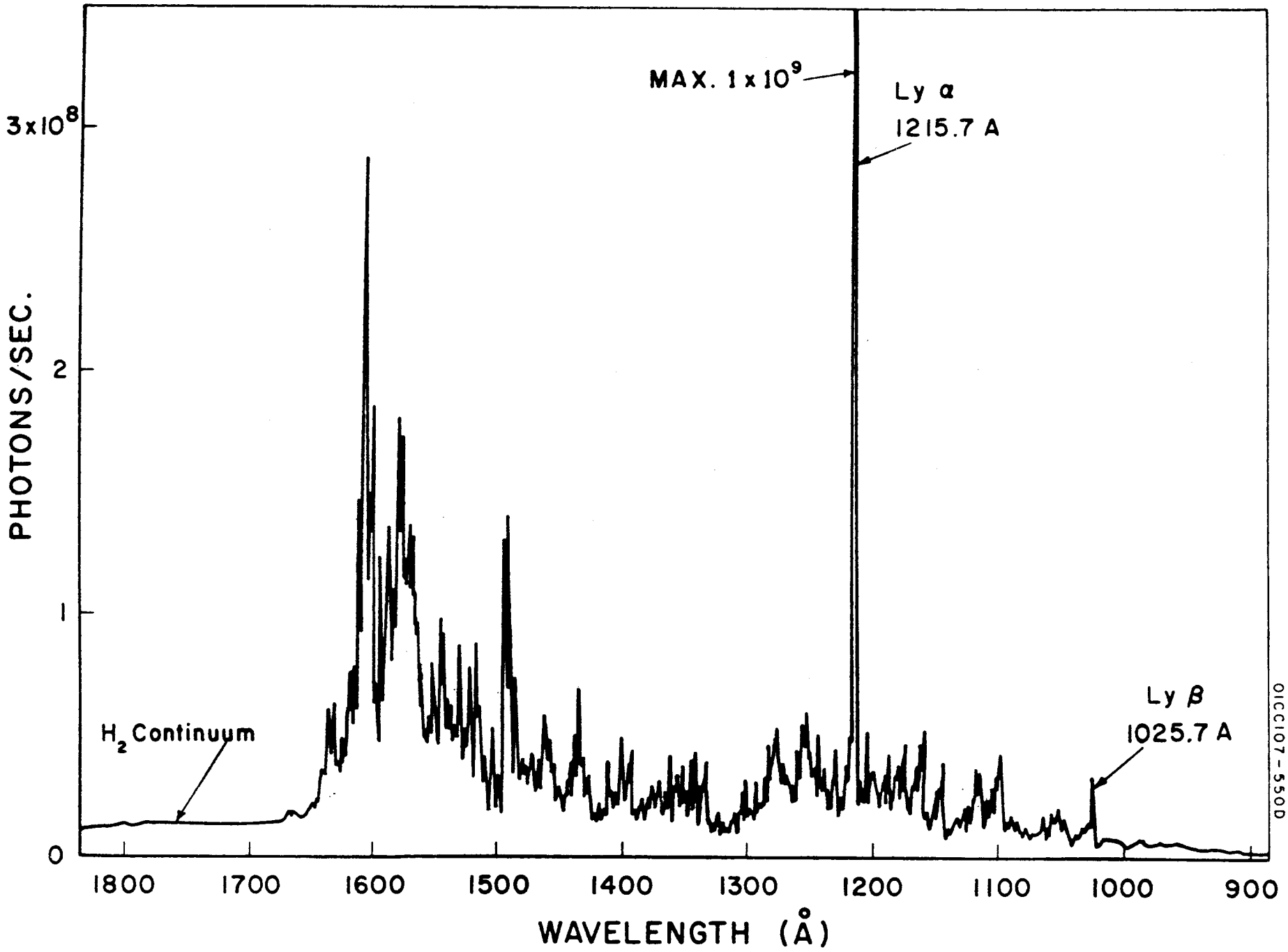

Figure 10. Hydrogen spectrum taken with an arc current of 0.9 amp. wavelength resolution is approximately 2 angstroms.

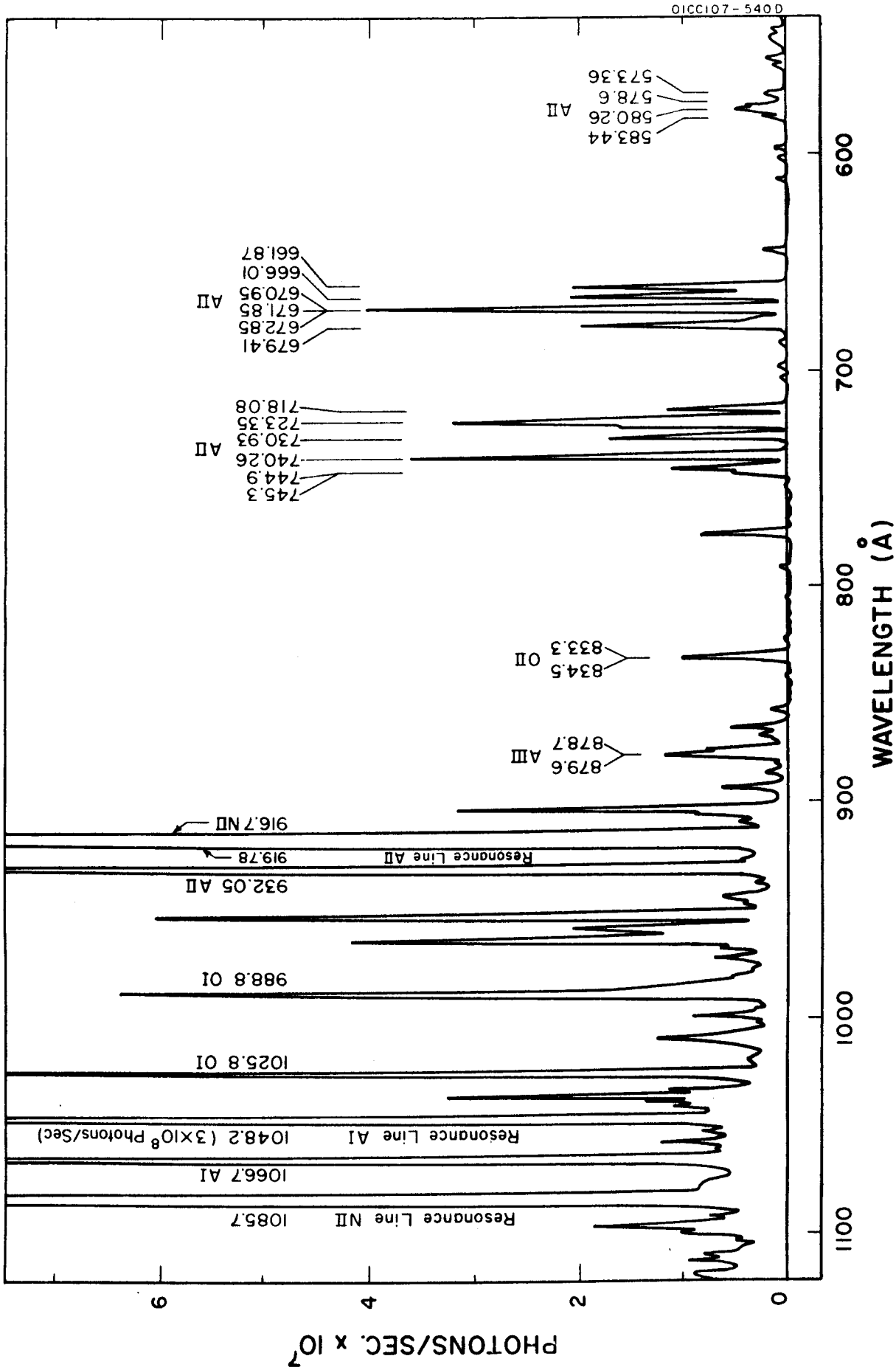

Figure 11. Argon spectrum taken with an arc current of 1.5 amp.

factor of five more intense than shown in Figure 11, whereas the A II series increased by only a factor of two. The presence of an air leak was indicated by radiation from atomic nitrogen and oxygen.

That the magnetic field confines the discharge to a very intense radiating plasma along the axis is evidenced by the fact that if the ceramic magnets are removed one by one, the light intensity decreases rapidly to the point of essentially zero light intensity at zero magnetic field.

The Duoplasmatron is suitable as a D.C. light source producing considerable intensity in the spectral region below 1000 A; however, for argon, these intensities are somewhat less than those of a 6 kv, 60 pps spark discharge. By increasing the arc discharge current, it appears possible to increase the intensity of the radiation to the point where it is comparable to that of the high voltage pulsed discharge.

D. MICROWAVE DISCHARGE

The first reported use of microwave frequencies to excite a discharge for use as a spectroscopic light source was by W. F. Meggers at the National Bureau of Standards.[19] He used a 110 Mc electrodeless discharge to excite the spectrum of Hg^{198} using the green 5461 A line as a standard of length. Jacobsen and Harrison,[20] studying these standard lamps, reported that the life and intensity of the lamps increased with

frequency in the range 10 to 3000 Mc. Since then, several other investigators[21-26] have described electrodeless discharge tubes excited in a microwave cavity. They used a Raytheon Microtherm Generator to produce radiation of 2450 Mc at a power output of 125 watts. Of these, the first report of their use as vacuum ultraviolet light sources was by Wilkinson.[25,26] Frost and McDowell[23] used them to produce line spectra in air and argon down to 600 A. P. Warneck[24] has described the use of a microwave discharge in hydrogen to produce the 1215.7 A Lyman-alpha line of atomic hydrogen for photochemical research. Recently, the Jarrell-Ash Company has produced the rare gas continua in a microwave cavity (see Section II). These light sources apparently are based on the researches of Wilkinson.[25]

The advantages of an electrodeless discharge are the absence of sputtered electrode material and impurities imbedded within the electrodes. The absence of sputtering prolongs the life of the windows.

The microwave light source investigated here was simply a long quartz tube placed within a microwave cavity. In a hydrogen-helium mixture, the microwave discharge produces perhaps the most monochromatic source of Lyman-alpha radiation. Figure 12 shows a spectrum taken with the hydrogen-helium mixture.

Spectra were observed in air and argon below 1000 A, but these were very weak. It is felt that the use of a capillary of a few mm bore rather than the 10 mm bore used here, would provide more intensity in the region below 1000 A.

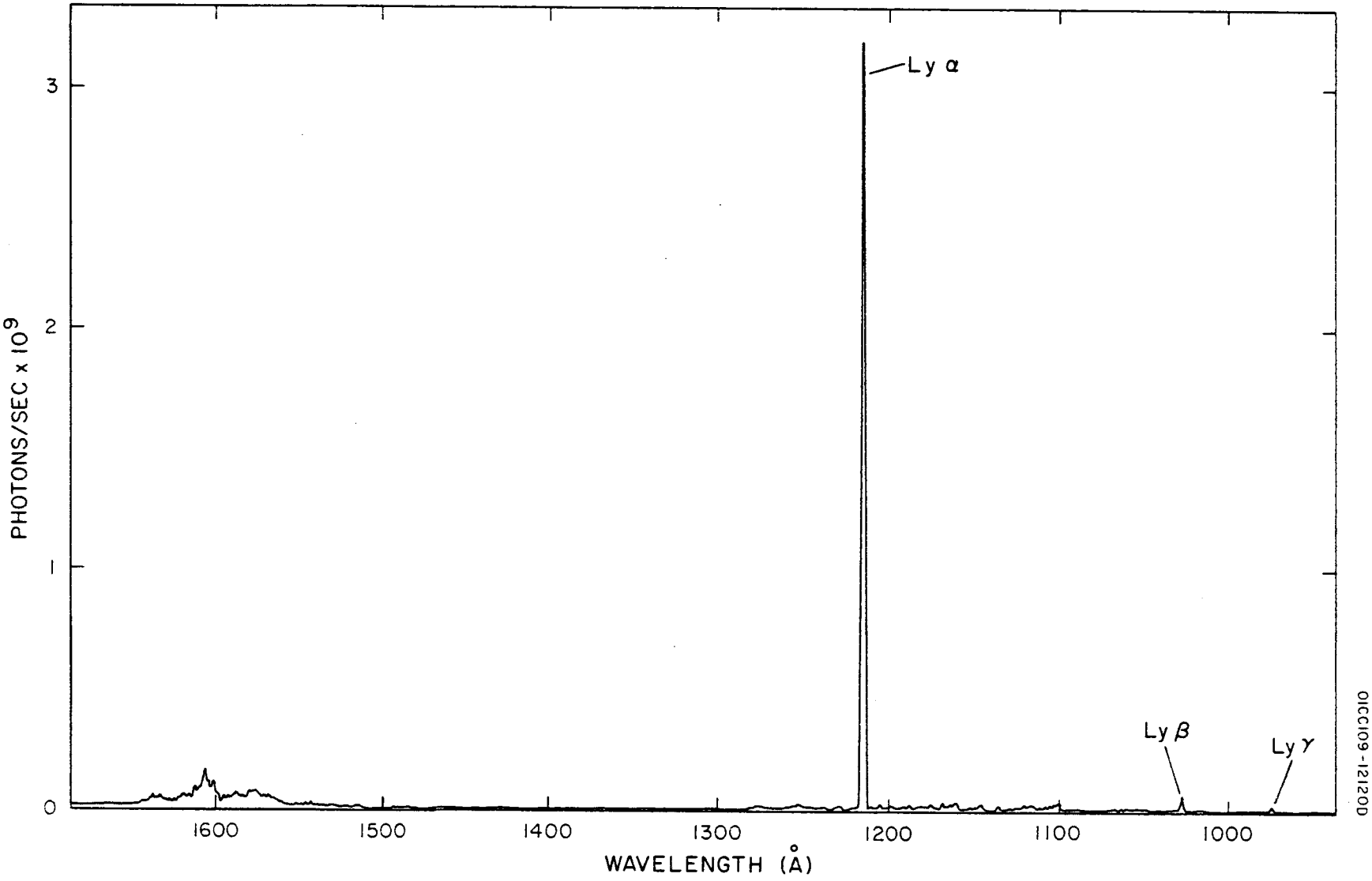

Figure 12. Hydrogen spectrum excited by microwaves in an H_2-He mixture. The spectrum is essentially monochromatic at Lyman-alpha.

IV. CONCLUSIONS

From the foregoing discussion it appears that several light sources exist which produce useful continua from 3500 A to 600 A of sufficient intensity to measure (employing photoelectric detection techniques) (a) absorption cross sections of gases and crystals and (b) reflectance and transmittance of thin films. In addition, it appears that in most cases, a resolution of one Angstrom or better can be achieved.

For photoionization measurements, it is possible to use the continua, especially the Hopfield continuum, if wider entrance and exit slits are used. The intensities are marginal, but by sacrificing resolution for intensity, one can still get valuable data previously unobtainable since the conventional high voltage spark spectrum below 1000 A has gaps between lines of as much as 20 A. However, the high voltage spark light source is still one of the most useful sources due to its greater intensity and low operating pressures eliminating elaborate differential pumping.

REFERENCES

1. Y. Tanaka, A.S. Jursa, and F.S. LeBlanc, J. Opt. Soc. Am., 48, 304 (1958).

2. R.E. Huffman, W.W. Hunt, Y. Tanaka, and R.L. Novak, J. Opt. Soc. Am., 51, 693 (1961).

3. R.E. Huffman, W.W. Hunt, Y. Tanaka, R.L. Novak, J.C. Larrabee, GRD Research Notes No. 61, AFCRL 663, 1961.

4. Reproduced by kind permission of Jarrell-Ash Co.

5. T. Lyman, Science, 64, 89 (1926).

6. W.H. Parkinson and E.M. Reeves, Proc. Roy. Soc., 262, 409 (1961).

7. W.R.S. Garton, Rev. Sci. Instr., 36, 11 (1959); Proc. Fourth Int. Conf. on Ionization Phenomena in Gases, p. 518, 1960.

8. W. Hunter, Private Communication.

9. J.A.R. Samson, J. Opt. Soc. Am., 52, 525 (1962).

10. F.S. Johnson, K. Watanabe, and R. Tousey, J. Opt. Soc. Am., 41, 702 (1951).

11. P. Johnson, J. Opt. Soc. Am., 42, 278 (1952).

12. P.L. Hartman and J.R. Nelson, J. Opt. Soc. Am., 47, 646 (1957); P.L. Hartman, J. Opt. Soc. Am., 51, 113 (1961).

13. The working drawings were kindly presented to GCA by Dr. P. Hartman, Cornell University, Ithaca, N.Y.

14. M.V. Ardenne, Tabellen der Elektronenphysik, Ionenphysik and Übermikroskopie, Deutschen Verlag der Wissenschaften, Berlin, Vol. I, p. 544 (1956).

15. C.D. Moak, H.E. Banta, J.N. Thurston, J.W. Johnson, and R.F. King, Rev. Sci. Instr., 30, 694 (1959).

16. H. Froehlich, Nukleonik, 1, 183 (1959).

17. B.S. Burton, Jr., "The Duoplasmatron," Presented at ARS Conference on Electrostatic Propulsion (Nov. 1960).

18. R.F.K. Herzog, Private Communication (Jan. 1962).

REFERENCES (continued)

19. W.F. Meggers, J. Opt. Soc. Am., 38, 7 (1948).

20. E. Jacobsen and G.R. Harrison, J. Opt. Soc. Am., 39, 1054 (1949).

21. G.H. Dieke and S.P. Cunningham, J. Opt. Soc. Am., 42, 187 (1952).

22. M. Zelikoff, P.H. Wyckoff, L.M. Aschenbrand, and R.S. Loomis, J. Opt. Soc. Am., 42, 818 (1952).

23. D.C. Frost and C.A. McDowell, Final Report on Ionization Potentials of Molecules, AF19(604)-2275, Project No. 7635 (1960).

24. P. Warneck, Applied Optics (to be published).

25. P.G. Wilkinson and Y. Tanaka, J. Opt. Soc. Am., 45, 344 (1955).

26. P.G. Wilkinson, J. Opt. Soc. Am., 45, 1044 (1955).

GCA Technical Report No. 63-1-N

PLANETARY AERONOMY IX:
THE DARK SIDE AIRGLOW OF VENUS

N. Jonathan and G. Doherty

February 1963

Contract No. NASw-395

Prepared for

National Aeronautics and Space Administration
Headquarters
Washington 25, D. C.

GEOPHYSICS CORPORATION OF AMERICA
Bedford, Massachusetts

TABLE OF CONTENTS

LIST OF FIGURES

LIST OF TABLES

THE DARK SIDE AIRGLOW OF VENUS

N. Jonathan and G. Doherty

SUMMARY

I. INTRODUCTION

Telescopic observations of Venus have shown a luminescence on the dark side similar to that which sometimes illuminates the whole moon during its first quarter.

Recent spectroscopic measurements have reported especially strong emission in the region 4410 - 4400 A.[1,2] The nature of the emissions is unestablished, but the possibility has been suggested that this luminescence arises as a result of the reaction between atomic oxygen and carbon monoxide.[3]

The chemiluminescence arising from the reaction of carbon monoxide and atomic oxygen has been investigated by a number of workers. A brief summary of the experimental methods and observations of Broida and Gaydon,[4] Clyne and Thrush,[5] and Mahan and Solo[6] were reviewed in the original report.[7] It was found that the results were not self-consistent. For example, Broida and Gaydon[4] associated their observed luminescence to excited carbon dioxide molecules formed during the three-body reaction:

$$CO + O + M \rightarrow CO_2^* + M.$$

Clyne and Thrush[5] explained their results on the basis of a three-body process involving atomic oxygen, carbon monoxide and the predominant species for stabilization of the excited state; a rather complex mechanism

resulted, which is discussed in detail in the original report. Finally, Mahan and Solo[6] used a stirred reactor in the pressure range 0.56 to 1.6 mm Hg and studied the light emission as a function of the amount of carbon dioxide which was produced. They propose a mechanism to explain their results, which involves two distinct two-body reactions resulting in the formation of both radiative and non-radiative carbon dioxide molecules. Full details of their mechanism are also given in the report.[7]

The present investigation is also concerned with a study of the chemiluminescence arising from the reaction of carbon monoxide and atomic oxygen. An experimental apparatus is employed which is similar to that of Mahan and Solo[6] but the measurements are performed in a completely different manner; the results can be considered independently.

On the basis of results and analyses from the present investigation, a new mechanism is proposed which can be successfully applied to the present data and to those of the previously cited investigators.[4,5,6]

A brief summary of the experimental procedures, results, and analyses are given in Sections II, III and IV.

II. EXPERIMENTAL

The details of the experimental procedure are given elsewhere.[7] Here, only a very brief sketch of this aspect is included for completeness.

A block diagram of the apparatus used is shown in Figure 1. Molecular oxygen or a mixture of molecular oxygen and inert gas is passed, via a flowmeter and valve, through a microwave discharge unit. This partially dissociates the molecular oxygen which then enters the reaction vessel after first passing through the Wood's light trap. Purified carbon monoxide enters the reaction vessel through another side arm via a needle valve.

The steady state concentration of oxygen atoms in the reaction vessel was measured at the end of each set of readings by the well-known titration method using nitrogen dioxide.

Two methods were used to observe the light emission from the carbon monoxide-atomic oxygen reaction. One was employed for determining the spectral distribution; the other for obtaining the over-all light emission.

The spectral distribution of the light emission was observed using a Perkin-Elmer model 112 G grating spectrometer, which had a single beam, double pass monochromator. Attempts were made to record the spectrum in the region from 2000 A - 6000 A. Above 3500 A, a Pyrex filter was inserted in order to avoid the presence of higher orders from the grating.

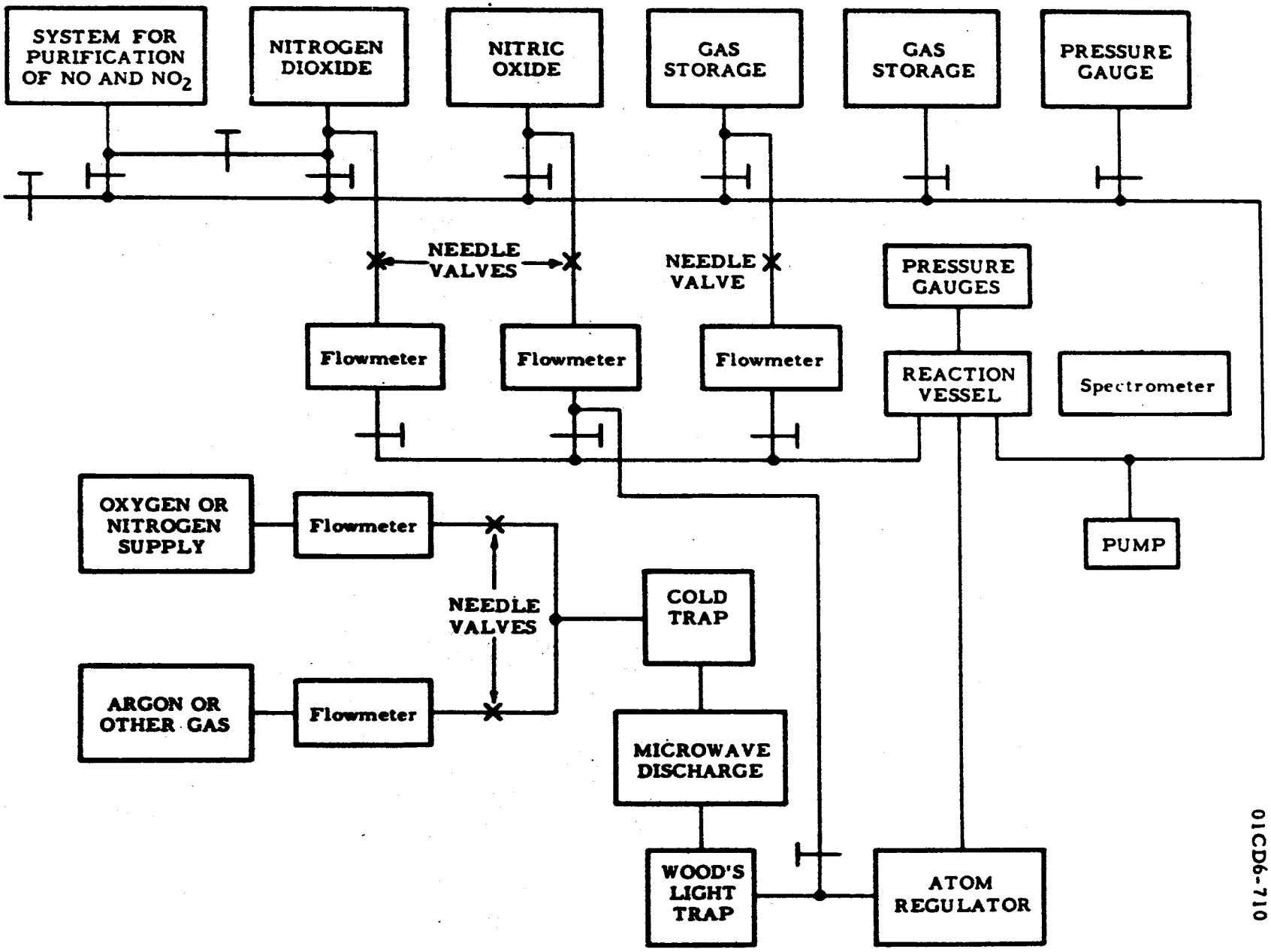

Figure 1. Block Diagram of Apparatus for Observation of Chemiluminescence.

The radiation passing through the monochromator was chopped on its second pass using a chopping frequency of 13 cps. This avoided the detection of the unchopped first pass radiation since the resulting signal was fed into an amplifier tuned to the chopping frequency. The signal was detected at the exit slit of the monochromator by an E.M.I. number 9558B tri-alkali photomultiplier tube which was mounted in a specially designed light-tight housing. The spectral region between 2000 A and 6000 A was scanned automatically.

The over-all light emission was measured by mounting an RCA 1P21 photomultiplier tube, in a light-tight housing, directly onto the aperture of the reaction cell. The resulting DC signal was fed into a Victoreen microammeter. Other details of this procedure are included elsewhere.[7]

III. RESULTS

The spectrum of the luminescence was obtained between pressure limits of 0.5 mm and 1.5 mm of mercury and at varying flow rates of oxygen, atomic oxygen and carbon monoxide. It is important to note, however, that very careful purification of the carbon monoxide is necessary. We found that if insufficiently pure carbon monoxide was used, then we obtained a much stronger light emission which consisted of a banded spectrum overlying an apparent continuum which appeared at somewhat longer wavelengths than the carbon monoxide-atomic oxygen continuum. The bands were readily identified as the emission from the CuCl system. It is to be noted that these bands are a frequent impurity in flames of burning carbon monoxide and also in the cool flame. Future investigators should be made aware of this observation.

The experimental program was continued using the photomultiplier setup which was described earlier. The net emission from the oxygen atom-carbon monoxide reaction was obtained by subtraction of background emission due to O + NO. The dependence of the glow on the concentration of carbon monoxide present was investigated. The light emission was then plotted as a function of the carbon monoxide concentration expressed in microns of mercury. The light emission was found to be linear with an increasing carbon monoxide concentration. A typical set of results is shown in Figure 2.

The light emission variation as a function of atomic oxygen concentration was also determined. The results are given in Figure 3

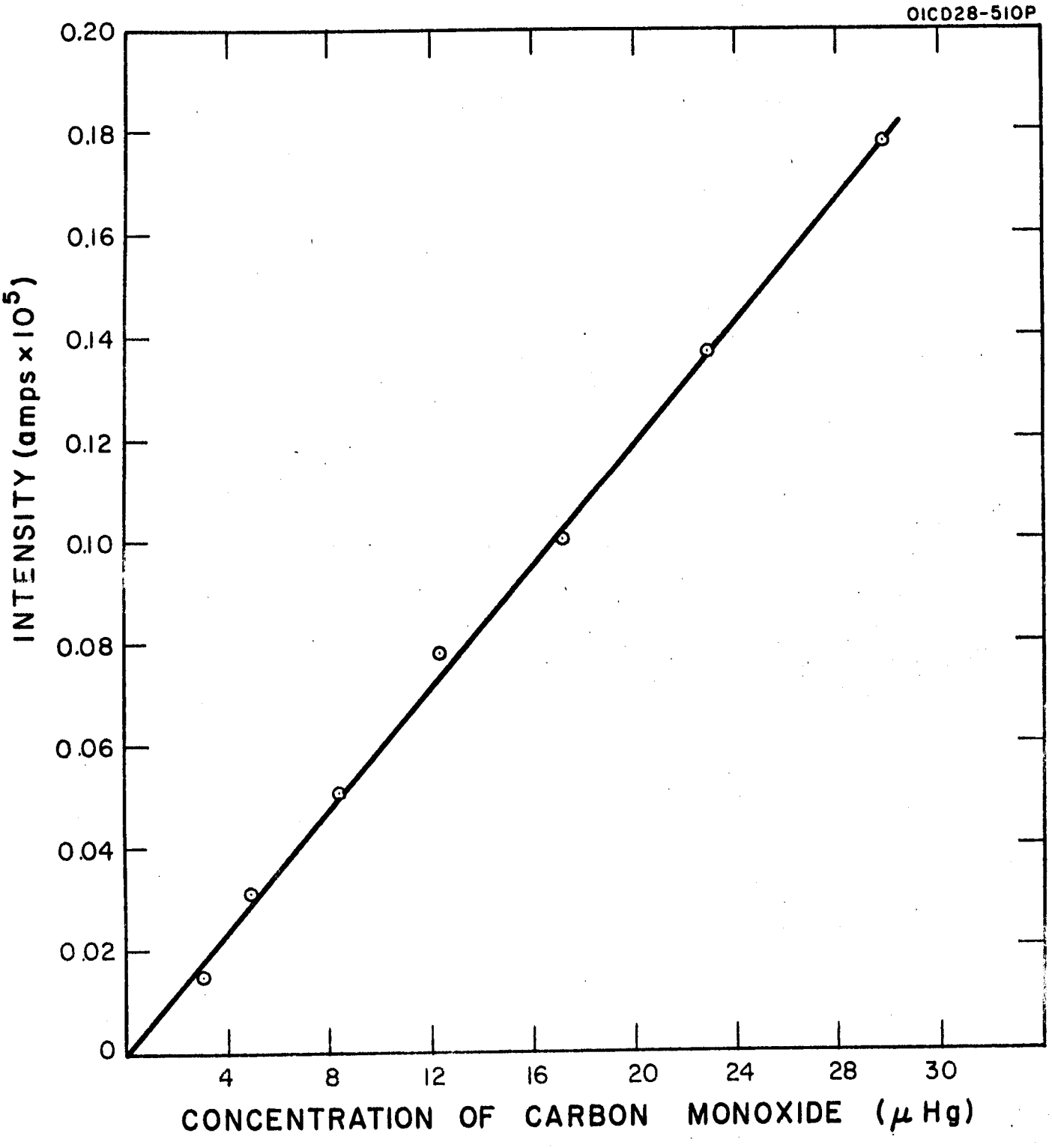

Figure 2. Graph of Light Emission Against Carbon Monoxide Concentration with Constant Oxygen Atom Concentration.

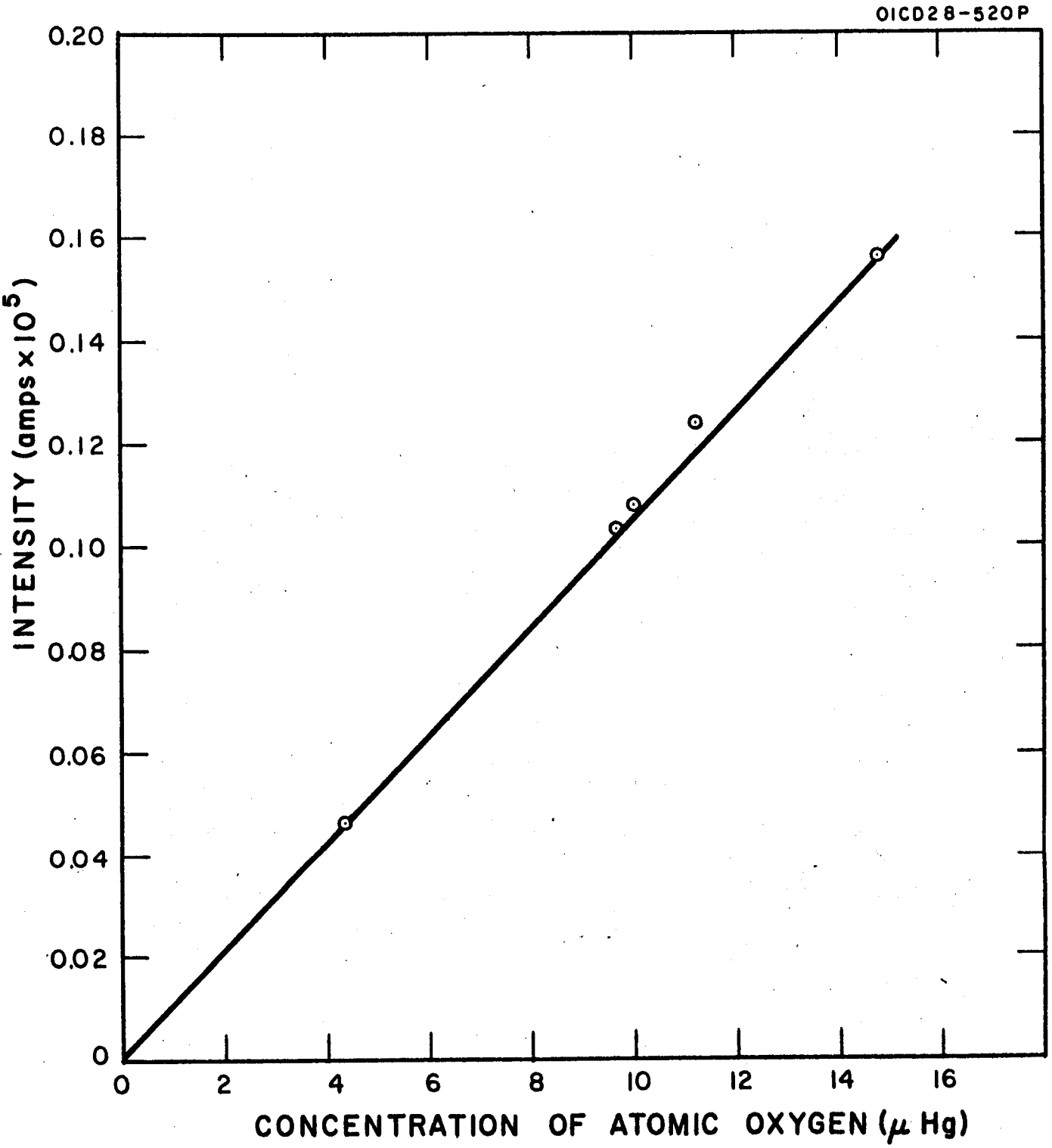

Figure 3. Graph of Light Emission Against Oxygen Atom Concentration with Constant Carbon Monoxide Concentration.

which shows that the light emission increases linearly with increasing atomic-oxygen concentration.

The effect of changing the amount of third body present was next established; the results are summarized in Figure 4, along with some extra readings. Figure 4 gives a clear indication of the lack of effect of varying amounts of the third body.

The dependence of the light emission on the type of third body present was investigated. The experiments were carried out by measuring the light emission using varying amounts of carbon monoxide, and diluting the molecular oxygen with either helium or argon so that the inert gas was the predominant third body. It was found that more light is emitted with argon and helium than there is with oxygen as a third body. These results are shown graphically in Figure 5.

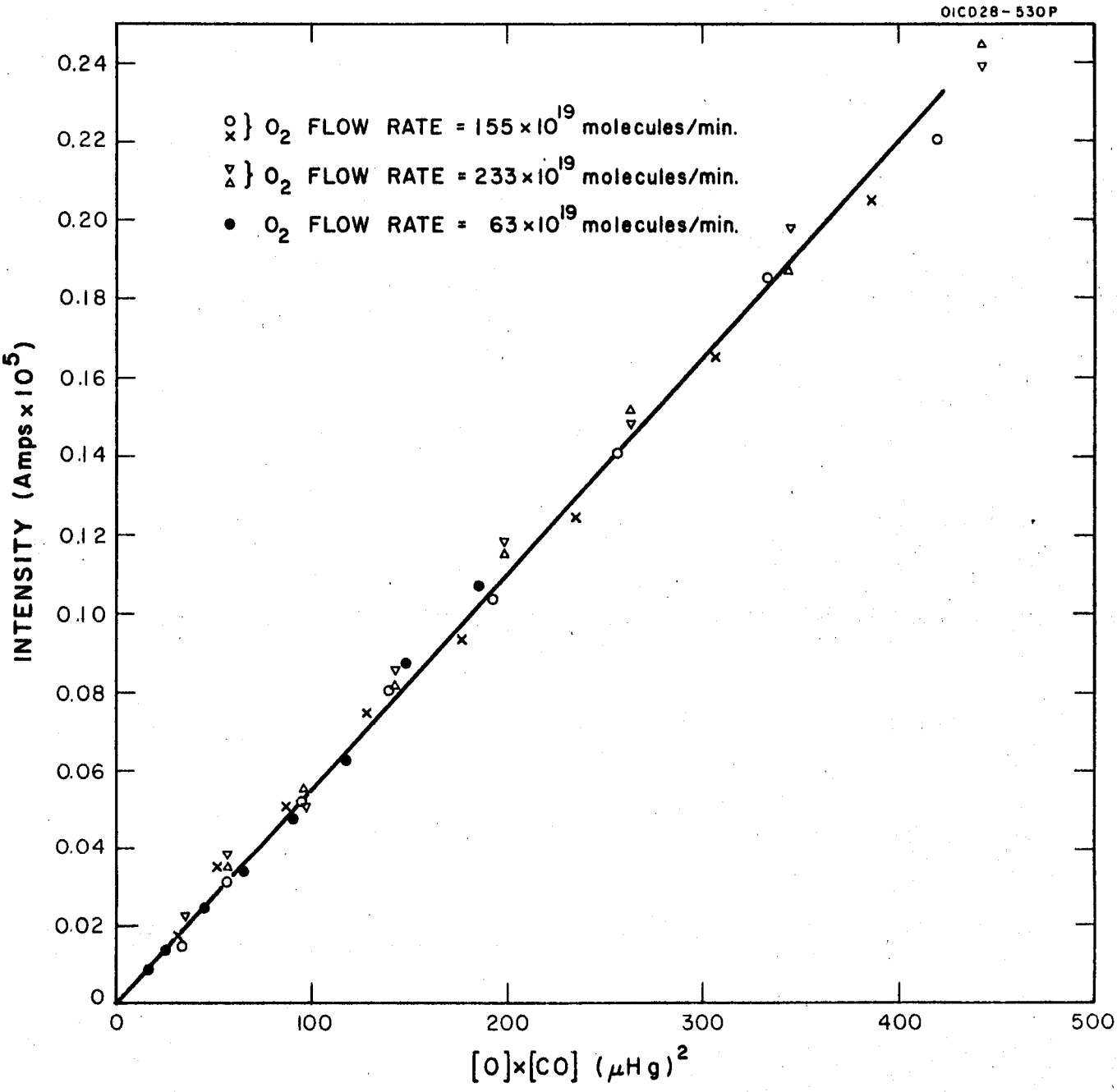

Figure 4. Plot of Intensity of Light Emission Against Concentration of Atomic Oxygen and Carbon Monoxide.

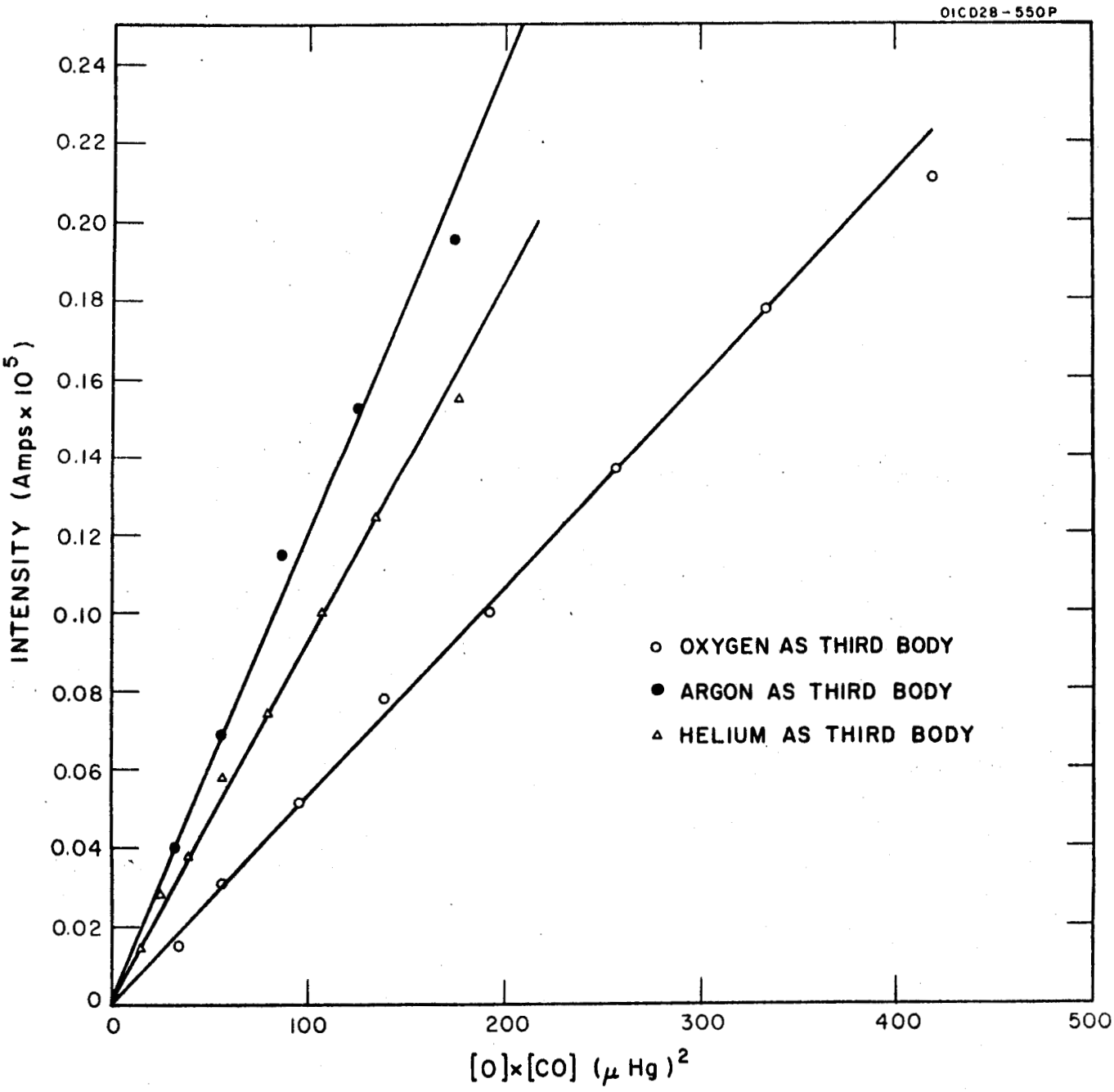

Figure 5. Effect of Variation of the Predominant Third Body on Intensity.

IV. DISCUSSION OF RESULTS

In the original document, the results have been discussed and interpreted in detail. For this purpose, it was necessary to include the results and interpretations of the works by Broida and Gaydon,[4] Clyne and Thrush,[5] and Mahan and Solo.[6] After a thorough review of these authors' works, in each instance they were systematically compared with the present results. In this manner, it was possible to derive a mechanism which was suitable for interpreting the present work and at the same time could serve as a mechanism which was compatible with the discordant results of the three previously cited authors.[4,5,6]

The detailed arguments are not repeated here since they are accessible in the full report.[7] However, it is important to note that the new mechanism proposed in the present work is the only one which is not in conflict with all the experimental observations.

In spite of the success of the present experiments, before we can draw any positive conclusions as to the importance of these chemiluminescent reactions to the Venus airglow, a study should be made at higher temperatures. In this regard, it might be noted that at room temperature, the luminescence is at least a factor of 2000 less than the O + NO reaction.

REFERENCES

1. Kozyrev, N. A., Izv. Krym. Astorfig. Obs. 12, 169 (1954).

2. Newkirk, G., Planet. Space Sci. 1, 32 (1959).

3. Jonathan, N. and Doherty, G., "Laboratory and Theoretical Studies in the Vacuum Ultraviolet," GCA Quarterly Progress Report, Contract No. NASw-395 (December, 1962).

4. Broida, H. P. and Gaydon, A. G., Trans. Far. Soc. 49, 1190 (1953).

5. Clyne, M. A. A. and Thrush, B. A., Proc. Roy. Soc. A269, 404 (1962).

6. Mahan, B. H. and Solo, R. B., J. Chem. Phys. 37, 2669 (1962).

7. Jonathan, N. and Doherty, G., "The Dark Side Airglow of Venus," GCA Technical Report No. 63-1-N, Contract NASw-395 (February 1963).